Dissertation

Finite-amplitude gravity waves in the atmosphere: traveling wave solutions and stability

Mark Schlutow

14. März 2017

eingereicht am

Fachbereich Mathematik und Informatik
Freie Universität Berlin

zur Erlangung des Grades eines
Doktors der Naturwissenschaften

Erstgutachter & Betreuer:
Prof. Dr. Rupert Klein

Zweitgutachter:
Prof. Dr. Ulrich Achatz

Drittgutachter:
Prof. Dr. Erich Becker

Tag der Disputation:
10. Juli 2017

Zusammenfassung

Basierend auf schwach asymptotischen Lösungen für nichtlineare Wentzel-Kramers-Brillouin Theorie für Schwerewellen mit finiter Amplitude in einer ungleichmäßig geschichteten Atmosphäre werden wandernde Wellenlösungen hergeleitet und bezüglich ihrer Stabilität untersucht. Von den nichtlinearen Eulergleichungen, welche für statisch instabile Wellen skaliert sind, leiten wir Modulationsgleichungen ab, die die Eulergleichungen im schwach asymptotischen Sinne lösen. Die Modulationsgleichungen beschreiben die zeitliche Entwicklung der Amplitude, Phase und des Grundstroms von führender Ordnung. Sie sind im Einklang mit der pseudoinkompressiblen Theorie, welche im Gegensatz zur Boussinesq-Theorie die Verstärkung eines Wellenpakets zulässt, wenn es in die obere Atmosphäre vordringt. Im Gegensatz zur anelastischen Theorie ist sie außerdem anwendbar im Falle starker Schichtung. Es werden zwei Klassen von wandernden Wellen als exakte Lösungen der Modulationsgleichungen entdeckt. Die erste Lösungsklasse propagiert nur horizontal, aber erlaubt dafür eine beliebig ungleichmäßige Hintergrundschichtung. Die zweite Klasse setzt eine gleichmäßige isotherme Schichtung voraus, bietet dafür aber auch eine Vertikalkomponente der Geschwindigkeit. Für die erste Klasse konnten partikuläre analytische Lösungen hergeleitet werden, die anschließend numerisch validiert werden. In den Simulationen wird die Erwartung über die Konvergenzordnung bezüglich des asymptotischen Parameters bei weitem übertroffen, sodass wir Konsistenz mit den vollen Eulergleichungen schlussfolgern. Desweiteren werden numerische Experimente mit den analytischen Lösungen als Referenz zur Konvergenzüberprüfung bezüglich der numerischen Auflösung durchgeführt. Es wird herausgestellt, dass die Lösungen der ersten Klasse Leewellen an Bergen ähnlich sind. Wir zeigen, dass sie den Grundstrom nur irreversibel verändern, falls sie brechen. Nichtsdestotrotz, aufgrund ihres nichtlinearen Verhaltens, tauschen sie kontinuierlich Energie mit dem Grundstrom aus, gesteuert durch die vertikale Windscherung des Grundstroms. Die zweite Klasse bietet Fronten ähnliche, horizontal periodisch wandernde Wellenlösungen, die immer aufwärts propagieren. Sie sind in ihrer Erscheinung vergleichbar mit Schiffswellen. Obwohl sie eine endliche Ausdehnung besitzen, bremsen die wandernden Wellenfronten den Grundstrom unumkehrbar ab, ohne aber dabei zu brechen, was der gängigen Theorie widerspricht. Bei diesem Prozess wird permanent Energie vom Grundstrom an die Welle übertragen. Durch die Anwendung der spektralen Stabilitätstheorie reproduzieren wir die Modulationsinstabilitäten für ebene Boussinesq-Wellen mit finiter Amplitude. Die Technik wird übenommen für unsere Modulationsgleichungen. Es stellt sich heraus, dass die wandernden Wellenfronten immer instabil sind gegenüber infinitesimalen Störungen. Wir linearisieren die skalierten Eulergleichungen um die allgemeinen wandernden Wellenlösungen. Mithilfe einer Skalierung passend zu dynamisch instabilen Wellen wenden wir eine WKB Näherung an, anstatt des üblichen Normalmoden-Ansatzen. Das entstandene System ist via Floquet-Theorie lösbar. Das Resultat dieser Untersuchung zeigt auf, dass die Dynamik kleinskaliger Störungen durch die Boussinesq-Theorie abgedeckt wird, welche vorhersagt, dass alle wandernden Wellenlösungen parametrisch instabil sind.

Abstract

Based on weak asymptotic solutions for nonlinear Wentzel-Kramers-Brillouin theory for finite-amplitude gravity waves in a non-uniformly stratified atmosphere, traveling wave solutions are derived and analyzed with respect to stability.

From the nonlinear Euler equations, which are scaled favorable for statically unstable gravity waves, we derive modulation equations describing the evolution of the leading order amplitude, phase, and induced mean flow. They are in line with pseudo-incompressible theory which allows, in contrast to Boussinesq theory, for amplification of wave packets when they travel deep into the higher atmosphere. And in contrast to anelastic theory, it is also valid for strong stratification.

Two classes of exact traveling wave solutions to the modulation equations are found. The first class propagates only in horizontal direction but applies to arbitrary non-uniform background stratification. The second class necessitates uniform, isothermal stratification but offers a vertical velocity component.

For the first class we discover particular analytic solutions that are also validated numerically. In simulations, they exceeded significantly the expectations at the order of convergence with respect to the asymptotic parameter, such that we conclude that they are consistent with the full Euler dynamics. Furthermore, numerical experiments with the analytic solution as a reference are used for a grid convergence study. It is pointed out that the solutions resemble the structure of mountain lee waves. We show that they fulfill the non-acceleration theorem. Nevertheless, due to their nonlinear behavior, the solutions of the first class constantly exchange energy with the mean flow controlled by the mean-flow vertical shear rate.

The second class features frontal-like, horizontal periodic solutions always traveling upwards. In their appearance, they are comparable with ship wakes. Although being of finite extend, the traveling wave front irreversibly decelerates the mean flow without breaking, which violates the non-acceleration theorem. In the process it constantly drains energy from the mean flow.

Applying a spectral stability analysis, we reproduce the modulational instabilities of finite plane Boussinesq waves. The technique is then adopted to our modulation equations. It turns out that the traveling wave fronts are always unstable against infinitesimal perturbations.

We linearize the scaled Euler equations at the most general traveling wave solutions. By a scaling suitable for dynamically unstable waves, we apply a WKB ansatz for the perturbation instead of the common normal-mode approach. The arisen system is solvable by Floquet theory. The outcome of this analysis reveals that the dynamics of small-scale perturbations is covered by Boussinesq theory which predicts parametric instability for all traveling wave solutions.

Contents

1 Introduction

The stratification of the earth's atmosphere gives rise to internal gravity waves which obtain kinetic energy and momentum from the mean flow when excited, transport them vertically as well as horizontally, and redistribute them by nonlinear interaction and breaking. By these processes, gravity waves have a major impact on the large-scale middle atmospheric circulation (Becker 2012; Fritts 2003).

Atmospheric gravity waves exhibit a considerable spectrum of wavelengths. Small-scale gravity waves have wavelengths of only about 100 m whereas large-scale waves posses horizontally wavelengths of several 1000 km. Global weather forecasting models have a resolution of approximately 10 km. Climate models typically are coarser resolved. Thus, they resolve only part of the gravity wave spectrum, the small-scale part needs to be parametrized (Alexander and Dunkerton 1999; McLandress 1998). Parametrization procedures estimate the impact of unresolved effects on the dynamics in terms of the resolved prognostic variables. They feedback the estimate as a correction to the resolved flow which is called the mean flow. In the feedback, conservation properties should be taken into account as the dynamical cores, i.e. the numerical model without the parametrizations, are usually designed to conserve energy, mass, and momentum. Therefore, the parametrizations should be based on the same governing equations which are in our context the Euler or rather the Navier-Stokes equations.

Gravity wave parametrizations rely on the following physical picture: Wave packets are excited in the lower atmosphere, usually the troposphere, by a flow over a mountain ridge for instance. The excitation transfers energy from the mean flow to the wave. The packet, and along with it the energy, propagates upwards from its origin where the wave grows in amplitude due to the thinning background density. This process is similar to surface waves on water. When waves from the deep ocean arrive at a shore they steepen up and amplify due to the flattening ocean bottom in the surf zone. Our atmospheric wave packets can propagate through the stratosphere deep into the higher atmosphere, i.e. the mesosphere over 50 km. Thereby, they interact with the mean flow obeying the non-acceleration principle (Bühler 2009) which states that the wave packet changes the mean flow irreversibly only when it breaks. A stable wave packet may alter the mean flow temporarily at a certain height but when it leaves by propagating farther up it restores the initial mean flow. Like the ocean waves when they come too close to the beach, such that they overturn and break, the atmospheric gravity wave packet reaches a height where the background air is so thin and the amplitude so high that the wave becomes unstable, overturns, breaks, produces turbulence, and dissipates. The energy that was carried by the wave transfers back to the mean flow and is hence

redistributed. In the breaking process the mean flow is finally accelerated by a drag.

This thesis is concerned with the instability mechanisms that lead to wave breaking. In theory and observations a whole zoo of different instability mechanisms is known that serve as criteria in the parametrizations to predict the position where wave drag is produced. Some of them are listed in the following.

If the perturbation of the background due to a wave locally leads to unstable stratification, such that dense air lies on top of thinner air, then the wave is said to be statically unstable. Note that the stratosphere provides a very stable background stratification due to its positive vertical temperature gradient. Gravity waves just propagate through and break in the mesosphere by the static instability in the most common scenarios. It is very unlikely that waves break by this mechanism in the stratosphere. Experimental observations by Haack et al. (2014) reveal, though, that turbulence plays a big role in the stratosphere which is probably induced by breaking gravity waves.

The associated instability mechanism, which is an open question in the community, could be shear. Atmospheric gravity waves can be characterized as shear waves as they produce a wind shear along the direction of their phase propagation. Statically stable waves can become unstable due to the shear if their local Richardson number becomes less than a quarter (Achatz 2007; Lelong and Dunkerton 1998; Liu et al. 2010; Miles 1961) which is known as Kelvin-Helmholtz instability (Goldstein 1931).

By means of Floquet theory, that is applicable for linear partial differential equations with periodic coefficients, parametric instabilities were considered by Drazin (1977), Lombard and Riley (1996), and Mied (1976). They exploited the convenient instance that monochromatic, plane waves in a uniform stratified background are exact solutions of the nonlinear Boussinesq equations. They found that even infinitesimal-amplitude waves are prone to parametric instabilities.

More recently, modulational instability effects taking weak nonlinear interactions with the mean flow into account were proposed by Dosser and Sutherland (2011a), Dosser and Sutherland (2011b), Sutherland (2001, 2006), and Tabaei and Akylas (2007). The ground for these studies was prepared by works of Grimshaw (1977) and Whitham (1974).

The underlying basis of all these analytical stability studies are traveling wave solutions. They are defined as stationary solutions in a translational coordinate system moving with a constant relative velocity. The aforementioned plane waves turn out to be of this kind. Once traveling wave solutions are found, one can linearize the transformed system at the traveling wave, which is stationary in the translational coordinates. The outcome provides an eigenvalue problem. If the linear operator exhibits eigenvalues with a positive real part, then the perturbation grows exponentially in time with the real part as its growth rate. In this case the traveling wave is said to be linear unstable.

All above-mentioned stability analyses assume a Boussinesq-type fluid. Achatz et al. (2010), Klein (2010), and Klein et al. (2010) tested the validity of the Boussinesq model, but also the anelastic model by Lipps and Hemler (1982), and the pseudo-incompressible model of Durran (1989) against the fully compressible

Euler equations. On the one hand, the findings suggest that the Boussinesq model holds for small-scale waves either with finite amplitude in uniform stratification or non-uniform stratification but infinitesimal amplitudes. However, in both cases the amplitude growth of an upward propagating wave cannot be captured. The anelastic theory provides a correction such that it allows for the amplification but on scales where stratification is much weaker as one would expect for the stratosphere but also for the mesosphere where waves usually break. On the other hand, the pseudo-incompressible model was confirmed to allow for the amplification on the typical scales that are involved.

Achatz et al. (2010) presented an extended theory: it was derived from a multiple-scale approach combined with Wentzel-Kramers-Brillouin (WKB) theory that allows variation of the wave envelope and phase on scales comparable with the pressure scale height with large, i.e. finite, amplitudes in arbitrarily strong stratification. The authors showed that the extended theory is in line with the pseudo-incompressible model. Its validity was also tested numerically by Rieper, Achatz, et al. (2013). With respect to the aforementioned effects that must be accounted for to establish a stability theory for gravity waves, which overcomes the limitations of the Boussinesq theory, this model provides the desired properties.

This thesis has two main objectives: First, we want to answer the question, whether traveling wave solutions to the extended theory exist and, if so, what do they look like? And second, what are their stability properties?

To achieve these goals this work is structured as follows. In Chapter 2 we will revisit the scaling assumptions of Achatz et al. (2010) to derive the governing equations: the scaled Euler equations. A spectral WKB ansatz for finite-amplitude waves will be exploited in Chapter 3. In addition to that, we will examine the notion of weak asymptotic solutions. This will lift the already well established theory on a stronger mathematical basis. Solvability constraints for the ansatz functions lead to the modulation equations which describe the evolution of the wave properties, such as amplitude, phase, and their influence on the mean flow. In Chapter 4 we will investigate the energy budget of the wave-mean-flow interaction and give a formulation of the non-acceleration theorem. Chapter 5 contains the answer to our first question. Here, we derive traveling wave solutions for the modulation equations which gives us leading order solutions for the governing equations. We will discover two distinct classes of traveling wave solutions. Both classes allow for a rich variety of parameter solutions. For the first class we will even find two different analytic solutions and for the second we will show existence and the structure of the wave. For both classes the wave-mean-flow energy exchange rate will be computed and the applicability of the non-acceleration theorem investigated. Chapter 6 is concerned with the numerical validation of the traveling wave solutions. The asymptotic parameter will by varied throughout the numerical experiments to find out if the asymptotic solution is consistent with the Euler dynamics. Subsequently, we will consider our asymptotic solution as the reference and proceed with a grid convergence study to validate the numerical model. In Chapter 7 we will investigate the existence of weak-asymptotic solutions which shall justify our approach. Thereby we will

introduce a curvilinear coordinate system that will help with the stability analyses in Chapter 8. This chapter will answer the second of our main questions. First, since the traveling waves are exact solutions to the modulation equations, we will linearize them and investigate the modulational stability in terms of the method of spectral stability analysis. Second, the governing equations will be linearized at the traveling waves which will result in a multiple scale problem. A WKB approach based on a scaling favoring shear-unstable waves will transfer it into a Floquet system. We will identify the structure with known results from literature.

2 The governing equations

In this chapter we will present a derivation of equations, that describe the dynamics of potentially unstable gravity waves in a hydrostatic background flow, starting from the dimensionless, fully compressible Euler equations. Because of their complexity we attempt to solve the Euler equations asymptotically. They are controlled by two non-dimensional characteristic parameters, the Mach and the Froude number, that measure the typical velocity in terms of the speed of sound and the flow inertia with regard to the gravitational acceleration, respectively. The first step towards an asymptotic solution will be to deduce a distinguished limit which couples the two characteristic parameters in a way that they approach zero depending on one another. For this purpose we must find in Section 2.1 a typical small number ε by scaling assumptions characterizing the physics of unstable gravity waves in the atmosphere. The Mach and the Froude number will become functions of ε and the limit $\varepsilon \to 0$ then generates the distinguished limit. The scaling assumptions will be induced by identifying the reference quantities and their relations to each other. Based on the multiple-scale asymptotic analysis of Achatz et al. (2010) we will introduce in Section 2.2 the gravity wave field as a fluctuation with certain amplitudes of the field's components against a hydrostatic background flow.

This chapter is based on a manuscript (Schlutow et al. 2017) which has been submitted to a peer reviewed journal.

2.1 Scaling the Euler equations for unstable gravity waves

We consider gravity waves in a two-dimensional domain neglecting the Coriolis force. Viscous effects as well as external heating sources are ignored, too. With respect to these basic assumptions the time evolution of the flow is governed by the compressible Euler equations for an ideal gas which may be written in non-dimensionalized form as

$$\begin{aligned} 0 &= D_t \mathbf{v} + \frac{1-\kappa}{\kappa} \frac{1}{\mathrm{Ma}^2} \theta \nabla \pi + \frac{1}{\mathrm{Fr}^2} \mathbf{e}_z \\ 0 &= D_t \theta \\ 0 &= D_t \pi + \frac{\kappa}{1-\kappa} \pi \nabla \cdot \mathbf{v} \end{aligned} \tag{2.1}$$

with (x, z) being the horizontal and vertical coordinate and the corresponding unit vectors $\mathbf{e}_x$ and $\mathbf{e}_z$. Here, $D_t = \partial_t + \mathbf{v} \cdot \nabla$ is the material derivative. The velocity vector field is denoted by $\mathbf{v}$. The Exner pressure is related to the usual pressure by

$$\pi = p^\kappa, \tag{2.2}$$

where κ is determined by the ratio of the the ideal gas constant R and the specific heat capacity at constant pressure c_p. From the temperature T we define the potential temperature to be

$$\theta = T/\pi. \tag{2.3}$$

The independent and dependent variables are non-dimensionalized according to Table 2.1. The Mach and the Froude number are given by $\mathrm{Ma} = v_{\mathrm{ref}}/C_s$ and

Dimensionful variable	x^*	z^*	t^*	$\mathbf{v}^*$	T^*	p^*
Dimensionless variable	x	z	t	$\mathbf{v}$	T	p
Reference value	x_{ref}	z_{ref}	t_{ref}	v_{ref}	T_{ref}	p_{ref}
Scaling	L_{ref}	L_{ref}	$\sqrt{g^{-1}H_\theta}$	$L_{\mathrm{ref}}\sqrt{gH_\theta^{-1}}$	$\kappa g R^{-1} H_\theta$	p_{ref}
Dimension in SI units	m	m	s	ms^{-1}	K	Pa

Table 2.1: Non-dimensionalization of variables

$\mathrm{Fr} = v_{\mathrm{ref}}/\sqrt{g z_{\mathrm{ref}}}$ with

$$C_s = \sqrt{\frac{1}{1-\kappa} R T_{\mathrm{ref}}} \tag{2.4}$$

being the speed of sound and g the gravitational acceleration. The objective is now to establish a distinguished limit which couples the Mach and the Froude number. Gravity waves are associated with motions slower than the speed of sound, so that the Mach number can safely be assumed to be small. In terms of scaling assumptions, we must figure out how the Froude number should change when the Mach number tends to zero, so that the physical properties characterizing gravity waves are captured asymptotically.

Grimshaw (1974) and Achatz et al. (2010) deduced the following scaling assumptions for large-amplitude gravity waves from linear theory:

1. Vertical and horizontal wave number are of the same order of magnitude, such that the spatial scaling is isotropic. Given a typical wavelength L_{ref} we let $x_{\mathrm{ref}} = z_{\mathrm{ref}} = L_{\mathrm{ref}}$.

2. The Brunt-Väisälä frequency, the pressure scale height, and the potential-temperature scale height may be defined as

$$N^2_{\mathrm{ref}} = \frac{\kappa g^2}{R T_{\mathrm{ref}}},\ H_p = \frac{R T_{\mathrm{ref}}}{g}, \text{ and } H_\theta = \frac{R T_{\mathrm{ref}}}{\kappa g}. \tag{2.5}$$

   It is worth noting that H_p and H_θ are of the same order in ε. Let us introduce a small dimensionless number $0 < \varepsilon \ll 1$ by assuming that the dominant wavelength is small in comparison with the scale height,

$$\varepsilon = L_{\mathrm{ref}}/H_\theta \tag{2.6}$$

   which will serve as a scale separation parameter.

3. A coarse estimate of the time scale is provided by $t_{\mathrm{ref}} = N_{\mathrm{ref}}^{-1}$.

4. The scaling of the velocity is obtained by a simple saturation argument (Achatz et al. 2010). The wave is said to be statically unstable if the sum of the vertical gradient of the buoyancy due to the wave and the background add up to be less than zero. Inducing this criterion into the polarization relation from the linear theory, links the buoyancy to the velocity and after some algebra it turns out that $u_{\mathrm{ref}} = w_{\mathrm{ref}} = L_{\mathrm{ref}} N_{\mathrm{ref}}$.

If we feed our dimensionless quantities with the scaling assumptions, we find the distinguished limit

$$\varepsilon = \sqrt{\frac{\kappa}{1-\kappa}}\mathrm{Ma} = \mathrm{Fr}^2 \tag{2.7}$$

that enslaves the Mach and the Froude number as ε tends to zero which is now the only parameter appearing in (2.1). The scaling of the reference variables is summarized in Table 2.1.

2.2 Multiple-scale analysis and the scaled Euler equations

The roughly estimated reference state is set to a hydrostatic atmosphere. Referring to scaling assumption 2 we can distinguish more precisely between two vertical length scales, the short wavelength of the potentially unstable gravity wave and the scale height of the reference atmosphere. The ratio of the two scales is ε. The scale separation can be achieved by a multiple-scale ansatz introducing a compressed vertical coordinate $Z = \varepsilon z$. Achatz et al. (2010) show that

$$\begin{pmatrix} \mathbf{v} \\ \theta \\ \pi \end{pmatrix} = \begin{pmatrix} \tilde{u}(x,z,t;\varepsilon) \\ \tilde{w}(x,z,t;\varepsilon) \\ \overline{\theta}(Z) + \varepsilon\tilde{\theta}(x,z,t;\varepsilon) \\ \overline{\pi}(Z) + \varepsilon^2\tilde{\pi}(x,z,t;\varepsilon) \end{pmatrix} \tag{2.8}$$

includes the essential ingredients which remain after carefully applying asymptotic analysis to leading order. In the velocity field the wave already appears at $O(1)$, because the background, which depends only on the stretched coordinate Z, is found to be hydrostatic, such that

$$d_Z\overline{\pi} = -\frac{1}{\overline{\theta}}. \tag{2.9}$$

Fluctuations from the background due to the wave in the potential temperature are $O(\varepsilon)$, whereas Exner pressure deviations first appear at $O(\varepsilon^2)$ in the wave field. That this assumption is indeed a reasonable, can be seen once again from linear theory. Another convincing argument is that $O(\varepsilon)$ fluctuations are potentially contaminated

with sound waves which we want to filter out. By means of the equation of state for ideal gases

$$\overline{\rho} = \frac{\overline{\pi}^{(1-\kappa)/\kappa}}{\overline{\theta}}, \tag{2.10}$$

which is found to be valid for the background, we introduce the background density $\overline{\rho}$. Additionally, the background temperature can be defined using (2.3) as

$$\overline{T} = \overline{\theta}\overline{\pi}. \tag{2.11}$$

To handle the background variables in a more convenient fashion, let us define the logarithmic background derivative of $\overline{f} \in \{\overline{\theta},\ \overline{\pi},\ \overline{\rho},\ \overline{T}\}$ as

$$\eta_f = d_Z \ln(\overline{f}). \tag{2.12}$$

Taking the derivative wrt Z of (2.10) and substituting with (2.12) we find that

$$\frac{1-\kappa}{\kappa}\eta_\pi = \eta_\rho + \eta_\theta. \tag{2.13}$$

We can identify $\eta_\theta = N^2$ to be the local Brunt-Väisälä frequency squared, $-\eta_\rho^{-1}$ may be interpreted as the local density scale height. Combining (2.9) – (2.13) it turns out that all background variables can be expressed by the background temperature,

$$\eta_\rho = -\eta_T - \frac{1}{\kappa\overline{T}} \text{ and } N^2 = \eta_T + \frac{1}{\overline{T}}. \tag{2.14}$$

So, once the vertical background temperature profile is known, all profiles of the remaining background variables are determined. If we now inject the distinguished limit (2.7) as well as the multiple-scale approach (2.8) into the compressible Euler equations (2.1) and substitute by (2.13), we arrive at a system of evolution equations

$$\begin{aligned} D_t u + \partial_x P &= -\varepsilon\, NB\partial_x P \\ D_t w + \partial_z P - NB &= -\varepsilon\,(NB\partial_z P - N^2 P) + \varepsilon^2 N^3 BP \\ D_t B + Nw &= -\varepsilon\,(N^2 + \eta_N) wB \\ \nabla\cdot\begin{pmatrix} u \\ w \end{pmatrix} &= -\varepsilon\,(N^2+\eta_\rho)w + \text{h. o. t.} \end{aligned} \tag{2.15}$$

for a new set of prognostic variables. This set is concatenated into the vector $U = (u, w, B, P)^T$ which is defined as

$$U = \left(\tilde{u},\ \tilde{w},\ \frac{1}{N}\frac{\tilde{\theta}}{\overline{\theta}},\ \overline{\theta}\tilde{\pi}\right)^T \tag{2.16}$$

where B and P relate to the buoyancy and the kinetic pressure, respectively. Some higher order terms (h. o. t.) are not given explicitly here for the sake of brevity. We

anticipate later derivations where they do not appear. However, they are taken into account completely in the asymptotic analysis. So, this system equals still the fully compressible Euler equations. We will refer to system (2.15) as scaled Euler equations. In the limit $\varepsilon \to 0$ and (x, z, t) kept constant it reduces to the well-known Boussinesq equations. However, in case we would neglect the h. o. t. terms at this point, we would obtain the pseudo-incompressible equations (Durran 1989), when using the same scaling assumptions with a the slowly varying background.

3 The asymptotic approximation

In this chapter we will apply a weak asymptotic scheme to derive the modulation equations whose traveling wave solutions and their stability are the main objective of this survey. In the previous chapter we found a distinguished limit from scaling assumptions suitable for unstable gravity waves and obtained the scaled Euler equations. This nonlinear system defines a multiple-scale problem as the wave field variables depend on fast coordinates whereas the coefficients of the PDE belong to the slowly varying background. In Section 3.1 we will introduce a nonlinear WKB approach that accounts for both scales. The notion of weak asymptotic solutions, which will be investigated in Section 3.2, will help us to deal with the nonlinear nature of the governing equations. The resulting asymptotic scheme will be used to extract leading (Section 3.3), first (Section 3.4), and second order equations (Section 3.5) whose solvability constraints will give us the modulation equations in Section 3.6.

3.1 A spectral WKB expansion

The scaled Euler equations are a set of nonlinear, first-order PDEs whose coefficients only depend on the stretched coordinate Z due to the background stratification. To account for the nonlinearities we exploit an asymptotic spectral expansion approach

$$U = \sum_{n=0}^{M} \sum_{|m|\leq n+1} \varepsilon^n \hat{U}_{n,m} e^{im\varepsilon^{-1}\Phi} + o(\varepsilon^M) \tag{3.1}$$

for the vector (2.16), in a way that resonant coupling of the wave with the mean flow, i.e. zeroth harmonics, already occurs in leading order (Chu and Mei 1970; Miura and Kruskal 1974). We restrict $\hat{U}_{n,-m} = \hat{U}^*_{n,m}$ for real-valuedness, where * indicates the complex conjugate of a variable. To account for the slowly varying background we additionally apply the WKB assumption that the coefficients and the phase are functions of only the slow variables $(X, Z, T) = \varepsilon(x, z, t)$, such that

$$(X, Z, T) \mapsto \hat{U}_{n,m}(X, Z, T),\ \Phi(X, Z, T). \tag{3.2}$$

The differential operators become

$$\partial_t = \varepsilon\partial_T \qquad \text{and} \qquad \nabla = \varepsilon\nabla_\varepsilon = \varepsilon(\partial_X, \partial_Z)^T. \tag{3.3}$$

So, when we apply this on the ansatz functions, e.g. with regard to the x-derivative, we obtain

$$\partial_x U = \varepsilon\partial_X \hat{U}_{0,0} + \left(\varepsilon\partial_X \hat{U}_{0,1} + i\hat{U}_{0,1}\partial_X\Phi\right) e^{i\varepsilon^{-1}\Phi} + \text{c. c.} + o(\varepsilon) \tag{3.4}$$

where c. c. stands for the complex conjugate of the previous terms. The derivatives with respect to z and t have the exact same structure. The phase should also be expanded in ε, like

$$\Phi = \Phi_0 + \varepsilon^2 \Phi_2 + \dots . \tag{3.5}$$

We only need the even gauge functions because effects by any Φ_n with n odd are already captured by $\arg(\hat{U}_{n,m})$. Since we will only analyze the system up to $M = 1$, these higher order effects do not matter in this work, so we simply keep $\Phi = \Phi_0$. By means of (3.3) we can define the local wave vector and the frequency,

$$\omega = -\partial_T \Phi, \tag{3.6}$$

$$\mathbf{k} = \nabla_\varepsilon \Phi. \tag{3.7}$$

3.2 The weak asymptotic scheme

This section discusses how to successively iterate the asymptotic solution in order to achieve an equation hierarchy. If we insert the ansatz (3.1) into the governing equations (2.15), we obtain an equation of the form

$$\sum_{k=0}^{M} \sum_{|l| \leq k+2} \varepsilon^k \mathcal{C}_{k,l}(X, Z, T) e^{il\varepsilon^{-1}\Phi(X,Z,T)} + o(\varepsilon^M) = 0. \tag{3.8}$$

The coefficients $\mathcal{C}_{k,l}$ represent the terms which contain the ansatz functions $\hat{U}_{n,m}, \Phi$, their derivatives, and the background variables. Our objective is to establish that the coefficients must be zero independently of k and l. This is usually achieved by an orthogonality argument that the harmonics are mutually perpendicular with respect to the inner product given by the average over the interval $[0, 2\pi]$ wrt the fast phase $\varepsilon^{-1}\Phi$ (Grimshaw 1974; Miura and Kruskal 1974; Tabaei and Akylas 2007; Whitham 1965). We encounter two issues with this approach if we want to apply it to our case: First, the fast phase does depend on ε, such that the phase lines squeeze together when ε tends to zero. And second, Φ is actually a function of space and time, therefore solving the integral requires an integration by substitution. We can circumnavigate these issues if we seek for asymptotic solutions in a weak sense (Danilov et al. 2003). Consider a differentiable, compactly supported test function S. We want to multiply S together with some test harmonic $\exp(-im\varepsilon^{-1}\Phi)$ to (3.8) and integrate over the entire real line with regard to the slow phase Φ. The aforementioned substitution shall be a bijective, continuously differentiable mapping, say

$$(X, Z, T) \mapsto F(X, Z, T) \tag{3.9}$$

which is independent of ε with $F = (\Phi, \Psi, \tau)$. We will present a particular mapping of this kind in Chapter 5. The weak formulation of (3.8) then reads

$$\sum_{k=0}^{M} \sum_{|l| \leq k+2} \varepsilon^k \int_{\mathbb{R}} S(\Phi)(\mathcal{C}_{k,l} \circ F^{-1})(\Phi, \Psi, \tau) e^{i(l-m)\varepsilon^{-1}\Phi} \mathrm{d}\Phi + o(\varepsilon^M) = 0. \tag{3.10}$$

We call (3.1) a weak asymptotic solution if it fulfills (3.10) for all $m \in \mathbb{N}$ and S. We may rewrite (3.10) for the forthcoming argument as

$$\sum_{k=0}^{M} \varepsilon^k \int_{\mathbb{R}} S\left(\mathcal{C}_{k,m} + \sum_{\substack{|l|\leq k+2 \\ l\neq m}} \mathcal{C}_{k,l} e^{i(l-m)\varepsilon^{-1}\Phi}\right) \mathrm{d}\Phi + o(\varepsilon^M) = 0. \tag{3.11}$$

One can show via integration by parts that the sum over l in (3.11) vanishes like $O(\varepsilon)$ when ε tends to zero, as

$$\int_{\mathbb{R}} S\mathcal{C}_{k,l} e^{i(l-m)\varepsilon^{-1}\Phi} \mathrm{d}\Phi = -\varepsilon \int_{\mathbb{R}} \frac{\partial S\mathcal{C}_{k,l}}{\partial \Phi} \frac{1}{i(l-m)} e^{i(l-m)\varepsilon^{-1}\Phi} \mathrm{d}\Phi = O(\varepsilon). \tag{3.12}$$

Here, we exploited that S has compact support. With (3.12) we can savely apply the limit $\varepsilon \to 0$ for (3.11) and iterate the solution: The sum over l in (3.11), i.e. the second summation, does not contribute to the leading order due to (3.12), such that $\mathcal{C}_{0,m} = 0$ for all m and S. In the next order these terms appear, but we can insert the leading order solution and find that they cancel out, such that also $\mathcal{C}_{1,m} = 0$ for all m and S. We can successively proceed to order $o(\varepsilon^M)$. To put it in a nutshell, it can be stated that $\mathcal{C}_{k,m} = 0$ provides a weak asymptotic solution for all k and m as $\varepsilon \to 0$.

3.3 Leading-order analysis

In the following sections we collect equations from the asymptotic scheme. From $\mathcal{C}_{0,0} = 0$ we find solenoidality of the velocity field of the primary harmonics,

$$ik_x \hat{u}_{0,1} + ik_z \hat{w}_{0,1} = 0. \tag{3.13}$$

And constraints for some mean-flow components

$$\hat{B}_{0,0} = \hat{w}_{0,0} = 0. \tag{3.14}$$

From $\mathcal{C}_{0,1} = 0$ we get a linear homogeneous system of equations

$$\mathcal{M}(-i\hat{\omega}, i\mathbf{k})\hat{U}_{0,1} = 0 \tag{3.15}$$

with the anti-Hermitian coefficient matrix

$$\mathcal{M}(-i\hat{\omega}, i\mathbf{k}) = \begin{pmatrix} -i\hat{\omega} & 0 & 0 & ik_x \\ 0 & -i\hat{\omega} & -N & ik_z \\ 0 & N & -i\hat{\omega} & 0 \\ ik_x & ik_z & 0 & 0 \end{pmatrix}. \tag{3.16}$$

Here, $\hat{\omega} = \omega - \hat{u}_{0,0}k_x$ represents the intrinsic frequency that is the frequency one observes in a reference frame moving with the leading order mean flow. It differs from ω only by a Doppler-shift term. Equations $\mathcal{C}_{0,2} = 0$ hold by the same solenoidality (3.13).

3.4 First-order analysis

From $\mathcal{C}_{1,0} = 0$ we obtain next order constraints for the mean flow

$$\begin{aligned}
\partial_T \hat{u}_{0,0} + \partial_X \hat{P}_{0,0} = &-\hat{u}^*_{0,1}\partial_X \hat{u}_{0,1} - \hat{w}^*_{0,1}\partial_Z \hat{u}_{0,1} \\
&-ik_z \hat{u}_{0,1}\hat{w}^*_{1,1} - ik_z \hat{u}_{1,1}\hat{w}^*_{0,1} \\
&-iNk_x \hat{B}_{0,1}\hat{P}^*_{0,1} + \text{c. c.}, \qquad (3.17)\\
(\partial_Z - N^2)\hat{P}_{0,0} - N\hat{B}_{1,0} = &-\hat{u}^*_{0,1}\partial_X \hat{w}_{0,1} - \hat{w}^*_{0,1}\partial_Z \hat{w}_{0,1} \\
&-ik_x \hat{u}_{1,1}\hat{w}^*_{0,1} - ik_x \hat{u}_{0,1}\hat{w}^*_{1,1} \\
&-iNk_z \hat{P}_{0,1}\hat{B}^*_{0,1} + \text{c. c.}, \qquad (3.18)\\
N\hat{w}_{1,0} = &-\hat{u}^*_{0,1}\partial_X \hat{B}_{0,1} - \hat{w}^*_{0,1}\partial_Z \hat{B}_{0,1} \\
&-(N^2 + \eta_N)\hat{w}^*_{0,1}\hat{B}_{0,1} + \text{c. c.}, \qquad (3.19)\\
\partial_X \hat{u}_{0,0} = &\, 0. \qquad (3.20)
\end{aligned}$$

Primary harmonics are fixed by $\mathcal{C}_{1,1} = 0$: it follows a linear inhomogeneous system for $\hat{U}_{1,1}$,

$$\mathcal{M}(-i\hat{\omega}, i\mathbf{k})\hat{U}_{1,1} + \mathcal{R}(\hat{U}_{1,2}, i\mathbf{k})\hat{U}_{0,-1} + \mathcal{L}(\delta_T, \nabla_\varepsilon)\hat{U}_{0,1} = 0 \qquad (3.21)$$

with $\mathcal{R}$ being a matrix

$$\mathcal{R}(\hat{U}_{1,2}, i\mathbf{k}) = \begin{pmatrix} ik_x\hat{u}_{1,2} - ik_z\hat{w}_{1,2} & 2ik_z\hat{u}_{1,2} & 0 & 0 \\ 2ik_x\hat{w}_{1,2} & ik_z\hat{w}_{1,2} - ik_x\hat{u}_{1,2} & 0 & 0 \\ 2ik_x\hat{B}_{1,2} & 2ik_z\hat{B}_{1,2} & -ik_x\hat{u}_{1,2} - ik_z\hat{w}_{1,2} & 0 \\ 0 & 0 & 0 & 0 \end{pmatrix} \qquad (3.22)$$

and $\mathcal{L}$ being a linear differential operator

$$\mathcal{L}(\delta_T, \nabla_\varepsilon) = \begin{pmatrix} \delta_T & \partial_Z\hat{u}_{0,0} & 0 & \partial_X \\ 0 & \delta_T & 0 & \partial_Z - N^2 \\ 0 & 0 & \delta_T & 0 \\ \partial_X & \partial_Z + N^2 + \eta_\rho & 0 & 0 \end{pmatrix} \qquad (3.23)$$

with $\delta_T = \partial_T + \hat{u}_{0,0}\partial_X + ik_x\hat{u}_{1,0} + ik_z\hat{w}_{1,0}$. Equations $\mathcal{C}_{1,2} = \mathcal{C}_{1,3} = 0$ yield the solenoidality,

$$ik_x\hat{u}_{1,2} + ik_z\hat{w}_{1,2} = 0, \qquad (3.24)$$

for the velocity field of the secondary harmonics.

3.5 Second-order analysis

From $\mathcal{C}_{2,0} = 0$ we obtain among others

$$\partial_X\hat{u}_{1,0} + (\partial_Z + N^2 + \eta_\rho)\hat{w}_{1,0} = 0. \qquad (3.25)$$

Here, we have already used the solenoidality (3.13). At this point we want to stop the iteration as we have found enough constraints to construct leading order solutions.

3.6 Derivation of the modulation equations

The objective of this section is to exploit solvability constraints from the asymptotic analysis (3.13)–(3.25) in order to derive a closed set of equations which we will denote as modulation equations. Equation (3.15) has non-trivial solution only if $\det(\mathcal{M}) = 0$ yielding the dispersion relation

$$\hat{\omega}^2 = \frac{N^2 k_x^2}{k_x^2 + k_z^2}. \tag{3.26}$$

Note that $\mathrm{sgn}(\hat{\omega}) = \pm 1$ indicates two different branches of the solution. By definition of the local wave vector (3.6), the dispersion relation is essentially a prognostic equation for Φ which is by definition of the frequency (3.7) of the form of a Hamilton-Jacobi equation. We find a particular vector $p \in \ker(\mathcal{M})$ providing the polarization relation

$$p(\mathbf{k}) = \left(-i\frac{k_z}{k_x}\frac{\hat{\omega}}{N},\ i\frac{\hat{\omega}}{N},\ 1,\ -i\frac{k_z}{k_x^2}\frac{\hat{\omega}^2}{N} \right)^T. \tag{3.27}$$

We deduce that $\mathrm{rank}(\mathcal{M}) = 3$. Since hence $\dim(\ker(\mathcal{M})) = 1$, we get a general solution for (3.15) by

$$\hat{U}_{0,1} = Ap \tag{3.28}$$

with a yet free complex valued scalar A, that we later refer to as wave amplitude. By means of solenoidality of the several harmonics in the velocity, (3.13) and (3.24), we can show that $\mathcal{R}(\hat{U}_{1,2}, \mathbf{k})\hat{U}_{0,-1} = 0$ which simplifies (3.21). A necessary condition for the solvability of (3.21) is that any vector $\mathcal{L}\hat{U}_{0,1} \in \mathrm{img}(\mathcal{M})$ has to be orthogonal to every $p \in \ker(\mathcal{M})$ by the Rank-nullity theorem:

$$0 = p^{*T}\mathcal{L}\hat{U}_{0,1}. \tag{3.29}$$

If equation (3.29) holds, then

$$0 = \hat{U}_{0,1}^{*T}\mathcal{L}\hat{U}_{0,1} + \text{c. c.}, \tag{3.30}$$

$$0 = \hat{U}_{0,1}^{*T}\mathcal{L}\hat{U}_{0,1} - \text{c. c.} \tag{3.31}$$

must be true independently, if $A \neq 0$, which will serve to fix the degrees of freedom in

$$A = |A| \exp(i \arg(A)). \tag{3.32}$$

This argument essentially means that the real and the imaginary part of the rhs of (3.29) must vanish. Equation (3.30) is true if

$$\partial_T|A|^2 + (\nabla_\varepsilon + \eta_\rho \mathbf{e}_z)\cdot(\mathbf{c}_g|A|^2) + |A|^2\frac{k_x}{\hat{\omega}}\frac{\partial\hat{\omega}}{\partial k_z}\partial_Z\hat{u}_{0,0} = 0 \tag{3.33}$$

which is derived using (3.20). With the help of the consistency relations, $\partial_T\mathbf{k}+\nabla_\varepsilon\omega = 0$ and $\partial_X k_z = \partial_Z k_x$ that we obtain by cross differentiating the definitions (3.6) and (3.7), we find

$$(\partial_T + \mathbf{c}_g\cdot\nabla_\varepsilon)\hat{\omega} = -k_x\frac{\partial\hat{\omega}}{\partial k_z}\partial_Z\hat{u}_{0,0} \tag{3.34}$$

with the group velocity

$$\mathbf{c}_g = \frac{\partial\hat{\omega}}{\partial\mathbf{k}} + \hat{u}_{0,0}\mathbf{e}_x. \tag{3.35}$$

Combining (3.33) and (3.34) results in an equation of motion,

$$\partial_T\frac{|A|^2}{\hat{\omega}} + (\nabla_\varepsilon + \eta_\rho\mathbf{e}_z)\cdot\left(\mathbf{c}_g\frac{|A|^2}{\hat{\omega}}\right) = 0, \tag{3.36}$$

for the specific wave action density $a = 2|A|^2/\hat{\omega}$. It is worthwhile mentioning that (3.36) is a conservation law for the wave action density $\mathcal{A} = \overline{\rho}a$. Let us return to the orthogonality of the kernel and the image vector (3.29). Exploiting (3.31) gives an equation of motion for the argument of A being basically some slow phase in addition to the fast phase Φ/ε, i.e.

$$(\partial_T + \mathbf{c}_g\cdot\nabla_\varepsilon)\arg(A) = -k_x\hat{u}_{1,0} \tag{3.37}$$

which contains the first order mean-flow horizontal wind. With the aid of the derivations from above, we can handle the mean-flow equations (3.17)-(3.20), and (3.25). Using solenoidality once more from (3.13) and (3.24) it is possible to settle all the terms depending on $\hat{U}_{1,1}$, so

$$\partial_T\hat{u}_{0,0} + \partial_X\hat{P}_{0,0} = -\partial_X|\hat{u}_{0,1}|^2 - (\partial_Z + \eta_\rho)(\hat{u}^*_{0,1}\hat{w}_{0,1}) + \text{c. c.}, \tag{3.38}$$

$$\hat{w}_{1,0} = 0, \tag{3.39}$$

$$\partial_X\hat{u}_{0,0} = 0, \tag{3.40}$$

$$\partial_X\hat{u}_{1,0} = 0. \tag{3.41}$$

If we plug (3.28) into (3.38), we obtain an equation of motion for the leading order mean-flow horizontal wind

$$\partial_T\hat{u}_{0,0} + \partial_X\hat{P}_{0,0} = -2(\nabla_\varepsilon + \eta_\rho\mathbf{e}_z)\cdot\left(k_x\frac{\partial\hat{\omega}}{\partial\mathbf{k}}\frac{|A|^2}{\hat{\omega}}\right). \tag{3.42}$$

The six equations (3.26), (3.36), (3.37), (3.40), (3.41), and (3.42), that we derived in this section, build a coupled system of equations for the six unknowns

$$\Phi,\ |A|,\ \arg(A),\ \hat{u}_{0,0},\ \hat{P}_{0,0},\ \text{and}\ \hat{u}_{1,0}.$$

These are the aforementioned modulation equations. Once they are solved, the leading order, weak asymptotic solution of the scaled Euler equations has been found. It is worth mentioning that further solvability constraints for the first order mean flow will show up when we keep iterating the asymptotic scheme. The equations are in line with the calculations of Achatz et al. (2010). However in addition, we explicitly provided a prognostic equation for the slow phase $\arg(A)$ and a constraint for the first order mean-flow horizontal wind since they contribute to the leading order solution. Equation (3.18) containing $\hat{B}_{1,0}$ can be considered to be uncoupled as it neither affects the leading order solution nor does it appear in one of the other modulation equations.

4 Wave-mean-flow interaction and energy balance

An important aspect of wave dynamics is the energy budget. As our theory allows for a wave-mean-flow interaction, we want to investigate the energy exchange.

4.1 The wave energy density

We can rewrite the equation of motion of the wave amplitude (3.33) in terms of the wave energy density, which we may define as $\widetilde{E} = 2\overline{\rho}|A|^2$, so

$$\partial_T \widetilde{E} + \nabla_\varepsilon \cdot \left(\mathbf{c}_g \widetilde{E}\right) = -k_x \frac{2\overline{\rho}|A|^2}{\hat{\omega}} \frac{\partial \hat{\omega}}{\partial k_z} \partial_Z \hat{u}_{0,0}. \tag{4.1}$$

On the lhs we find a conservative flux, that transports energy with the group velocity, and on the rhs an energy source term that is associated with the vertical shear of the mean-flow horizontal wind.

4.2 The mean-flow kinetic energy density

Let us now consider the mean-flow equation (3.42). Multiplying it by $\hat{u}_{0,0}$, using the chain rule and (3.20), give us an evolution equation for the mean-flow kinetic energy density $\overline{E} = \overline{\rho}\hat{u}_{0,0}^2/2$, so

$$\partial_T \overline{E} + \nabla_\varepsilon \cdot \left(\overline{\rho}\hat{u}_{0,0}\hat{P}_{0,0}\mathbf{e}_x + k_x \frac{2\overline{\rho}|A|^2}{\hat{\omega}} \frac{\partial \hat{\omega}}{\partial k_z} \hat{u}_{0,0}\mathbf{e}_z \right) = k_x \frac{2\overline{\rho}|A|^2}{\hat{\omega}} \frac{\partial \hat{\omega}}{\partial k_z} \partial_Z \hat{u}_{0,0}. \tag{4.2}$$

On the lhs we also find a conservative flux and on the rhs the same energy source term as in (4.1) but with the opposite sign making it an energy exchange rate.

4.3 The energy budget

If we sum up (4.1) and (4.2), we obtain a conservation law for the total energy density $E = \widetilde{E} + \overline{E}$. We will refer to the energy exchange rate, i.e. the rhs of (4.2), as

$$q = k_x \frac{2\overline{\rho}|A|^2}{\hat{\omega}} \frac{\partial \hat{\omega}}{\partial k_z} \partial_Z \hat{u}_{0,0} = k_x \mathcal{A} c_{gz} \partial_Z \hat{u}_{0,0}. \tag{4.3}$$

In conclusion, the total energy is conserved by the modulation equations. The sign of the exchange rate determines the direction of energy flow. E.g., an upward propagating wave packet with downward-facing phase speed vector transfers energy to the mean flow if the vertical shear is positive and vice versa.

4.4 The non-acceleration theorem

Another important aspect of wave-mean-flow interaction is the non-acceleration theorem that shall be investigated in this section. Let us consider horizontally periodic gravity waves. So, the phase simplifies to

$$\Phi = K_x X + \hat{\Phi}(Z, T), \tag{4.4}$$

where K_x is some constant horizontal wave number, and the horizontal derivatives in the modulation equations vanishes. Those kinds of wave solutions were examined by Rieper, Achatz, et al. (2013) and Bölöni et al. (2016). In this case the evolution equation for the mean-flow horizontal wind (3.42) can be written as

$$\overline{\rho}\partial_T \hat{u}_{00} = \partial_Z(K_x c_{gz}\mathcal{A}). \tag{4.5}$$

We want to find out how a vertically propagating wave packet changes the mean-flow wind. The answer to this question is the basis for gravity wave parametrizations in numerical weather forecasting and climate models.

Let us assume for this purpose that the wave action density $\mathcal{A}$ is compactly supported on a vertical range. This assumption corresponds to a typical wave packet having finite extent. We now compute the net acceleration of the mean-flow horizontal wind by integrating (4.5) over an interval Ω enclosing completely the support of the wave. So,

$$\partial_T \int_\Omega \overline{\rho}\hat{u}_{00} = \left[K_x c_{gz}\mathcal{A}\right]_{\partial\Omega} = 0. \tag{4.6}$$

The integral vanishes as we assumed a compactly supported wave packet, so that at the boundary $\partial\Omega$ the wave action density is zero. This result implies that wave packets with finite extent can only induce a lasting, i.e. irreversible, change in mean flow if they break and dissipate thereby (Bühler 2009). We will present in the following chapters solutions to the modulation equations that surely interact with the mean flow due to a verifiable energy exchange but do not necessarily fulfill the non-acceleration theorem.

5 Traveling wave solutions of the modulation equations

In the previous chapters we derived the modulation equations as a weak asymptotic approximations to the scaled Euler equations. This chapter is concerned with exact solutions to the modulation equations.

A key aspect for derivations of stability properties are traveling wave solutions. These are stationary, i.e. time-independent, solutions in a translational coordinate system. Performing a coordinate transformation of the governing equations and linearizing at the traveling wave solution results in an eigenvalue problem (due to the stationarity) for the time evolution of a small perturbation. The eigenvalues tell us whether the perturbation is bounded or whether it grows in time which implies instability. If we find traveling wave solutions for the modulation equations, we automatically obtain weak asymptotic traveling wave solutions for the scaled Euler equations. Why this is the case, will be answered in this chapter.

Consider the translational coordinate system $\Gamma = (\xi, \zeta, \tau)$ defined by the transformation $(X, Z, T) \mapsto \Gamma(X, Z, T)$:

$$\begin{pmatrix} \xi \\ \zeta \end{pmatrix} = \begin{pmatrix} X \\ Z \end{pmatrix} - \mathbf{C}T \text{ and } \tau = T, \tag{5.1}$$

with $\mathbf{C}$ being the constant relative velocity. Note that the unit vectors are preserved and the mapping is one-to-one. The nabla operator and the time derivative become

$$\nabla_\varepsilon = \mathbf{e}_x \partial_\xi + \mathbf{e}_z \partial_\zeta \tag{5.2}$$

and

$$\partial_T = \partial_\tau - \mathbf{C} \cdot \nabla_\varepsilon, \tag{5.3}$$

respectively. The modulation equations in the new coordinates may be written as

$$-(\partial_\tau - \mathbf{C} \cdot \nabla_\varepsilon)\Phi = \hat{\omega}(\mathbf{k}) + \hat{u}_{0,0} k_x, \tag{5.4}$$

$$(\partial_\tau - \mathbf{C} \cdot \nabla_\varepsilon)a + (\nabla_\varepsilon + \eta_\rho \mathbf{e}_z) \cdot (\mathbf{c}_g a) = 0, \tag{5.5}$$

$$\left(\partial_\tau + (\mathbf{c}_g - \mathbf{C}) \cdot \nabla_\varepsilon\right) \arg(A) = -k_x \hat{u}_{1,0}, \tag{5.6}$$

$$(\partial_\tau - C_z \partial_\zeta)\hat{u}_{0,0} + \partial_\xi \hat{P}_{0,0} = -(\nabla_\varepsilon + \eta_\rho \mathbf{e}_z) \cdot \left(k_x \frac{\partial \hat{\omega}}{\partial \mathbf{k}} a \right), \tag{5.7}$$

$$\partial_\xi \hat{u}_{0,0} = 0, \tag{5.8}$$

$$\partial_\xi \hat{u}_{1,0} = 0. \tag{5.9}$$

For the sake of simplification, we replaced $|A|$ by the specific wave action density $a = 2|A|^2/\hat{\omega}$. These equations depend on the background variables N and η_ρ which are functions of $Z = \zeta + C_z\tau$ due to the transformation, so they now depend in particular on time. In other words, the background is not hydrostatic anymore in the translational reference frame since the frame moves relatively to the background. We conclude that stationary solutions can only exist in two disjoint cases:

C1 The reference frame does not move vertically, such that $C_z = 0$. In this case we find that $Z = \zeta$ and hence the background is again time-independent. We will refer to this case as horizontally traveling wave solution. It will be examined in Section 5.1.

C2 The background variables, i.e. η_ρ and N, are constant in the first place and $C_z \neq 0$. If we combine the definition of the background temperature (2.11) with (2.13), we obtain

$$\frac{\kappa - 1}{\kappa}\frac{1}{\overline{T}} = \eta_\rho + N^2. \tag{5.10}$$

From this brief calculation we can deduce that the background temperature must be constant if the rhs is constant. By this point we will refer to this case as isothermal traveling wave solution which will be investigated in Section 5.2.

These arguments also hold for the scaled Euler equations because they exhibit the very same background variables as coefficients. So in general, we can say that traveling waves as solutions for the governing equations can only exist if either C1 or C2 is satisfied.

In both cases, a stationary solution to (5.4) is given by

$$\Phi(\xi, \zeta) = K_x\xi + \int_{\zeta_0}^{\zeta} k_z(\zeta')\mathrm{d}\zeta' \tag{5.11}$$

where K_x is a constant being, without loss of generality, positive and k_z the root of the 4th order polynomial derived from the dispersion relation

$$\left(C_z k_z + (C_x - \hat{u}_{00})K_x\right)^2 = \frac{N^2 K_x^2}{K_x^2 + k_z^2}. \tag{5.12}$$

The point ζ_0 denotes a reference point for the boundary conditions and may be chosen as $\zeta_0 = 0$, i.e. the bottom.

5.1 The horizontally traveling wave solution

In this section we want to investigate the horizontally traveling wave solution (C1), where $C_z = 0$ and $\zeta = Z$, because it is possible to find analytic, explicit solutions in this case, even for arbitrary stratification. These solutions already possess some

interesting properties such as nonlinear phase and amplitude, as well as arbitrary mean-flow horizontal wind.

If $C_z = 0$, then $\hat{u}_{0,0}$ disappears in (5.7), and hence (5.8) is solved by any real function

$$\hat{u}_{0,0}(\zeta) = u_{f0}(\zeta). \tag{5.13}$$

It can be interpreted rather as a background flow than a mean flow as it is still a solution to the hydrostatic background equations. Although we did not show the equation, an evolution equation for $\hat{u}_{1,0}$ emerges at higher order in the asymptotic iteration. But fortunately, the same argument holds due to (5.9), so it turns out that

$$\hat{u}_{1,0}(\zeta) = u_{f1}(\zeta) \tag{5.14}$$

is also an arbitrary function. Equation (5.12) reduces to a quadratic polynomial that is solved by

$$k_z(\zeta) = \pm\sqrt{\frac{N^2(\zeta)}{(C_x - u_{f0}(\zeta))^2} - K_x^2}. \tag{5.15}$$

It is worth pointing out that a negative discriminant results in an exponential growth or decay of the wave in the vertical direction corresponding to a reflective layer. To prevent this, we constrain $N/K_x > |C_z - u_{f0}|$ at any point. Also, we must not have $u_{f0} = C_x$ at any point as it possibly causes singularities which corresponds to a critical layer.

To solve (5.5), we drop the time derivative and rewrite it as

$$\partial_\zeta G + \frac{c_{gx} - C_x}{c_{gz}} \partial_\xi G = 0 \tag{5.16}$$

which is an equation for the vertical wave action flux $G = \overline{\rho} c_{gz} a$. Its validity requires that $c_{gz} \neq 0$ which is fulfilled if $k_z \neq 0$ and bounded. This manipulation is feasible as $\mathbf{c}_g$ depends only on ζ due to (5.13) and (5.15). As soon as we find a solution for G, the amplitude can then be computed by

$$|A|^2 = \frac{\hat{\omega}}{2\overline{\rho} c_{gz}} G. \tag{5.17}$$

By the method of characteristics a solution is given by

$$G(\xi, \zeta) = G_0(\Psi) \tag{5.18}$$

with

$$\Psi(\xi, \zeta) = K_x \xi - K_x \int_{\zeta_0}^{\zeta} \frac{c_{gx}(\zeta') - C_x}{c_{gz}(\zeta')} \mathrm{d}\zeta'. \tag{5.19}$$

The function G_0 can be determined by a boundary condition at ζ_0. Equation (5.19) can be further simplified if we plug in the definition (3.35) and use the dispersion relation (5.4),

$$\Psi(\xi,\zeta) = K_x\xi - \int_{\zeta_0}^{\zeta} \frac{K_x^2}{k_z(\zeta')}\mathrm{d}\zeta'. \tag{5.20}$$

Note that the characteristic curves given through Ψ are locally orthogonal on every line with constant phase Φ. This remarkable property only shall be stated here unproved. It will be investigated in detail in Chapter 7 where we will draw conclusions about the existence of weak asymptotic solutions using this very fact. In Section 8.2 the orthogonality will furthermore play a key role for some stability analyzes. Taking advantage of (5.9) we can compute a solution to (5.6) by separation of variables resulting in

$$\arg(A)(\xi,\zeta) = L_\Psi\Psi(\xi,\zeta) - K_x\int_{\zeta_0}^{\zeta} \frac{u_{f1}(\zeta')}{c_{gz}(\zeta')}\mathrm{d}\zeta' \tag{5.21}$$

with L_Ψ some constant. A general solution to (5.7) is found when inserting (5.5)

$$P_{0,0}(\xi,\zeta) = K_x\big(u_{f0}(\zeta) - C_x\big)a(\xi,\zeta) + P_f(\zeta) \tag{5.22}$$

with P_f some function.

5.1.1 Wave-mean-flow interaction of the horizontally traveling wave solution

Let us consider the energy budget for the C1 traveling wave solutions. With the aid of (5.18) we can compute the energy exchange rate as presented in Chapter 4 as

$$q = K_x G\partial_Z u_{f0}. \tag{5.23}$$

If G is locally confined, the energy exchange between wave and mean flow happens therefore on the characteristic curves defined by Ψ. And is strongest where the characteristic curve of the peak of G meets the level of strongest vertical shear.

The horizontally traveling waves fulfill the non-acceleration theorem as presented in Section 4.4 since the mean-flow horizontal wind is time-independent. Nevertheless, the wave is able to exchange constantly energy with the mean flow. This result is also quite counter-intuitive as the horizontally traveling waves are not horizontally periodic, which was actually a prerequisite.

5.1.2 Analytic solution for some non-uniform stratification

We were able to derive a complete general solution in the case of a horizontally traveling wave. However, the solution is still not explicit since integrals emerged for Φ, Ψ and $\arg(A)$. They may be solved numerically. Though, for some particular

background stratification profiles and horizontal mean-flow winds these integrals may have analytic solutions.

Consider a background with constant mean flow, such that

$$u_{f0} = U_f = \text{const. and } u_{f1} = 0, \tag{5.24}$$

and a stratification profile

$$N^2(\zeta) = N^2_{\min} + (N^2_{\max} - N^2_{\min}) \left(1 + \left(\frac{\zeta - \zeta_{\text{pos}}}{\Delta\zeta}\right)^2\right)^{-2} \tag{5.25}$$

which represents a bell function with a peak of $N^2_{\max}$ positioned at ζ_{pos} and width $\Delta\zeta$. For $\zeta \to \pm\infty$ it converges to $N^2_{\max}$. When we insert these assumptions into (5.15), we obtain

$$k_z(\zeta) = \pm K_x \frac{\sqrt{N^2_{\max} - N^2_{\min}}}{N_{\min}} \left(1 + \left(\frac{\zeta - \zeta_{\text{pos}}}{\Delta\zeta}\right)^2\right)^{-1}. \tag{5.26}$$

Here, we chose

$$C_x = N_{\min}/K_x + U_f. \tag{5.27}$$

It can be integrated by means of standard antiderivatives yielding

$$\Phi(\xi, \zeta) = K_x\xi \pm K_x\Delta\zeta \frac{\sqrt{N^2_{\max} - N^2_{\min}}}{N_{\min}} \arctan\left(\frac{\zeta - \zeta_{\text{pos}}}{\Delta\zeta}\right) \tag{5.28}$$

and

$$\Psi(\xi, \zeta) = K_x\xi \mp K_x\Delta\zeta \frac{|N_{\min}|}{\sqrt{N^2_{\max} - N^2_{\min}}} \left(\frac{\zeta - \zeta_{\text{pos}}}{\Delta\zeta} + \frac{1}{3}\left(\frac{\zeta - \zeta_{\text{pos}}}{\Delta\zeta}\right)^3\right). \tag{5.29}$$

The slow phase simply becomes $\arg(A) = L_\Psi\Psi$.

In conclusion, for this particular stratification we found an analytic traveling wave solution. It is plotted in Figure 5.1 for some choice of $O(1)$-parameters and G_0 a bell function. This traveling wave is characterized by spatial modulation of phase as well as amplitude which is completely controlled by the stratification (see Panel a). The structure is that of a locally confined wave packet. For $\Delta\zeta \to \infty$ the background tends to uniformity and the wave merges to a plane wave. As the wave travels to the right, an observer at position x_{obs} (see Panel b) would experience an upward propagating wave packet with downward traveling wave troughs and crests. As we decided for a constant mean-flow horizontal wind, there is no shear. So, there is no energy exchange between the wave and the mean flow.

If $C_x = 0$, the result resembles a stationary wave in the original (X, Z)-coordinates. Such a wave can be interpreted as a mountain lee wave. The orography then may fix the boundary condition for G_0.

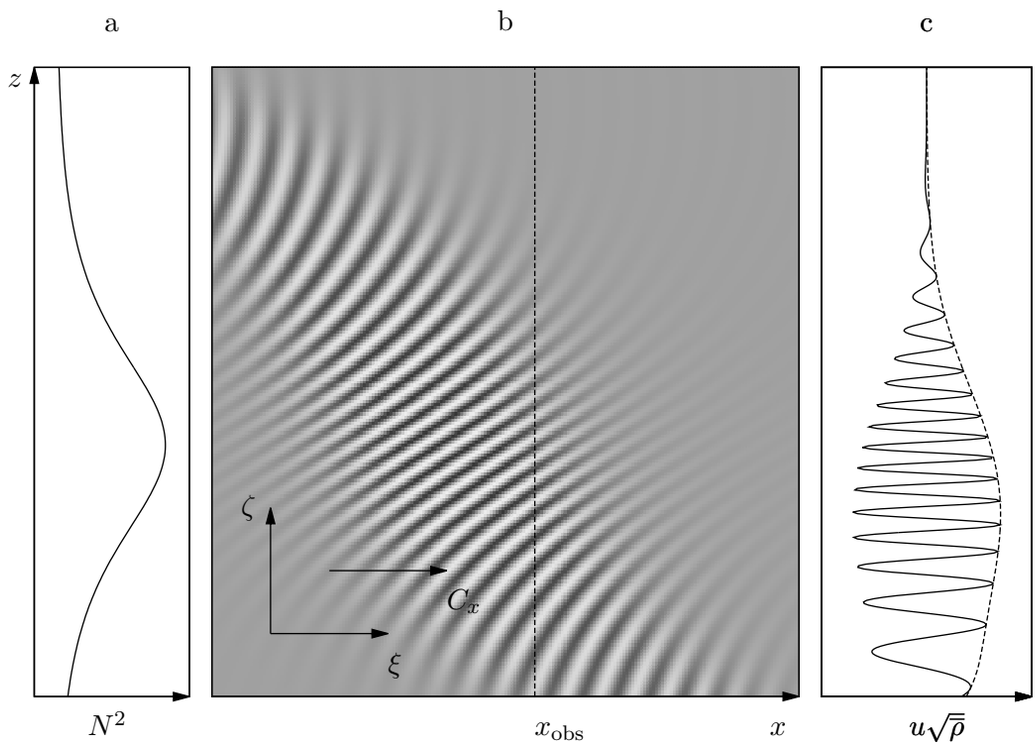

Figure 5.1: Illustration of the horizontally traveling wave solution without mean flow experiencing non-uniform stratification. (panel a) Squared Brunt-Väisälä frequency profile. (panel b) Horizontal wind component multiplied by the square root of the background density in the stationary coordinate system (x, z). Also, the translational coordinate system (ξ, ζ) that moves with the constant velocity C_x to the right. (panel c) Profile that one would observe at x_{obs}.

5.1.3 Analytic solution for a sheared mean flow

It is also possible to construct analytic traveling waves where $N = \text{const.}$, corresponding to an isothermal background, and $u_{f0}(\zeta)$ a prescribed profile. How this is achieved will be shown in this subsection. We may write

$$u_{f0}(\zeta) = U_f + \Lambda\zeta \tag{5.30}$$

as a linear function where U_f is again constant and Λ the mean-flow vertical shear rate. This choice is of particular interest because the wave-mean-flow energy exchange rate reduces to

$$q = K_x G \Lambda \tag{5.31}$$

according to (5.23) which implies that the exchange rate is proportional to the shear rate. As G depends solely on the characteristic function Ψ, so does q and if G has, say, compact support with respect to the characteristic, then the energy exchange between wave and mean flow can happen only on this support. The lower boundary conditions may determine the shape of G, the characteristic is defined by an analytic function containing some parameters as we will show next, and hence the wave-mean-flow interaction can be computed explicitly. This probably provides an interesting model to examine mountain lee waves and their impact on the mean-flow circulation where the boundary condition of G is given by the shape of the mountain.

For the sake of simplicity we choose again $u_{f1} = 0$. The vertical wave number from (5.15) becomes

$$k_z(\zeta) = \pm\sqrt{\frac{N^2}{(C_x - U_f - \Lambda\zeta)^2} - K_x^2}. \tag{5.32}$$

In order to integrate it with regard to (5.11) we substitute by

$$\chi(\zeta) = \frac{K_x}{N}(C_x - U_f - \Lambda\zeta) \tag{5.33}$$

such that

$$\mathrm{d}\zeta = -\frac{N}{K_x\Lambda}\mathrm{d}\chi. \tag{5.34}$$

The phase can be computed subsequently by standard antiderivatives resulting in

$$\Phi(\xi,\zeta) = K_x\xi - \frac{N}{K_x\Lambda}\left[\chi k_z(\chi) \mp \operatorname{arsech}(\chi)\right]_{\chi(0)}^{\chi(\zeta)} \tag{5.35}$$

with arsech denoting the inverse hyperbolic secant function. This integration necessitates that the constraint

$$1 > \chi^2(\zeta) \tag{5.36}$$

holds on the entire integration domain to prevent the critical layers (cf. Section 5.1). The characteristic function (5.19) is also given by standard antiderivatives as

$$\Psi(\xi,\zeta) = K_x\xi \mp \frac{N}{\Lambda}\left[\sqrt{1-\chi^2}\right]_{\chi(0)}^{\chi(\zeta)}. \tag{5.37}$$

The amplitude of the wave depends on the background density due to (5.17). Since we require that $N = \text{const.}$, the background atmosphere must be isothermal which can be readily seen by (2.14). Combining these two equations it follows that

$$\eta_\rho = -\kappa^{-1}N^2. \tag{5.38}$$

And hence by integrating

$$\overline{\rho}(\zeta) = \rho_0 e^{-\kappa^{-1}N^2\zeta} \tag{5.39}$$

exhibits an exponentially decaying background density profile. As the amplitude is proportional to the inverse of $\overline{\rho}$, it increases in turn exponentially with height. Large amplitudes give rise to nonlinear interaction with the mean flow and also to instabilities.

5.1.4 The plane wave

The plane wave is a particular solution for the horizontally traveling wave class. It occurs if the background is isothermal, such that N and η_ρ are constant. Also the mean-flow horizontal wind u_{f0} must not have a shear. In this environment, we see from (5.15) that the vertical wave number $k_z(\zeta) = K_z = \text{const.}$ becomes independent of altitude making it a plane wave. Also the characteristics Ψ would be straight lines perpendicular to the phase lines. If we additionally assume that the vertical wave action flux $G_0(\Psi) = G_{/\!/\!/}$ is as well just a number, then the wave extends to infinity and the amplitude grows with height due to (5.17). Such a wave would be indistinguishable from an upward propagating wave: let us consider the phase of the plane wave in the translational coordinate system Γ, so

$$\Phi = K_x\xi + K_z\zeta \tag{5.40}$$

transforming it into the stationary coordinate system according to (5.1), we may write it like

$$\Phi = K_xX + K_zZ - \mathbf{C}\cdot\mathbf{K}\ T. \tag{5.41}$$

So, the frequency is given by $\mathbf{C}\cdot\mathbf{K}$ which might have, by the nature of the scalar product, many realizations resulting in the same value. As we actually consider the C1 traveling wave where $C_z = 0$, we have

$$\mathbf{C}\cdot\mathbf{K} = C_xK_x. \tag{5.42}$$

But the same value could have been realized likewise by

$$\mathbf{C} \cdot \mathbf{K} = C_z K_z \tag{5.43}$$

by choosing C_z accordingly and $C_x = 0$ which would correspond to a vertically traveling wave solution. It is important to note that this works only for plane waves because one has to use the linearity of the phase function to get a scalar product. Another important aspect worth mentioning is that, if we consider the plane wave solution for the horizontally traveling wave class as an upward propagating wave, then this wave is not a traveling wave solution anymore in terms of our definition. Because the amplitude depends exponentially on height. In a translational coordinate system with $C_z \neq 0$ the height dependency would result in a time-dependency after the transformation. Therefore, the solution is not stationary in Γ anymore which is key in the traveling wave definition.

5.2 The isothermal, horizontally periodic traveling wave solution

This section examines Case C2, that is the isothermal traveling wave solution, where N^2 and η_ρ are constant. In this case a complete leading order solution of the scaled Euler equations cannot be achieved as we did not provide the explicit evolution equation for $\hat{u}_{1,0}$, which is mandatory to compute $\arg(A)$ in (5.6). This is because the argument in (5.13) does not hold here since $C_z \neq 0$. However, the remaining modulation equations are uncoupled, so they may possess some insightful solution.

Even though the 4th order polynomial in (5.12) has an analytic solution, its calculation does not provide any further enlightenment. We differentiate (5.4) instead wrt ζ, which avoids lengthy terms and gives us an evolution equation for the vertical wave number. Closure of the system as well as substantial simplification can be gained if we restrict ourselves to horizontally periodic traveling waves, such that the horizontal derivatives in the modulation equations drop out. Thus, we may rewrite the modulation equations like

$$(\partial_\tau - C_z\partial_\zeta)k_z + \partial_\zeta(\hat{\omega}(k_z) + K_x\hat{u}_{0,0}) = 0, \tag{5.44}$$

$$(\partial_\tau - C_z\partial_\zeta)a + (\partial_\zeta + \eta_\rho)(\hat{\omega}'(k_z)a) = 0, \tag{5.45}$$

$$(\partial_\tau - C_z\partial_\zeta)\hat{u}_{0,0} = -K_x(\partial_\zeta + \eta_\rho)(\hat{\omega}'(k_z)a). \tag{5.46}$$

Since K_x and N are now constant, we handle the intrinsic frequency as a function of k_z only, so

$$\hat{\omega}(k_z) = \pm\frac{NK_x}{\sqrt{K_x^2 + k_z^2}}. \tag{5.47}$$

The prime indicates the derivative wrt k_z, such that $\hat{\omega}' = c_{gz}$.

This system has been studied numerically by Rieper, Achatz, et al. (2013). A similiar system has been investigated by Dosser and Sutherland (2011b). If we combine (5.45) with (5.46) and integrate, we obtain

$$\hat{u}_{0,0} = K_x a + u_0 \tag{5.48}$$

with $u_0 = u_0(\zeta + C_z\tau)$ some yet undetermined function. Injecting into (5.44), so

$$\partial_\tau k_z + \partial_\zeta\big(\hat{\omega}(k_z) - C_z k_z + K_x^2 a + K_x u_0\big) = 0, \tag{5.49}$$

$$\partial_\tau a + \partial_\zeta\left[(\hat{\omega}'(k_z) - C_z)a\right] = -\eta_\rho \hat{\omega}'(k_z)a, \tag{5.50}$$

reduces the number of equations. As we seek for stationary solutions in the translational reference frame, we drop the time derivatives and set $u_0(\zeta + C_z\tau) = \text{const.}$ to get rid off its $\tau-$dependency. By that we can integrate (5.49) and solve for

$$a = \frac{\hat{\omega} - C_z k_z}{-K_x^2} + a_0. \tag{5.51}$$

The constant a_0 absorbed u_0. Hereinafter, we handle a as function of k_z. Inserting it into (5.50) yields a one-dimensional, nonlinear, autonomous ODE for k_z. After some basic manipulation it can be written as

$$\partial_\zeta k_z = f(k_z) \text{ with } f(k_z) = \frac{2\eta_\rho}{K_x^2}\,\frac{\hat{\omega}'(k_z)a(k_z)}{a^{2\prime\prime}(k_z)}. \tag{5.52}$$

Since the ODE is autonomous, one can separate the variables and integrate. But this approach is not fruitful due to the fact that the inverse of the nonlinear f does not feature an analytical antiderivative. We want to choose a more illuminating approach. The ODE has equilibrium solutions if the numerator of f vanishes, which happens either for $\hat{\omega}'(k_z^-) = 0$ or for $a(k_z^+) = 0$. By definition (3.35) it turns out that $k_z^- = 0$. Instead of solving (5.51) for k_z^+, which means again finding the root of a quartic function, we can use it to fix its constant

$$a_0 = \frac{\hat{\omega}(k_z^+) - C_z k_z^+}{K_x^2}. \tag{5.53}$$

Both equilibria seem uninteresting at first glance: for k_z^+ the amplitude vanishes and for k_z^- there is no oscillation in the vertical, such that wave vector is purely horizontal. But maybe some solution exists connecting both equilibria asymptotically which can then be considered as asymptotic rest states, such that

$$\lim_{|\zeta|\to\infty} k_z = k_z^\pm. \tag{5.54}$$

Such a solution may be called traveling wave front as $a \to 0$ for $\zeta \to +\infty$. The other way around, if $a \to 0$ for $\zeta \to -\infty$, we may call it traveling wave back (cf. Sandstede 2002).

5.2.1 The traveling wave front

Consider, without loss of generality, $k_z^+ < 0$ and an initial condition $k_z(0) = k_z^0 \in I = (k_z^+, k_z^-)$. We want to settle two questions: first, for which initial condition and set of parameters does a solution exist? And second, to which of the two asymptotic rest states does the solution converge? That is to determine the sign of f of (5.52). As we seek for upward propagating wave packets, we shall set $\mathrm{sgn}(\hat{\omega}) = +1$, such that $\hat{\omega}' > 0$ on I. To guarantee that $|A| \in \mathbb{R}^+$, we must constrain $a > 0$ on I. In particular, we require $a(k_z^-) = a_- > 0$ which we can use to settle

$$C_z = \frac{\hat{\omega}(k_z^+) - N - K_x^2 a_-}{k_z^+}. \tag{5.55}$$

It emerges that $C_z > 0$, because we can estimate $\hat{\omega}(k_z^+) < N$ for all $k_z^+ < 0$. Under the previous assumptions, our wave always propagates upwards. Note that by (2.14) and $\eta_T = 0$ (isothermal background), we get

$$\eta_\rho = -\kappa^{-1} N^2. \tag{5.56}$$

So, the numerator of f is negative on I. In order to obtain the sign of the denominator, we must consider

$$\frac{a^{2\prime\prime}(k_z)}{2} = a'^2(k_z) + a(k_z)a''(k_z) \tag{5.57}$$

where

$$a'(k_z) = \frac{\hat{\omega}'(k_z) - C_z}{-K_x^2} \text{ and } a''(k_z) = \frac{\hat{\omega}''(k_z)}{-K_x^2}. \tag{5.58}$$

If we evaluate (5.57) at $k_z^- = 0$, we find that

$$\frac{a^{2\prime\prime}(k_z^-)}{2} = \frac{C_z^2}{K_x^4} + \frac{a_- N}{K_x^4} > 0. \tag{5.59}$$

As the denominator must not assume a root, a cannot have a saddle point on I. Neither is a allowed to exhibit a local maximum, because $a^{2\prime\prime}$ would switch sign and would particularly assume a root as it is continuous. The continuity of a also prohibits a local minimum, since it would imply a local maximum which we already ruled out. In conclusion, a must not have any critical points which yields the restriction $a' > 0$ on I, i.e. a is strictly increasing. This is fulfilled regarding (5.58) if $\hat{\omega}' < C_z$ on I. It turns out that

$$\underset{k_z \in (k_z^+, 0)}{\arg\max}\, \hat{\omega}'(k_z) = \max\left(k_z^+, -\frac{K_x}{\sqrt{2}}\right). \tag{5.60}$$

This gives us a critical relative velocity for the existence of bounded traveling waves

$$C_z^{\mathrm{crit}}(k_z^+) = \begin{cases} \hat{\omega}'(-K_x/\sqrt{2}), & \text{if } k_z^+ < -K_x/\sqrt{2} \\ \hat{\omega}'(k_z^+), & \text{if } -K_x/\sqrt{2} \le k_z^+ < 0 \end{cases} \tag{5.61}$$

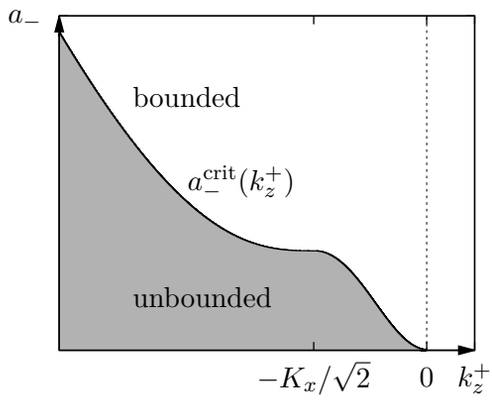

Figure 5.2: Critical asymptotic specific wave action density.

where

$$\hat{\omega}'(-K_x/\sqrt{2}) = \frac{2}{3\sqrt{3}}\frac{N}{K_x}. \tag{5.62}$$

Demanding $C_z > C_z^{\mathrm{crit}}(k_z^+)$ generates by (5.55) a lower bound on

$$a_- > a_-^{\mathrm{crit}}(k_z^+) = \frac{\hat{\omega}(k_z^+) - k_z^+ C_z^{\mathrm{crit}}(k_z^+) - N}{K_x^2}. \tag{5.63}$$

The critical asymptotic specific wave action density a_-^{crit} is illustrated in Figure 5.2. Given that the previous constraints hold: by continuity $a^{2''}$ is positive on I and the sign of f is therefore negative. This means, for any $k_z^0 \in I$ the solution converges to the asymptotic rest state k_z^+ as $\zeta \to +\infty$. Vice versa, for $\zeta \to -\infty$ the solution tends to $k_z^- = 0$. So, as long as for some k_z^+ we choose a_-, such that it is in the white zone in Figure 5.2, the solution converges. As soon as $a_- < a_-^{\mathrm{crit}}$ (grey zone), the solution will run into a singularity and grow without bounds.

We want to point out that C_z is also the vertical component of the phase velocity. Multiplying by k_z gives us the frequency in the stationary coordinate system. We may interpret (5.61) in terms of a critical frequency for a traveling wave solution. In particular, for a lower boundary condition, that is an initial condition in the stationary system, this leads to a minimal frequency for the existence of traveling wave solutions.

The ODE (5.52) can be solved with the explicit Euler method. For some $O(1)$-parameters, that fulfill the requirements, a particular solution is plotted in Figure 5.3.

Panel a shows the directly computed solution of the vertical wavenumber k_z, Panel b has the specific wave action density a derived from (5.51), and Panel c the leading order horizontal wind

$$u_* = \hat{u}_{0,0} + (\hat{u}_{0,1} e^{i\Phi\varepsilon^{-1}} + \mathrm{c.\,c.}), \tag{5.64}$$

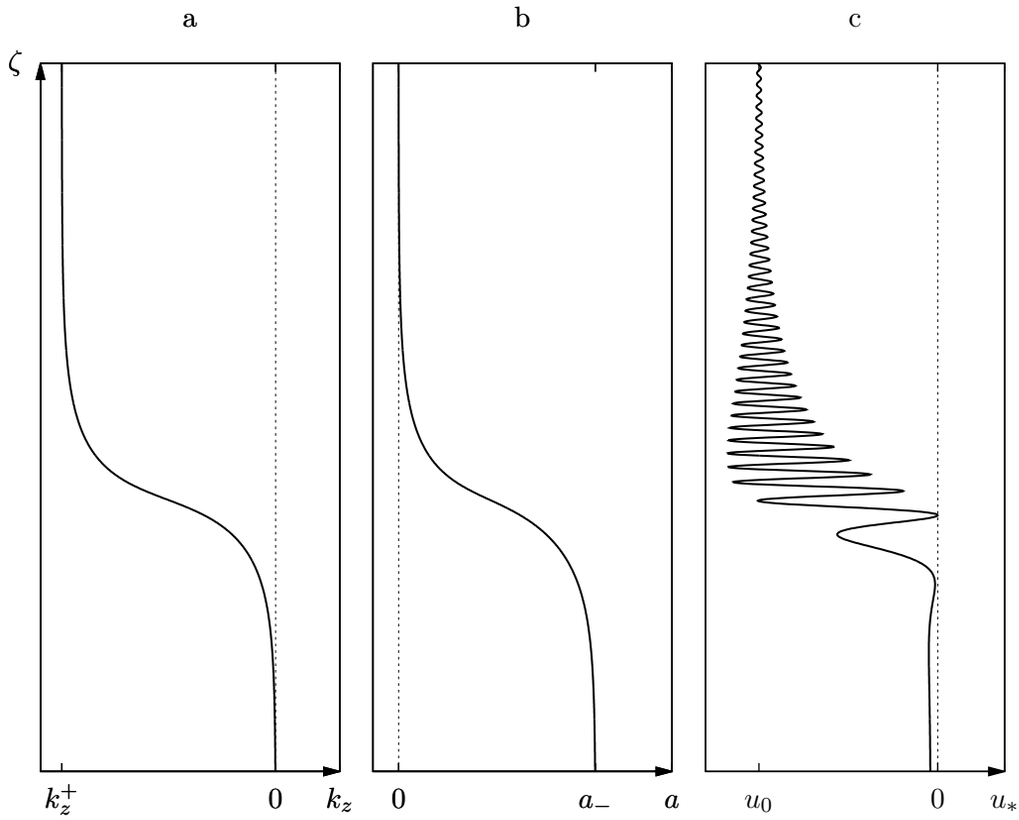

Figure 5.3: Illustration of the isothermal, horizontally periodic traveling wave computed by the explicit Euler method. Panel a: vertical wave number. Panel b: specific wave action density. Panel c: horizontal wind.

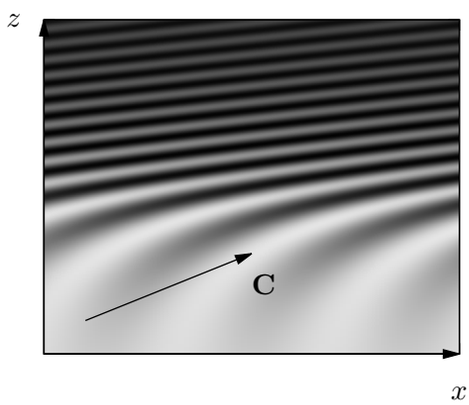

Figure 5.4: Horizontal wind u_* of the isothermal, horizontally periodic traveling wave solution.

which is also shown in Figure 5.4 from a two-dimensional perspective. We chose $u_0 = -K_x a_-$ for (5.48). To compute Φ from (5.11), we applied the very same Euler method. To compute $\hat{u}_{0,1}$ according to (3.28), we set $\arg(A) = \text{const.}$ because we lack an equation for it. The error produced by this oversimplification occurs in the wake of the front when k_z tends to zero, such that the slow phase $\arg(A)$ becomes vertically dominant and maybe produces some long wavelength vertical oscillation. From the two-dimensional point of view, the leading term in Φ is then still $K_x\xi$. However, this will not change the overall picture as the induced mean flow regarding (5.48) is not affected by the slow phase. Again this traveling wave solution is characterized by spatial modulation of amplitude as well as phase.

5.2.2 Wave-mean-flow interaction of the traveling wave front

The specific wave action density and therefore the amplitude remain constant in the wake of the front. So at first glance, it seems like the traveling wave induces wave energy into the mean flow. This conclusion would be logical because one would usually expect increasing amplitude with height due to the thinning air when the wave propagates upwards and due to the fact that the wave energy scales with the background density. This "extra" energy should then accelerate the mean flow. But this interpretation turns out to be incorrect, which becomes clear if we compute the wave-mean-flow energy exchange rate from Chapter 4 in the stationary coordinate system,

$$q = K_x^2 \overline{\rho} a(k_z) \hat{\omega}'(k_z) a'(k_z) \partial_Z k_z < 0. \tag{5.65}$$

Here, we used (5.48) and the estimates from this section. We can already conclude that energy is exchanged directly in the front where the gradient is located. The rate is always negative. On the contrary, the wave gains energy from the mean flow and the mean-flow horizontal wind decelerates.

This surprising behavior dissolves if we also consider the wave energy flux from (4.1). It tells us that the wave energy is transported with the group velocity $\hat{\omega}'$. But the front moves with C_z which is always greater than $\hat{\omega}'$ as we suppressed any critical points for a.

In summary, the fast traveling wave front only sustains if it obtains energy from the mean flow. It thereby violates the non-acceleration theorem as presented in Section 4.4: although the wave front is horizontal periodic and exhibits a finite extent, it accelerates the mean flow irreversibly without dissipating.

5.2.3 The traveling wave back

We will demonstrate in this subsection that backs as solutions to (5.52) cannot exist, regardless whether it propagates up- or downwards. A back is a solution that connects both asymptotic rest states $\lim_{\zeta \to \pm\infty} k_z(\zeta) = k_z^{\pm}$ such that $k_z^+ = 0$ and $a(k_z^-) = 0$, i.e. the opposite of the frontal solution in the previous subsection as $a_+ \neq 0$. A back would indeed pose an interesting solution because it might

correspond to a pulse with regard to the wave action density $\mathcal{A} = \overline{\rho}a$. Therefore, we consider it worthwhile investigating the isothermal, horizontally periodic traveling wave back. Firstly, we want to clarify why a back relates to a pulse of wave action density. A pulse (definition: see e.g. Sandstede 2002) satisfies

$$0 = \lim_{\zeta \to \pm\infty} \mathcal{A}(\zeta) = \lim_{\zeta \to \pm\infty} \overline{\rho}(Z)a(\zeta) = \rho_0 e^{C_z \tau} \lim_{\zeta \to \pm\infty} \frac{a(\zeta)}{e^{-\eta_\rho \zeta}} \tag{5.66}$$

for every $\tau < \infty$, so it converges for both limits towards the same rest state namely zero. For the limit $\zeta \to +\infty$ the denominator in the last step of the equation sequence tends to infinity and $a \to a_+$, so the whole fraction tends readily to zero. In the other case $\zeta \to -\infty$ the limit $a \to 0$ does not suffice as the denominator also approaches zero. However, we can use the rule of L'Hopital,

$$\lim_{\zeta \to -\infty} \frac{a(\zeta)}{e^{-\eta_\rho \zeta}} = \lim_{\zeta \to -\infty} \frac{\partial_\zeta a}{(-\eta_\rho) e^{-\eta_\rho \zeta}}. \tag{5.67}$$

We can identify

$$\partial_\zeta a = a'(k_z) \partial_\zeta k_z = a'(k_z) f(k_z). \tag{5.68}$$

By definition we know that $f(k_z) \to f(k_z^-) = 0$ as $\zeta \to -\infty$ which gives us a keen hint that the claim might be true. But one still has to show that $a'(k_z)f(k_z)$ converges faster to zero than the denominator of (5.67) to prove the convergence of the whole fraction. This task remains unresolved in this work. Its outcome however becomes pointless as soon as we can show that backs cannot exist anyway.

Pretending that the aforementioned claim is true a back with respect to the "specific" wave action density would relate to a pulse with respect to the "usual" wave action density. Since the wave-energy density from (4.1) can be written in terms of the wave action density as $\widetilde{E} = \mathcal{A}\hat{\omega}$, such a pulse would represent a locally confined wave packet possessing a finite wave energy. This property makes the back worthwhile investigating, in particular.

In order to show that backs are indeed impossible as solutions for the modulation equations, we consider the vertical wave number at minus infinity k_z^- which is either positive or negative. Let us assume traveling wave backs exist: if on the one hand for example $k_z^- < 0$, we must have $f(k_z) > 0$ on $I = (k_z^-, 0)$, to ensure that $k_z \to 0$ as $\zeta \to +\infty$. If on the other hand $k_z^- > 0$, we must claim the exact opposite.

To investigate the sign, we may rewrite the right hand side of the ODE (5.52) as

$$f(k_z) = -\eta_\rho \frac{2}{a^{2\prime\prime}(k_z)} \frac{\hat{\omega}(k_z)a(k_z)}{K_x^2 k^2} k_z \tag{5.69}$$

when we substitute $\hat{\omega}'(k_z) = -\hat{\omega}(k_z)k_z/k^2$. Where k denotes the Euclidean norm of the vector $\mathbf{k}$. The denominator of (5.69) is always positive as

$$\frac{a^{2\prime\prime}(k_z^-)}{2} = \left(a'(k_z^-)\right)^2 > 0, \tag{5.70}$$

which we obtain from (5.57), and due to the fact that the denominator cannot assume a root on I because otherwise the solution diverges. When we take a closer look onto the nominator of f, we find that $\hat{\omega}a = 2|A|^2 > 0$ by definition and $-\eta_\rho > 0$. So, the sign of f depends solely on k_z itself. If $k_z < 0$, it turns out that $f(k_z) < 0$ and vice versa. But this contradicts the demands for the existence of traveling wave backs. The result is independent of the vertical relative translational velocity C_z. So, neither up- nor downward traveling wave backs can solve the modulation equations despite their potentially interesting qualities. On the other hand we have just shown: if there is a solution connecting both asymptotic rest states, then it must be a front.

5.2.4 The isothermal traveling wave with sheared mean-flow wind

For the derivation of the traveling wave front we faced the same issue as before in Chapter 5 when we discussed, for which instances traveling wave solutions to the modulation equations can exist in general. We were challenged by the appearance of Z-dependencies in the coefficients of the PDE's. Transforming them into the translational coordinate system resulted consequently in a time dependency, due to $Z = \zeta + C_z\tau$. This makes intuitively sense as an observer now moves relatively to the varying background at rest. For the traveling wave front we encountered this problem for the integration constant u_0 of the mean flow from (5.48). As it gave us an extra degree of freedom, we readily set it constant. However, there is another approach providing traveling wave solutions,

$$u_0(\zeta + C_z\tau) = u_0(Z) = U_f + \Lambda Z = U_f + \Lambda(\zeta + C_z\tau) \tag{5.71}$$

incorporating a linear Z-dependency with the constant shear rate Λ (cf. Section 5.1.3). This ansatz indeed allows for traveling wave solutions, because u_0 occurs only in (5.49) inside the derivative. If we perform the derivative with respect to ζ on the mean flow, then we obtain the constant $K_x\Lambda$ that simply adds a source term on the right hand side. The resulting ODE is also autonomous. But it cannot be simplified to a single autonomous ODE like (5.52) which generated the traveling wave front. A two dimensional ODE complicates the solution but may give rise to up- and downward traveling pulse, front, and back solutions (cf. Section 5.2.3). This interesting problem remains an open question, here.

5.2.5 The plane wave revisited

The isothermal traveling wave solution class possesses plane waves as a particular solution when $C_z = 0$. The plane wave is adjoined from the frontal solution class, because if the vertical relative translational velocity vanishes, we can allow u_0 from (5.48) to depend on altitude as $Z = \zeta$. Choosing u_0 such that $\hat{u}_{0,0} = 0$ we can construct an exact solution of the modulation equations like

$$k_z = K_z = \text{const. and } a = \mathcal{A}_{/\!/\!/}\overline{\rho}^{-1}(\zeta) \text{ with } \mathcal{A}_{/\!/\!/} = \text{const.}. \tag{5.72}$$

This plane wave is exactly the same as the one we considered in Section 5.1.4 where we derived plane waves as solutions to the horizontally traveling wave case. So, the plane wave solution is an element of both traveling wave solution classes and thereby provides a link connecting them.

6 Numerical validation of the traveling wave solutions

In the previous chapters we found that traveling wave solutions for the modulation equations and consequently for the scaled Euler equations appear in two cases. For the first case (C1), when the atmosphere is non-uniformly stratified, we were able to derive analytic solutions for the modulation equations. These traveling wave solutions can only travel in the horizontal direction. They solve the scaled Euler equations asymptotically. For the second case (C2) we managed to show existence and the structure of traveling wave fronts that are horizontally periodic in an isothermal atmosphere. These waves travel horizontally and vertically. In this and the following chapters we want to test the consistency of these solutions. The analytic traveling wave solutions of the C1-case will be validated numerically, so we can check the range of validity as the traveling wave solutions could be unstable intrinsically or only sustain for very small, even unrealistic ε. For this purpose, we will use a conservative solver of the Euler equations in the following section. The C2-case will be analyzed with respect to stability in Section 8.1.2 where we investigate the stability of the modulation equations and compare with findings from Boussinesq theory. General stability analysis of the scaled Euler will be examined in Section 8.2.

6.1 The conservative solver of the Euler equations

As a reference we will use the Pseudo-Incompressible Flow Solver with Implicit Turbulence (pincFloit) model, presented by Rieper, Achatz, et al. (2013), as solver for the Euler equations. This finite-volume flow solver conserves energy, momentum as well as mass and suits therefore the purpose well. It is sound-proof and hence allows for larger time steps as dictated by the speed of sound due to the Courant-Friedrichs-Lewy (CFL) criterion. Within the framework of the model it is possible to simulate with almost unconstrained background stratifications apart from the uniform, isothermal atmosphere. The fidelity of the model was tested against standard cases. Rieper, Hickel, et al. (2013) applied pincFloit to check the range of validity of the extended WKB theory for gravity waves of Achatz et al. (2010) which is the basis for our traveling wave solutions. Recently, Bölöni et al. (2016) and Muraschko et al. (2015) derived a numerical solver for the modulation equations based on a Lagrangian ray-tracing approach for horizontally homogeneous GW packets that was also tested with the aid of pincFloit. It discretizes the governing equations on an equidistant staggered C-grid. From the alternative schemes, that

the model provides, it proved practical to apply the third order, low storage Runge-Kutta time stepping scheme, which is total variation diminishing. This is combined with the monotonic upstream-centered scheme for conservation laws (MUSCL) for spatial discretization and a monotonized central flux limiter. As the name of the model implies, it is capable of solving the compressible Navier-Stokes equations. But since this survey is only interested in the Euler equations, any diffusion or dissipation are switched off.

6.2 Experimantal setup

The objective is to simulate the analytic solutions of the C1 traveling wave solutions with non-uniform stratification as given by the equations (5.25)-(5.29). These traveling wave solutions have no compact support. Inevitably, the wave will touch the boundary of the computational domain. In order to prevent reflection we prescribe the analytic solution on the boundary cells for all times. We choose a particularly challenging test case such that the background stratification and the amplitude varies like $O(1)$ on the whole domain. The mean-flow horizontal wind is chosen in a way that the horizontal translational, relative velocity C_x vanishes, so

$$U_f = -N_{\min}/K_x. \tag{6.1}$$

By this choice the traveling wave is stationary in the fix coordinate system, such that $(\xi, \zeta) = (X, Z)$, which makes it convenient to compare the initial condition with the final state. The wave amplitude is set to be of the same order as the mean flow to provoke nonlinear coupling. So, the setup can be viewed as a wave that wants inherently to migrate to the right with a constant horizontal group velocity but faces an opposing wind of the exact same velocity. If the model manages to balance these tendencies the outcome stands at rest.

l_x/km	l_z/km	$N_{\min}$	$N_{\max}$	$\Delta\zeta$	K_x	L_Ψ	$\Delta\Psi$	$G_{\max}$	$\operatorname{sgn}(k_z)$
60	60	0.5	1.5	0.7	1.5	-0.3	1.0	3×10^{-5}	-1

Table 6.1: Parameters that are the same for all experiments. $G_{\max}$ seems very small at first glance but to compute the amplitude it scaled with the density.

The parameters that define the traveling wave and the background universally for all upcoming experiments are presented in Table 6.1. Here, l_x and l_z are the dimensionful domain size. The initial wave action flux is given by another bell shaped function

$$G(X, Z) = G_{\max}\left(1 + \left(\frac{\Psi(X, Z) - \Psi(X_{\text{pos}}, Z_{\text{pos}})}{\Delta\Psi}\right)^4\right)^{-2} \tag{6.2}$$

where $G_{\max}$ is the maximum flux at the peak.

To prescribe the stratification in the model, we have to provide the background density, Exner pressure, and potential temperature. The latter can be computed by means of standard antiderivatives from (5.25)

$$\begin{aligned}\overline{\theta}(Z) &= \exp\left(\int_0^Z N^2(Z)\mathrm{d}Z'\right)\\ &= \exp\left(N_{\min}^2 Z' + \frac{\Delta Z}{2}(N_{\max}^2 - N_{\min}^2)\left[\frac{\chi}{1+\chi^2} + \arctan\chi\right]_{\chi(0)}^{\chi(Z)}\right).\end{aligned} \tag{6.3}$$

For the integration we applied the substitution $\chi(Z) = (Z - Z_{\text{pos}})/\Delta Z$ such that $\mathrm{d}Z = \Delta Z \mathrm{d}\chi$. We set $Z_0 = 0$ which is the model bottom. The background Exner pressure is defined through the hydrostatic equation (2.9),

$$\partial_Z \overline{\pi} = -\frac{1}{\overline{\theta}}, \tag{6.4}$$

which we must integrate numerically. This is achieved by a simple Euler forward scheme with very high resolution. It looks costly at first glance but it only needs to be computed once at start. The integration constant is chosen to be $\overline{\pi}(0) = 1$. The background density is obtained directly from the equation of state (2.10) as

$$\overline{\rho} = \frac{\overline{\pi}^{\frac{1-\kappa}{\kappa}}}{\overline{\theta}}. \tag{6.5}$$

Instead of the total density the model evolves its deviation from the background. The setup was tested with zero vertical wind, a vertically sheared horizontal wind having a maximum of 140 ms^{-1}, and zero density deviation as initial conditions. The background was determined as given by Table 6.1. By a choice of $\varepsilon = 0.1$ the Brunt-Väisälä frequency varies on the whole domain from $N_{\min}$ to $N_{\max}$, such that the difference is already $O(1)$. If the boundary conditions and the background are implemented correctly, this initial condition is stationary.

Any numerical errors are measured by the weighted norms of the numerically simulated field (num) minus the expected (true) field. Hereinafter, we consider the horizontal wind field as we did not find any significant differences from the other fields in terms of errors. We define the weighted error norms as

$$\begin{aligned} l_1 &= \frac{I(|u^*_{\text{true}} - u^*_{\text{num}}|)}{I(|u^*_{\text{true}}|)},\\ l_2 &= \left(\frac{I(|u^*_{\text{true}} - u^*_{\text{num}}|^2)}{I(|u^*_{\text{true}}|^2)}\right)^{1/2},\\ l_\infty &= \frac{\max_{x^*,z^*}(|u^*_{\text{true}} - u^*_{\text{num}}|)}{\max_{x^*,z^*}(|u^*_{\text{true}}|)}\end{aligned} \tag{6.6}$$

where I denotes the numerical approximation to the integral

$$I(u) \approx \int_0^{l_x}\int_0^{l_z} u(x^*, z^*)\mathrm{d}z^*\mathrm{d}x^*. \tag{6.7}$$

The numerical quadrature exploits the trapezoidal rule.

For the simple first test case, even after a simulation time of $100 \times t_{\text{ref}}$ there was no detectable error. The error norms were all zero to machine accuracy.

6.3 Experiments with varying scale separation parameter

To test the consistency of the C1 traveling wave solutions, the scale separation parameter ε is altered whereas all other parameters, as given in Table 6.1 determining the properties of the traveling wave solution, are kept constant. The analytical asymptotic solution in non-dimensional form can be written as

$$U_{\text{true}} = \hat{U}_{0,0} + \left(\hat{U}_{0,1} e^{i\varepsilon^{-1}\Phi} + \text{c. c.}\right) + O(\varepsilon) \tag{6.8}$$

for $\varepsilon \to 0$ and (X, Z, T) fixed. We call the solution consistent if we can reproduce the analytical order of convergence of $M = 1$ numerically for a broad range of ε. In Chapter 2 by scaling assumption 3 we defined

$$\varepsilon = \frac{L_{\text{ref}}}{H_\theta}. \tag{6.9}$$

So, to alter ε there are two obvious choices: either one varies the dominant wavelength L_{ref} and keeps the potential temperature scale height H_θ fixed or one varies H_θ, which can be interpreted as altering the reference temperature T_{ref}, and keeps L_{ref} fixed. It is, of course, also possible to change both at once but we will argue subsequently that one choice is superior to the others.

If we decrease L_{ref} so does ε but the wavelength also reduces. This alters the number of grid cells per wavelength. Consequently, if we change the resolution accordingly, we can not distinguish effects on the error by change in resolution from those of changing ε. Proceeding all the experiments with the highest resolution necessary for the smallest ε emerged, after some test runs, to be computationally needlessly expensive. On the other hand, if we keep L_{ref} constant and alter H_θ exclusively, the number of grid cells per wavelength does not change. However, as t_{ref} is defined through the inverse of the reference Brunt-Väisälä frequency (see Chapter 2 scaling assumption 4), which in turn can be written according to (2.5) as $N^2_{\text{ref}} = g/H_\theta$, the number of time steps per wave period changes. So, in line with the model setup we would need to adapt the Courant-Friedrichs-Lewy (CFL) number. For stationary solutions though this does not have much of an effect and therefore the choice of varying ε by varying H_θ is superior. We set $L_{\text{ref}} = 3.053\,\text{km}$ fixed and link correspondingly to (6.9) $H_\theta = L_{\text{ref}}/\varepsilon$. We chose a resolution of 256×512 grid cells, which corresponds to approximately 18 grid cells per wave period which is a reasonable value to resolve all important features.

As we vary ε we must constrain that $T = \varepsilon t = O(1)$, which fulfills a necessity of the asymptotic ansatz, and hence the overall simulation time must change like

$$t^*_{\text{end}} = O\left(\frac{t_{\text{ref}}}{\varepsilon}\right) = O\left(\varepsilon^{-2/3}\right) \quad \text{since} \quad t_{\text{ref}} = \sqrt{H_\theta/g} = O(\varepsilon^{-1/2}). \tag{6.10}$$

Table 6.2 presents the parameters defining each experiment. In particular, the simulation time t^*_{end} is shown in the rightmost column. The potential temperature scale height varies from roughly 17 to 46 km throughout the simulations which gives us a considerable range for the scale separation.

Experiment	Parameters					
	n_x	n_z	L_{ref}/km	H_θ/km	ε	t^*_{end}/s
1.01	256	512	3.053	45.57	0.067	1204
1.02	256	512	3.053	37.23	0.082	889
1.03	256	512	3.053	30.53	0.100	660
1.04	256	512	3.053	25.03	0.122	490
1.05	256	512	3.053	20.35	0.150	360
1.06	256	512	3.053	16.59	0.184	264

Table 6.2: Parameters for experiments with varying ε.

The simulation results of the Experiments 1.01 to 1.05 are plotted in Figure 6.1. The stratification, dimensionful total horizontal wind, and its relative deviation from the analytic solution, i.e. $u^*_{\text{true}} - u^*_{\text{num}}$, are depicted. For smallest $\varepsilon = 0.067$ (top row) the stratification is moderate and the amplitude envelope, which is given by the wave action flux G, is also rather broad in width. The horizontal wind oscillates around a mean flow of about $12\,\text{ms}^{-1}$ with an amplitude of $3\,\text{ms}^{-1}$. The lines of constant phase are nearly straight, so are the characteristic lines Ψ, which define the shape of the envelope. With even smaller ε the wave will get closer to the uniform stratified regime with infinitesimal amplitude which can be captured by the Boussinesq theory. The relative error after the simulation is as expected very small, much less then 1 % at the peaks. Remarkably, the error is almost perfectly in phase with the initial wave at least in the middle of the domain. This means that errors are not generated by non-stationary effects. The wave does not move at all, the peaks are slightly smeared out, probably, by some numerical dissipation. By increasing ε, the width of the stratification peak narrows and also the envelope confines. The mean-flow horizontal wind gets stronger and we can expect nonlinear effects. For $\varepsilon = 0.1$ (third row) the mean flow approaches $15\,\text{ms}^{-1}$ and the horizontal wind varies with $\pm 10\,\text{ms}^{-1}$ which produces some substantial shear. In this case, we observe clearly some error sources at the upper boundary. These are numerical errors. As we prescribe the expected analytic solution at the boundaries, even small deviations of the numerical solution in the domain can cause discontinuities directly on the boundary. These shocks than propagate into the domain which can be seen in the case of $\varepsilon = 0.122$ (fourth row). For even higher ε, nonlinear effects start to dominate the error production. In the experiment where $\varepsilon = 0.15$ (fifth row), the mean flow is about $18\,\text{ms}^{-1}$ and the horizontal wind oscillates from 0 to -40 ms^{-1} which is not included in the color scale of Figure 6.1 anymore. Here, we find some quadrupole structure in the relative error field that indicates phase shifts by some

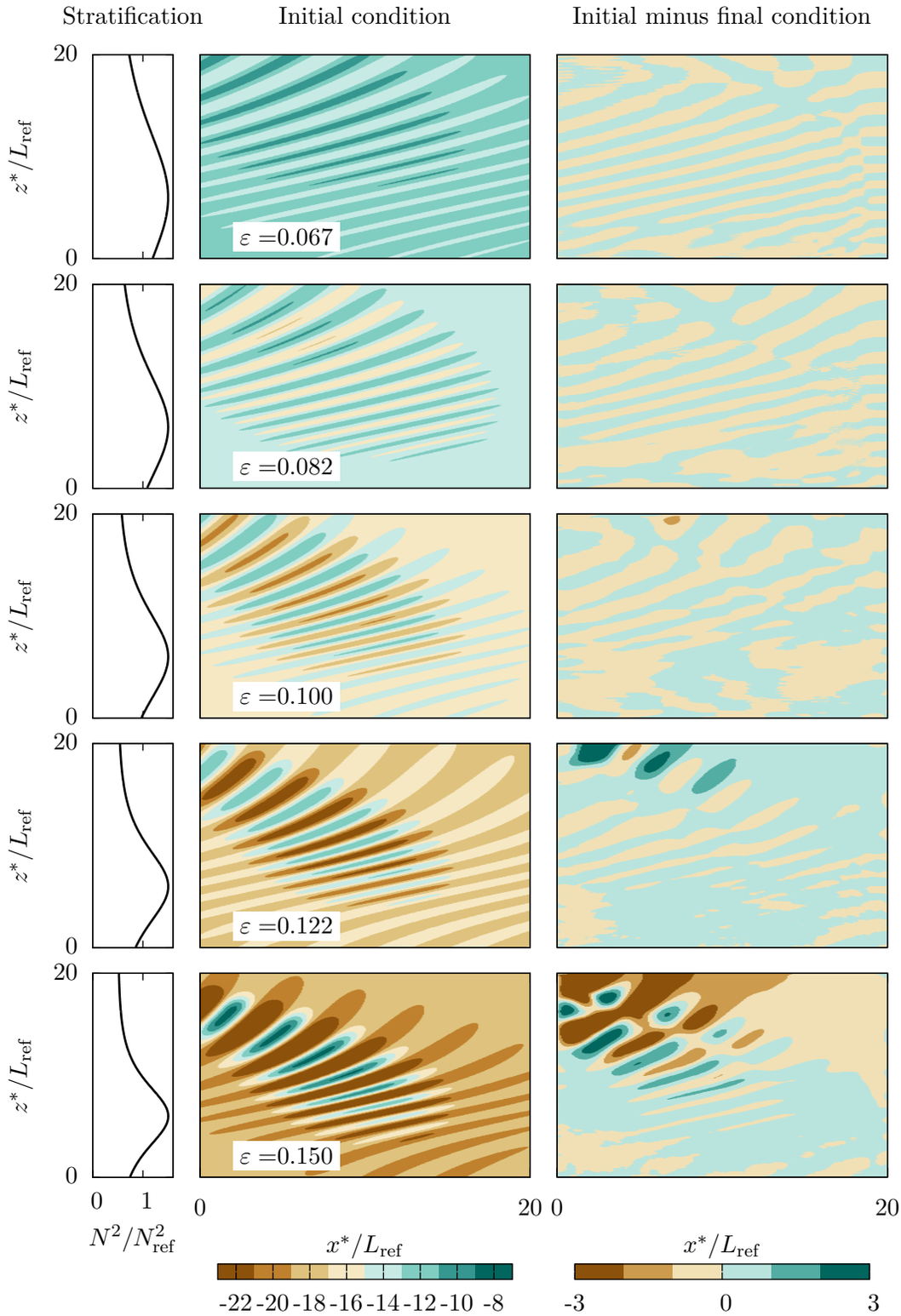

Figure 6.1: Numerical validation of the traveling waves for various ε. (left column) local squared Brunt-Väisälä frequency. (middle) Initial total horizontal wind u^*_{true} in ms^{-1}. (right) Error after simulation time t^*_{end}.

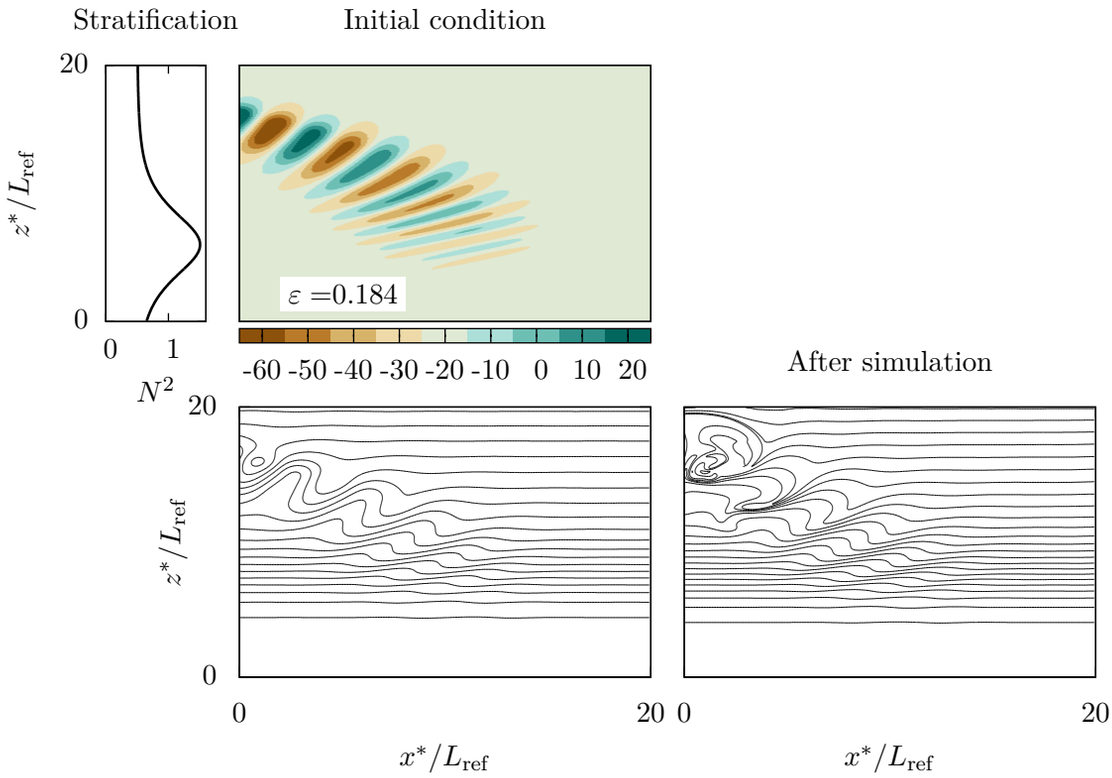

Figure 6.2: (top row) Same as in Figure 6.1 for Experiment 1.06. (bottom left) Isolines of the initial total potential temperature $\theta = \overline{\theta} + \theta'$. (bottom right) same after t^*_{end}. At the beginning this traveling wave is statically unstable as the isolines overturn.

instability process which may be triggered by the boundary discontinuities. The local error exceeds $3\,\text{ms}^{-1}$ at some points.

In Figure 6.2 the traveling wave for $\varepsilon = 0.184$ is shown separately. Note that the color scheme is adjusted to visualize its highly confined envelope and strong peaks as the mean flow is about $22\,\text{ms}^{-1}$ and the horizontal wind alternates with almost $\pm 50\,\text{ms}^{-1}$. The width of the wave packet at higher altitudes is already smaller than on wavelength L_{ref}. This wave is excluded from the further analysis since it is intrinsically unstable. Its unstable nature can be observed in the bottom row of Figure 6.2 where the isolines of the total potential temperature are shown. It can be seen clearly the initial condition has negative vertical slopes which makes it statically unstable. The static stability of our traveling waves will be discussed in detail in Section 8.1.

For Experiment 1 we computed the error norms according to (6.6). The results are shown in Figure 6.3 where we plotted the error norms against ε on a log-log scale. A least square fit gives us the analytical order of convergence M assuming

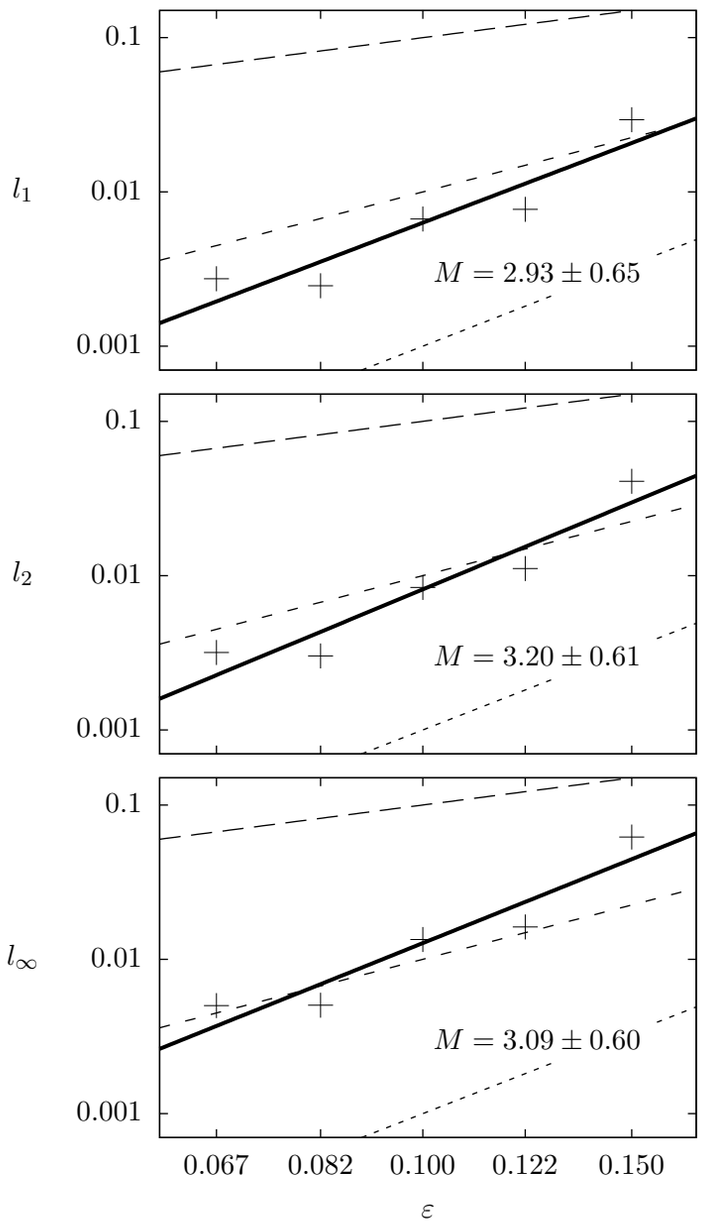

Figure 6.3: Convergence of the error norms with regard to ε for Experiment 2. (solid line) Linear regression on a log-log scale applying the least square method reveals an analytical order of convergence M and its standard deviation. (long dashed) first order, (medium dashed) second order, and (short dashed) third order lines.

that the error norms converge like

$$l_n = C\varepsilon^M \text{ for } n = 1, 2, \infty. \tag{6.11}$$

We also computed its standard deviation which are depicted aside the fitted lines. For all three norms we obtain convergence like $O(\varepsilon^3)$. Even after subtracting the rounded error margin of 1 from the order, this is apparently still included in the expected $O(\varepsilon)$-convergence with a comfortable cushion. For larger ε the model probably overestimates the norms due to the numerical errors at the boundaries propagating into the domain and triggering instabilities. We tested the influence of this effect by changing the integration domain of the norms like

$$I(u) \approx \int_{\delta}^{l_x-\delta} \int_{\delta}^{l_z-\delta} u(x^*, z^*) \mathrm{d}z^* \mathrm{d}x^* \tag{6.12}$$

and δ some positive fixed number. So, we focus on a smaller box and ignore cells that are potentially influenced by the boundaries. For some values of δ we recalculated the error norms for every ε. There was no significant effect on the order of convergence. So either (i) the hypothesis of boundary discontinuities propagating into the domain causing instabilities is wrong or (ii) they already contaminate the whole domain after the simulation time as they propagate faster than expected or (iii) instabilities are excited by other processes. This remains an open question. However, for small ε the norms are presumably also overrated as the amplitudes become so small that nonlinear coupling between the wave and the mean flow becomes inefficient and numerical damping takes over.

In conclusion, the horizontally traveling wave solution (C1) can be considered consistent with regard to numerical simulations of the Euler equations as we tested for a significant range of ε with a numerically challenging set of parameters. We identified some error sources distorting our results, but the estimates of the order of convergence are solid against those considerations.

We can generalize the setup easily to also simulate non-stationary waves by making the boundaries time-dependent. With the aid of this enhancement we are also able to simulate the isothermal, horizontally periodic traveling wave fronts (C2). These simulations shall remain an open task.

However, the model setup proves feasible to simulate instabilities and breaking events as we have seen in Figure 6.2. This is quite remarkable as to the knowledge of the authors, there are no numerical simulations of breaking finite-amplitude gravity waves in a strong stratified atmosphere within the pseudo-incompressible framework available in the literature.

6.4 Experiments with varying resolution, a grid convergence study

We used numerical simulations of the Euler dynamics to test the consistency of our asymptotic traveling wave solutions in the previous section. They performed

very well and sustained for long periods with regard to the reference time. This nature of the traveling wave solutions motivates us to use them as a test case suite for numerical solvers. The pincFloit solver, e.g., is used by Bölöni et al. (2016) to validate a parametrization for finite-amplitude gravity waves in a slowly varying background which is designed for global circulation models. So, there is certainly a need for validating the solvers with respect to exactly those kind of waves.

In this section we will use the horizontally traveling wave solution with non-uniform stratification to conduct a grid convergence studies for the pincFloit model. As a reference wave we use the one from Experiment 1.03 of Section 6.3 where $\varepsilon = 0.1$. For the experiments we simulate the reference wave and vary the resolution according to Table 6.3. The CFL number is kept constant with a value of 0.5. So,

Experiment	Parameters						
	n_x	n_z	$\Delta t^*/s$	L_{ref}/km	H_θ/km	ε	$t^*_{\text{end}}/\text{s}$
2.01	128	256	2.00	3.053	30.53	0.100	660
2.02/1.03	256	512	1.00	3.053	30.53	0.100	660
2.03	512	1024	0.50	3.053	30.53	0.100	660
2.04	1024	2048	0.25	3.053	30.53	0.100	660

Table 6.3: Parameters for experiments with varying resolution.

the time steps are changed as well due to the constraint

$$\Delta t^* = \text{CFL} \min\left(\frac{\Delta x^*}{u^*_{\max}}, \frac{\Delta z^*}{w^*_{\max}}\right) \tag{6.13}$$

where Δx^* and Δz^* denote the horizontal and vertical grid spacing. The maximum winds on the domain $u^*_{\max}$ and $w^*_{\max}$ are determined by the initial condition.

We perform each experiment according to Table 6.3 and compute the errors against the high resolution reference case 2.04 possessing 1024×2048 grid cells which we now label as u^*_{true}. The weighted error norms are computed as given by (6.6) for each of the experiments 2.01 to 2.03. They are plotted in Figure 6.4 on a log-log scale against the resolution. The order of convergence of the numerical error is denoted by p. It can be computed in terms of the weighted error norms like

$$l_n = C(\Delta z^*)^p \propto n_z^{-p} \text{ for } n = 1, 2, \infty \tag{6.14}$$

if we apply a least square fit. The fitting lines are depicted in Figure 6.4 together with the calculated p and its standard deviation. We conclude that within the error margins the numerical error converges with an order of approximately 1 as the grid spacing tends to zero. This order is not quite expected as we use a Runge-Kutta time stepping scheme of order 3 in combination with the MUSCL scheme which has order 2. However, our result is in line with the findings of Rieper, Hickel, et al. (2013, p 868) who resolved the discrepancy: the model discretizes the pseudo-incompressible equations which include a divergence constraint. Since the pressure has no explicit

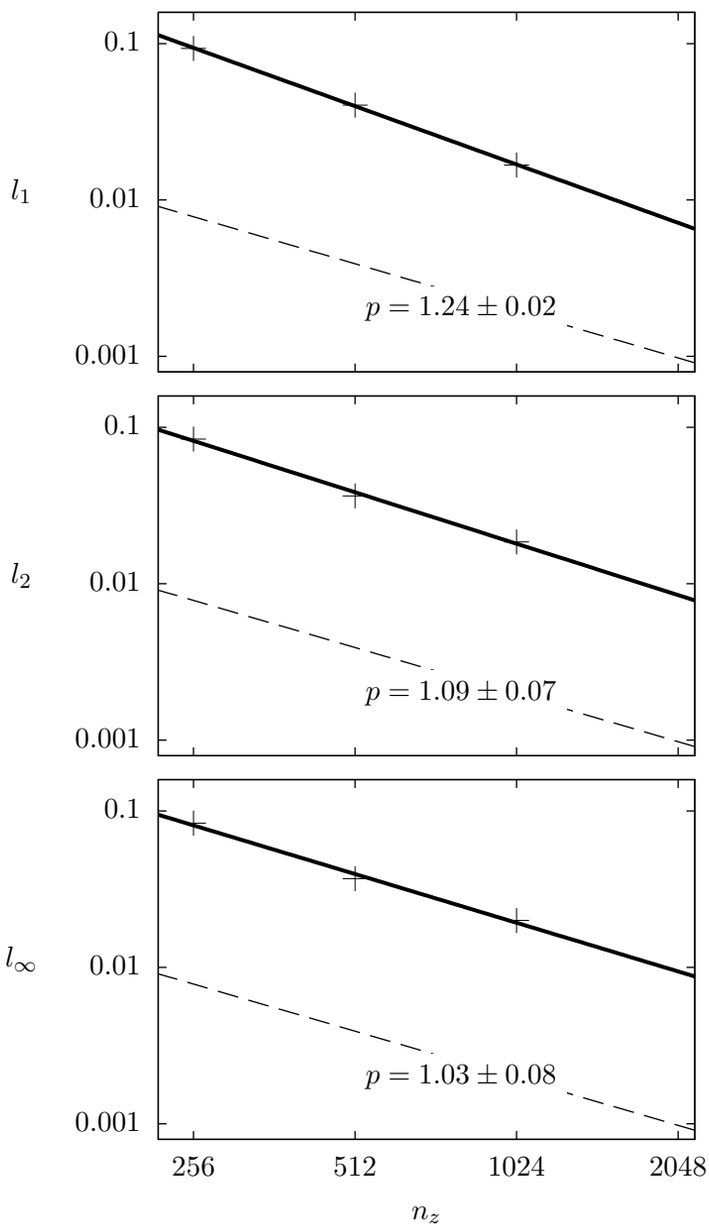

Figure 6.4: Grid convergence study. (solid line) Linear regression on a log-log scale applying the least square method reveals an numerical order of convergence p and its standard deviation. (dashed) First order line.

prognostic equation, the momentum equation is solved every time step with the pressure from the previous step. Next, the momentum and the pressure are corrected to match the divergence constraint. This correction is applied every Runge-Kutta step which deteriorates the convergence order of the overall numerical scheme. However, the authors also note that the method increases the rate of convergence C. They replaced in a numerical test case the Runge-Kutta scheme by a forward Euler and found that the rate of convergence was one order of magnitude smaller for the Euler scheme, so they concluded to favor the Runge-Kutta.

The numerical test case, the authors applied, was a simple one-dimensional wave packet in uniformly stratified background. We now generalized these tests with a much more complicated wave and background which provides a tool to check for many potential model limitations.

7 Existence of weak asymptotic solutions and the curvilinear coordinates

This chapter shall answer an open question on weak asymptotic solutions. We introduced this technique in Section 3.2 where we showed that the coefficients in the Fourier-like WKB-ansatz decouple with regard to their harmonics in the asymptotic expansion when one seeks for weak asymptotic solutions. In order to obtain the weak formulation of the original problem we postulated the existence of a mapping in terms of a coordinate transformation that allowed us to substitute the original slow Cartesian variables in the integral by the phase Φ of the wave and the according counterparts spanning a basis. The integral was inspired by the common method to average over the fast phase $\varepsilon^{-1}\Phi$ and using orthogonality of the harmonics which became problematic with regard to the asymptotic series expansion. The problem arose because our fast phase depends on space, time, and the asymptotic parameter. So, the orthogonality comes with a small error whose size, i.e. the asymptotic order, was unclear when applying the average. With the weak asymptotic scheme we were able to compute this error explicitly which provided an equation hierarchy that we then used to compute the modulation equations.

The open question, however, lies in the existence of the substitution. In Section 3.2 we claimed a mapping

$$F(X,Z,T) = \big(\Phi(X,Z,T), \Psi(X,Z,T), \tau(X,Z,T)\big) \tag{7.1}$$

to be bijective and differentiable. The objective of this chapter is now to give this mapping explicitly in terms of an orthogonal, curvilinear coordinate transformation. This shall close the loop about the weak asymptotic solutions and furthermore provides us with a tool that we will use in later chapters about stability of traveling wave solutions (see Chapter 8.2). For an introduction of the method used in the following derivations see e.g. Lebedev et al. (2010).

We observed already in Section 5.1 that the characteristic curves Ψ, that solved the wave action conservation law for horizontally traveling waves, are locally orthogonal on every line with constant phase Φ. This quality is also illustrated in Figure 5.1 where one can guess that the amplitude peak may follow a curve being orthogonal on the phase lines.

Inspired by this observation let us introduce a mapping $\Theta = (\Phi, \Psi)$ that projects

the translational (ξ, ζ)-coordinates onto

$$\Phi(\xi, \zeta) = K_x \xi + \int_{\zeta_0}^{\zeta} k_z(\zeta') \mathrm{d}\zeta', \tag{7.2}$$

$$\Psi(\xi, \zeta) = K_x \xi - \int_{\zeta_0}^{\zeta} \frac{K_x^2}{k_z(\zeta')} \mathrm{d}\zeta' \tag{7.3}$$

which are the solutions we found in (5.11) and (5.20). The integrals are well behaved, i.e. monotone and continuous, if $k_z \lesseqgtr 0$ on the domain.

This mapping is obviously differentiable. In order to show that the mapping is indeed a coordinate transformation, i.e. bijective, let us compute the Jacobian of Θ

$$\mathcal{J}_\Theta(\xi, \zeta) = \begin{pmatrix} \partial_\xi \Phi & \partial_\zeta \Phi \\ \partial_\xi \Psi & \partial_\zeta \Psi \end{pmatrix} = \begin{pmatrix} K_x & k_z(\zeta) \\ K_x & -K_x^2 / k_z(\zeta) \end{pmatrix}. \tag{7.4}$$

The Jacobian of the inverse transformation

$$\mathcal{J}_{\Theta^{-1}}(\Phi, \Psi) = \begin{pmatrix} \partial_\Phi \xi & \partial_\Psi \xi \\ \partial_\Phi \zeta & \partial_\Psi \zeta \end{pmatrix} \tag{7.5}$$

is unknown at this point, but it can be calculated if the inverse function theorem holds which requires that $\mathcal{J}_\Theta$ is invertible. If

$$\det(\mathcal{J}_\Theta) = -\frac{K_x k^2}{k_z} \neq 0, \tag{7.6}$$

the requirement is fulfilled which is true as long as $k_z(\zeta), K_x \neq 0$ on the domain. The constraint on k_z was already a prerequisite for the integrals in the definition of the mapping. In terms of this argument we have shown that the mapping is indeed bijective. In order to show that it is also locally orthogonal, we now compute the inverse of the Jacobian

$$\mathcal{J}_\Theta^{-1}(\xi, \zeta) = \frac{1}{k^2(\zeta)} \begin{pmatrix} K_x & k_z^2(\zeta)/K_x \\ k_z(\zeta) & -k_z(\zeta) \end{pmatrix}. \tag{7.7}$$

The inverse function theorem tells us that

$$\mathcal{J}_{\Theta^{-1}} = \mathcal{J}_\Theta^{-1} \tag{7.8}$$

which we apply to derive the (contravariant) unit vectors being defined by

$$\mathbf{e}_\Phi = \frac{\mathbf{h}_\Phi}{\|\mathbf{h}_\Phi\|} \quad \text{and} \quad \mathbf{e}_\Psi = \frac{\mathbf{h}_\Psi}{\|\mathbf{h}_\Psi\|} \tag{7.9}$$

where $\mathbf{h}_\Phi$ and $\mathbf{h}_\Psi$ denote the natural basis vectors. Their vector norms are called Lamé coefficients (Lebedev et al. 2010, p. 113). They are defined through the inverse Jacobian by

$$(\mathbf{h}_\Phi, \mathbf{h}_\Psi) = \mathcal{J}_{\Theta^{-1}} \tag{7.10}$$

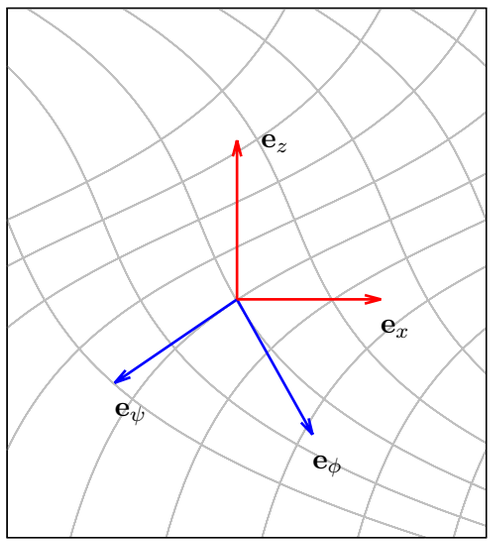

Figure 7.1: Illustration of the curvilinear coordinate system. The gray curves represent lines of constant phase Φ and characteristics Ψ originating from a non-plane wave, respectively. The red vector base spans the Cartesian space. The blue unit vectors indicate the locally orthogonal coordinates. Note that in the curved coordinates an observer experiences plane waves.

since the Jacobian exhibits the tangent vectors of the curves obtained by varying one coordinate and keeping the others fixed. If we use (7.8) and plug in the components of (7.7), we obtain the contravariant unit vectors through the Cartesian unit vectors

$$\mathbf{e}_\Phi = \frac{K_x}{k}\mathbf{e}_x + \frac{k_z}{k}\mathbf{e}_z, \tag{7.11}$$

$$\mathbf{e}_\Psi = \frac{k_z}{k}\mathbf{e}_x - \frac{K_x}{k}\mathbf{e}_z. \tag{7.12}$$

Computing the scalar product of these two,

$$\mathbf{e}_\Phi \cdot \mathbf{e}_\Psi = 0, \tag{7.13}$$

proves that the mapping is locally orthogonal and therefore a coordinate transformation in the desired sense. How this transformation looks like is illustrated in Figure 7.1 where we plotted the covariant, i.e. Cartesian, and the contravariant unit vectors.

With the aid of the previous considerations we can now deduce the substitution that was needed for the weak asymptotic scheme. Let us define

$$F(X, Z, T) = \Theta \circ \Gamma(X, Z, T) \tag{7.14}$$

where Γ is the translational coordinate transformation defined by (5.1) of Chapter 5 making F some coordinate transformation having the properties of being translational, orthogonal, and curvilinear. Since Γ is bijective, so is F. It therefore fulfills the requirements for the substitution in the weak asymptotic formulation of the governing equations: it was claimed to be differentiable and bijective.

As the solution for the phase (5.11) holds also for the isothermal traveling wave solution (C2), we can construct the curvilinear, translational transformation there as well. In conclusion, this discussion justifies the validity of the weak asymptotic scheme in hindsight.

8 Stability of the traveling wave solutions

In the following chapter we will examine the stability of the traveling wave solutions that we derived in the previous chapters.

The common static stability criterion (cf. Achatz 2007) is that the vertical gradient of total potential temperature, which corresponds to the squared total Brunt-Väisälä frequency, must not be negative. If at some point the gradient drops below zero, the total Brunt-Väisälä frequency becomes imaginary. Linear theory tells us that in this case exponentially growing modes of small perturbation can exist which leads to instability. This argument can be illustrated by the observation that dense air on top of light air produces a buoyant acceleration that causes small scale motion inducing turbulence. The gradient of the total potential temperature can be written in terms of the ansatz (2.8) as

$$\partial_z \theta = \partial_z(\overline{\theta} + \varepsilon\tilde{\theta}) = \varepsilon \partial_Z \overline{\theta} + \varepsilon \partial_z \tilde{\theta} \tag{8.1}$$

since the background only depends on the compressed coordinates. By definition (2.16) we have that $\tilde{\theta} = N\overline{\theta}B$. Inserting the WKB ansatz (3.1) and getting rid of Φ by assuming the worst case scenario, yield

$$\min_{\Phi\in(0,2\pi)} \partial_z \theta = \varepsilon \left(\partial_Z \overline{\theta} - 2N\overline{\theta} k_z |\hat{B}_{0,1}| \right) + O(\varepsilon^2). \tag{8.2}$$

With the aid of the polarization relation (3.27), this is positive to leading order if

$$2k_z|A| < N. \tag{8.3}$$

The same result differing only by the normalization factor of two was also obtained by Bölöni et al. (2016).

If we now insert the exact results of the horizontally traveling wave solution from Section 5.1, we find that this wave is stable as long as

$$2|k_z|k^2 \overline{\rho}^{-1} G_0 < N^2. \tag{8.4}$$

We want to test the analytic solution for the traveling wave solutions with non-uniform stratification and constant mean flow. In terms of the constant mean flow (5.24) and the chosen relative translational velocity (5.27), the inequality (8.4) becomes

$$\frac{2K_x^2}{N_{\min}^2} \sqrt{\frac{K_x^2 N^2}{N_{\min}^2} - K_x^2}\; G_0 < \overline{\rho}. \tag{8.5}$$

We can estimate $N \leq N_{\max}$ and $G_0 \leq G_{\max}$. So, the parameter for the analytic horizontally traveling wave solution with non-uniform stratification should be chosen such that

$$\frac{2K_x^3}{N_{\min}^2}\sqrt{\frac{N_{\max}^2}{N_{\min}^2}-1}\; G_{\max} < \overline{\rho} \text{ on the whole domain} \tag{8.6}$$

to ensure static stability. In our numerical simulations this threshold was meet for the case where $\varepsilon = 0.184$ (see Figure 6.2) at about $10\, L_{\text{ref}}$ in the vertical from the origin. This simulation already shows the limitations of this basic stability criterion since at the predicted level the wave stabilized whereas a strong instability, which leads to overturning, developed approximately one or two wavelength units above this point. Numerical dissipation may play a role in stabilizing the wave at the predicted breaking point. However, the discrepancy is so big that it cannot be explained by dissipation alone. The limitation of the criterion originates from the fact that linear theory was employed. It is derived from Boussinesq theory with uniform stratification. But since our traveling waves are nonlinear weak asymptotic solutions of the scaled Euler equations, the static stability argument can only provide a heuristic hint for the real instability level. Understanding the nature of the instability mechanism that lead to breaking of the nonlinear waves derived here shall motivate the following sections.

As we have got exact solutions to the modulation equations, it seems quite natural to start our analysis with regard to them. For this purpose we will introduce the notion of spectral stability in Section 8.1. We will demonstrate this technique with the help of the finite amplitude Boussinesq model with uniform stratification which possesses plane wave solutions. The result is the well known modulational stability criterion. We continue in Section 8.1.2 to investigate the spectral stability of the isothermal traveling wave front from Section 5.2.1. In Section 8.2 we will ask for stability of traveling wave solutions in general as asymptotic solutions to the governing, scaled Euler equations.

8.1 Stability of the modulation equations

This section is committed to the stability of traveling wave solutions against the modulation equations. For this purpose we will linerize the modulation equations in the translational coordinate system at the exact traveling wave solution. The linerized equations will give us an evolution equation for the perturbation. Since the traveling waves are stationary in the moving frame of reference, the evolution equation will be solved through an eigenvalue problem of a linear differential operator which may depend on space. The so-called temporal eigenvalues will determine the stability.

They lie in the spectrum of the linear operator which is the set of complex eigenvalues that fulfill the eigenvalue problem. The spectrum may contain isolated numbers in the complex plane (point spectrum) but it can also incorporate a

continuum of points (essential spectrum). Whether a point belongs to the essential or the point spectrum is closely related to the Fredholm properties of the operator which allows to characterize the operator by the difference of the dimension of the kernel minus the codimension of the range being called the Fredholm index.

If the spectrum has points on the right half of the complex plane, we call the traveling wave spectrally unstable. Note that spectral stability is a prerequisite for linear stability. So, if we find spectral instability, this implies then linear instability. An introduction to spectral stability is given by Kapitula and Promislow (2013). We will mostly follow Sandstede (2002).

We will first demonstrate this concept for finite-amplitude plane waves of the Boussinesq theory. The resulting differential operator does not depend on space, so that the spectrum can be calculated straightforwardly. The outcome is well known as we will reproduce the modulational stability of Whitham (1974) that was applied in the atmospheric context for Boussinesq waves by Grimshaw (1977) and Sutherland (2001).

We will then proceed to exploit the spectral stability technique to examine the isothermal traveling wave front from Section 5.2.1. Here, the linear operator will depend on space. But due to the frontal structure of the solution, we will be able to calculate the limit operator which will yield the borders of the essential spectrum, the Fredholm borders which are curves in the complex plane. The aforementioned Fredholm index will then help to clarify, whether the essential spectrum lies to the left or to the right of the Fredholm border with regard to its orientation.

8.1.1 Spectral stability of the Boussinesq plane wave

Let us introduce the concept of spectral stability for a common type of wave equations. We start our calculations with the modulation equations for two-dimensional, horizontally periodic gravity waves in a Boussinesq-type system. It accounts for a wave-mean-flow interaction and has uniform stratification. For the derivation of these equations see, e.g., Muraschko et al. (2013). We may give this coupled set of equations here in flux form

$$\partial_T k_z + \partial_Z\big(\hat{\omega}(k_z) + K_x \hat{u}_{0,0}\big) = 0, \tag{8.7}$$

$$\partial_T a + \partial_Z\big(\hat{\omega}'(k_z) a\big) = 0, \tag{8.8}$$

$$\partial_T \hat{u}_{0,0} + \partial_Z\big(K_x \hat{\omega}'(k_z) a\big) = 0. \tag{8.9}$$

All the variables have the same meaning as before. It is worth mentioning that in Muraschko et al. (2013) the equations are formulated in the wave action density $\mathcal{A} = \overline{\rho} a$ rather than the "specific" wave action density a. In the Boussinesq model the background density is constant, thus they differ only by a factor. The distinction to our modulation equations (5.44)-(5.46) lies in the missing source term on the right hand side. Which makes intuitively sense, because this term originated in our model from the background density. As the Boussinesq model does not account for the slowly varying background density, this term is neglected.

Equations (8.8) and (8.9) can be combined which yields

$$\partial_T(\hat{u}_{0,0} - K_x a) = 0. \tag{8.10}$$

This equation connects the pseudo-momentum $K_x a$ with the mean flow. It can be integrated, so we obtain

$$\hat{u}_{0,0}(Z,T) = K_x a(Z,T) + u_0(Z) \tag{8.11}$$

where the initial condition at $T = 0$ fixes $u_0(Z) = \hat{u}_{0,0}(Z,0) - K_x a(Z,0)$. Inserting this result into the original system reduces the number of equations.

$$\partial_T k_z + \partial_Z(\hat{\omega}(k_z) + K_x^2 a + K_x u_0(Z)) = 0, \tag{8.12}$$
$$\partial_T a + \partial_Z(\hat{\omega}'(k_z) a) = 0. \tag{8.13}$$

This system reads in vector form

$$\partial_T y + \partial_Z F(y;Z) = 0 \tag{8.14}$$

where $y = (k_z, a)^T$. The flux

$$F(y;Z) = \begin{pmatrix} \hat{\omega}(k_z) + K_x^2 a + K_x u_0(Z) \\ \hat{\omega}'(k_z) a \end{pmatrix} \tag{8.15}$$

depends explicitly on Z due to the mean flow. For the purpose of stability analysis, we seek for a traveling wave solution, so we transform the coordinates according to $\zeta = Z - C_z T$ and $\tau = T$ from (5.1) which yields

$$\partial_\tau y + \partial_\zeta\big(F(y;\zeta + C_z\tau) - C_z y\big) = 0. \tag{8.16}$$

The flux now depends explicitly on time due to $u_0(Z) = u_0(\zeta + C_z\tau)$ in the translational coordinate system. Traveling waves are defined to be stationary in this moving frame of reference. Thus, we drop the time derivative and restrict the initial condition $u_0 = \text{const.}$ to get rid of the time dependency in the flux. Any stationary solution then fulfills

$$\partial_\zeta\big(F(y) - C_z y\big) = 0. \tag{8.17}$$

This can be solved by any constant vector $Y = (K_z, a_{/\!/\!/})^T$. It resembles a plane wave possessing a constant envelope and a linear phase function. Linearization of (8.16) at Y yields

$$\partial_\tau y + \big(\mathcal{J}_F(Y) - C_z\,\mathrm{id}\big)\partial_\zeta y = 0 \tag{8.18}$$

where the Jacobian of the flux is found to be

$$\mathcal{J}_F(y) = \begin{pmatrix} \hat{\omega}'(k_z) & K_x^2 \\ a\hat{\omega}''(k_z) & \hat{\omega}'(k_z) \end{pmatrix}. \tag{8.19}$$

The spectral stability of the traveling wave Y is determined by the eigenvalue problem

$$\mathcal{L}_Y y = \lambda y \tag{8.20}$$

with the linear differential operator

$$\mathcal{L}_Y = -\big(\mathcal{J}_F(Y) - C_z \,\mathrm{id}\big)\partial_\zeta \tag{8.21}$$

generated by the ansatz

$$y(\zeta, \tau) = y(\zeta) e^{\lambda \tau}. \tag{8.22}$$

The spectrum of a linear operator is defined as

$$\mathrm{spec}(\mathcal{L}_Y) = \{\lambda \in \mathbb{C} \mid (\mathcal{L}_Y - \mathrm{id}\,\lambda) \text{ is not invertible}\}. \tag{8.23}$$

It can be separated into the essential and point spectrum, such that

$$\mathrm{spec}(\mathcal{L}_Y) = \mathrm{spec}_{\mathrm{ess}}(\mathcal{L}_Y) \cup \mathrm{spec}_{\mathrm{pt}}(\mathcal{L}_Y). \tag{8.24}$$

The wave is said to be spectrally stable if no $\lambda \in \mathrm{spec}(\mathcal{L}_Y)$ has positive real part and is unstable otherwise.

To solve the eigenvalue problem (8.20), it can be written as an ODE of the form

$$\partial_\zeta y = \mathcal{B}(\lambda) y \tag{8.25}$$

where

$$\mathcal{B}(\lambda) = -\big(\mathcal{J}_F(Y) - C_z \,\mathrm{id}\big)^{-1} \lambda \tag{8.26}$$

is a spatially constant matrix. The ODE has a general solution in terms of the Fourier transformation

$$y(\zeta) = \frac{1}{\sqrt{2\pi}} \int_{\mathbb{R}} \tilde{y}(\mu) e^{-i\mu\zeta} \mathrm{d}\mu \tag{8.27}$$

which translates the ODE into an algebraic equation

$$\big(\mathcal{B}(\lambda) + i\mu \,\mathrm{id}\big)\tilde{y} = 0. \tag{8.28}$$

It has non-trivial solutions only if

$$\det\big(\mathcal{B}(\lambda) + i\mu \,\mathrm{id}\big) = 0 \tag{8.29}$$

giving us the essential spectrum of the linear operator $\mathcal{L}_Y$,

$$\lambda = i\mu\big(\hat{\omega}'(K_z) - C_z \pm K_x \sqrt{a_{/\!/\!/} \hat{\omega}''(K_z)}\big) \text{ for } \mu \in \mathbb{R}. \tag{8.30}$$

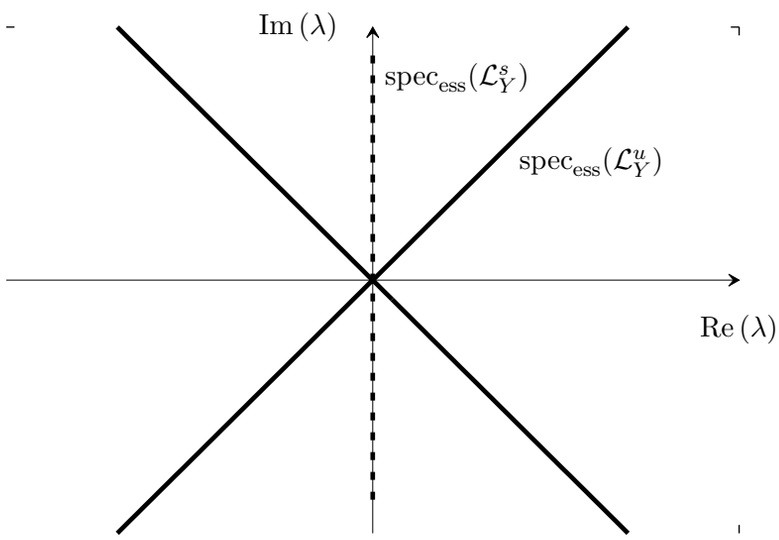

Figure 8.1: Essential spectra of the linear differential operator $\mathcal{L}_Y$ for plane Boussinesq waves. (dashed line) Stable essential spectrum where $a_{/\!/\!/}\hat{\omega}''(K_z) \geq 0$. (solid lines) The two branches of the unstable essential spectrum where $a_{/\!/\!/}\hat{\omega}''(K_z) < 0$.

The essential spectrum consists of straight lines in the complex plane parametrized by μ. Note that the spectrum has no isolated points and hence no point spectrum. We say the traveling plane wave is (essentially spectrally) stable if $\mathrm{Re}(\lambda) \leq 0$ for all $\mu \in \mathbb{R}$. Thus, we deduce from (8.30) that stability is only possible as long as

$$a_{/\!/\!/}\hat{\omega}''(K_z) \geq 0 \tag{8.31}$$

which is the well-known result for modulational stability (see Grimshaw 1977; Sutherland 2001; Whitham 1974). The spectrum of $\mathcal{L}_Y$ is depicted in Figure 8.1 for both the stable and the unstable case.

In the stable case, the essential spectrum $\mathrm{spec}_{\mathrm{ess}}(\mathcal{L}_Y^s)$ coincides with the imaginary axis. For an unstable setting we obtain two branches of $\mathrm{spec}_{\mathrm{ess}}(\mathcal{L}_Y^u)$ due to the non-uniqueness of the square root in (8.30). If $a_{/\!/\!/}\hat{\omega}''(K_z) < 0$, which occurs if

$$\sqrt{2}|K_z| < |K_x|, \tag{8.32}$$

then the growth rate of the instability is then given by

$$|\mathrm{Re}(\lambda)| = |\mu K_x|\sqrt{|a_{/\!/\!/}\hat{\omega}''(K_z)|}, \tag{8.33}$$

which increases linearly with μ. So, we can conclude that highest wave number perturbations, which corresponds to smallest wavelength, produce the highest instability growth rates.

8.1.2 Spectral stability of the isothermal traveling wave front

In the previous section we demonstrated spectral stability for the finite-amplitude gravity waves in the uniform Boussinesq theory. In this section we will apply the same techniques for the isothermal traveling wave front which we discovered in Section 5.2.1. The front is an exact solution to our modulation equations that we derived in Section 3.6 in the isothermal case C1. These modulation equations constitute a generalization to the Boussinesq model as they take the slowly changing background density into account. Let us rewrite them here in the translational moving frame of reference according to (5.49) and (5.50)

$$\partial_\tau k_z + \partial_\zeta(\hat{\omega}(k_z) - C_z k_z + K_x^2 a + K_x u_0) = 0, \tag{8.34}$$

$$\partial_\tau a + \partial_\zeta\left[(\hat{\omega}'(k_z) - C_z)a\right] = -\eta_\rho \hat{\omega}'(k_z)a. \tag{8.35}$$

Where again $u_0 = \mathrm{const.}$. For the following analysis we reformulate them in vector form resulting in

$$\partial_\tau y + \partial_\zeta(F(y) - C_z y) = G(y) \tag{8.36}$$

for the solution vector $y = (k_z, a)^T$. The flux F and an inhomogeneity G are given by

$$F(y) = \begin{pmatrix} \hat{\omega}(k_z) + K_x^2 a + K_x u_0 \\ \hat{\omega}'(k_z)a \end{pmatrix} \tag{8.37}$$

and

$$G(y) = \begin{pmatrix} 0 \\ -\eta_\rho \hat{\omega}'(k_z) a \end{pmatrix}, \tag{8.38}$$

respectively. These modulation equations differ from the uniform Boussinesq ones (8.12) and (8.13) by the inhomogeneity G which depends on η_ρ. Note that they do not equalize in the limit $\eta_\rho \to 0$ because due to the hydrostatic background we also have from (5.56)

$$\eta_\rho = -\kappa^{-1} N^2, \tag{8.39}$$

such that with vanishing η_ρ the intrinsic frequency $\hat{\omega}$, since it depends on N, would also disappear.

We have shown in Section 5.2.1 that the isothermal modulation equations posses a horizontally periodic, stationary solution $Y = Y(\zeta)$ with the property

$$\lim_{\zeta \to \pm\infty} Y(\zeta) = Y^{\pm}. \tag{8.40}$$

We found two asymptotic rest states at plus and minus infinity, $Y^- = (0, a^-)^T$ and $Y^+ = (k_z^+, 0)^T$ with $a^- > 0$ and $k_z^+ < 0$ that the solution connects via a front.

To assess the stability, let us study the evolution of an infinitesimal perturbation by linearizing (8.36) at Y, so

$$\partial_\tau y + \partial_\zeta \left[(\mathcal{J}_F(Y) - C_z \,\mathrm{id}) y \right] = \mathcal{J}_G(Y) y. \tag{8.41}$$

The Jacobians of the flux and the inhomogeneity are found to be

$$\mathcal{J}_F(y) = \begin{pmatrix} \hat{\omega}'(k_z) & K_x^2 \\ a\hat{\omega}''(k_z) & \hat{\omega}'(k_z) \end{pmatrix} \tag{8.42}$$

and

$$\mathcal{J}_G(y) = \begin{pmatrix} 0 & 0 \\ -\eta_\rho a \hat{\omega}''(k_z) & -\eta_\rho \hat{\omega}'(k_z) \end{pmatrix}. \tag{8.43}$$

The perturbation must be of the form

$$y(\zeta, \tau) = y(\zeta) e^{\lambda \tau} \tag{8.44}$$

which again yields an eigenvalue problem

$$\mathcal{L}_Y y = \lambda y \tag{8.45}$$

for a linear differential operator

$$\mathcal{L}_Y = \mathcal{J}_G(Y) - \partial_\zeta \mathcal{J}_F(Y) + (C_z \,\mathrm{id} - \mathcal{J}_F(Y)) \partial_\zeta. \tag{8.46}$$

The eigenvalue problem can be rewritten as a non-autonomous ODE of the form

$$\partial_\zeta y = \mathcal{B}(\zeta;\lambda)y \tag{8.47}$$

with the non-constant coefficient matrix

$$\mathcal{B}(\zeta;\lambda) = \big(C_z\,\mathrm{id} - \mathcal{J}_F(Y)\big)^{-1}\big(\lambda\,\mathrm{id} - \mathcal{J}_G(Y) + \partial_\zeta \mathcal{J}_F(Y)\big). \tag{8.48}$$

The inverse of the Jacobian of the flux exists if the traveling wave front fulfills the lower bound (5.63) on the asymptotic rest state at minus infinity

$$a_- > a_-^{\mathrm{crit}}(k_z^+) \tag{8.49}$$

that we derived in Section 5.2.1. Note that, in contrast to the previous section, the matrix $\mathcal{B}$ depends on ζ because, $Y = Y(\zeta)$, the traveling wave front varies spatially.

We cannot solve the ODE straightforwardly by a Fourier transformation due to the ζ-dependency. Still, it is feasible to compute the spectrum of $\mathcal{L}_Y$ analytically. For this purpose let us introduce the Fredholm properties. We call a closed linear operator $\mathcal{L}$ Fredholm if it has finite dimension of its kernel and finite codimension of its image (cf. Sandstede 2002). The Fredholm index is then defined by

$$\mathrm{ind}(\mathcal{L}) = \dim\ker(\mathcal{L}) - \mathrm{codim}\,\mathrm{img}(\mathcal{L}). \tag{8.50}$$

It is now possible to define the essential spectrum in terms of the Fredholm properties by

$$\mathrm{spec}_{\mathrm{ess}}(\mathcal{L}) = \{\lambda \in \mathbb{C} \,|\, (\mathcal{L} - \lambda\,\mathrm{id}) \text{ is } \textit{not} \text{ Fredholm with index } 0\}. \tag{8.51}$$

Let us now consider the asymptotic operator $\mathcal{L}_Y^\infty$ being defined through

$$\mathcal{L}_Y^\infty = \begin{cases} \mathcal{L}_{Y^-} & \text{if } \zeta < 0, \\ \mathcal{L}_{Y^+} & \text{if } \zeta > 0. \end{cases} \tag{8.52}$$

The original operator $\mathcal{L}_Y$ is considered to be a perturbation of the asymptotic operator. One can now show that well-behaved perturbations do not change the Fredholm properties of an operator (Kato 1995, Theorem 5.35).

In terms of this preparation we can compute the essential spectrum of the asymptotic operator. It is given by the ODEs that are generated by the asymptotic coefficient matrices

$$\mathcal{B}^\pm(\lambda) = \lim_{\zeta\to\pm\infty} \mathcal{B}(\zeta;\lambda). \tag{8.53}$$

We solve the two ODEs with constant coefficients for $\zeta < 0$ and $\zeta > 0$, respectively. The eigenvalues of $\mathcal{B}^\pm(\lambda)$ must satisfy

$$\det\big(\mathcal{B}^\pm(\lambda) + \nu^\pm\,\mathrm{id}\big) = 0. \tag{8.54}$$

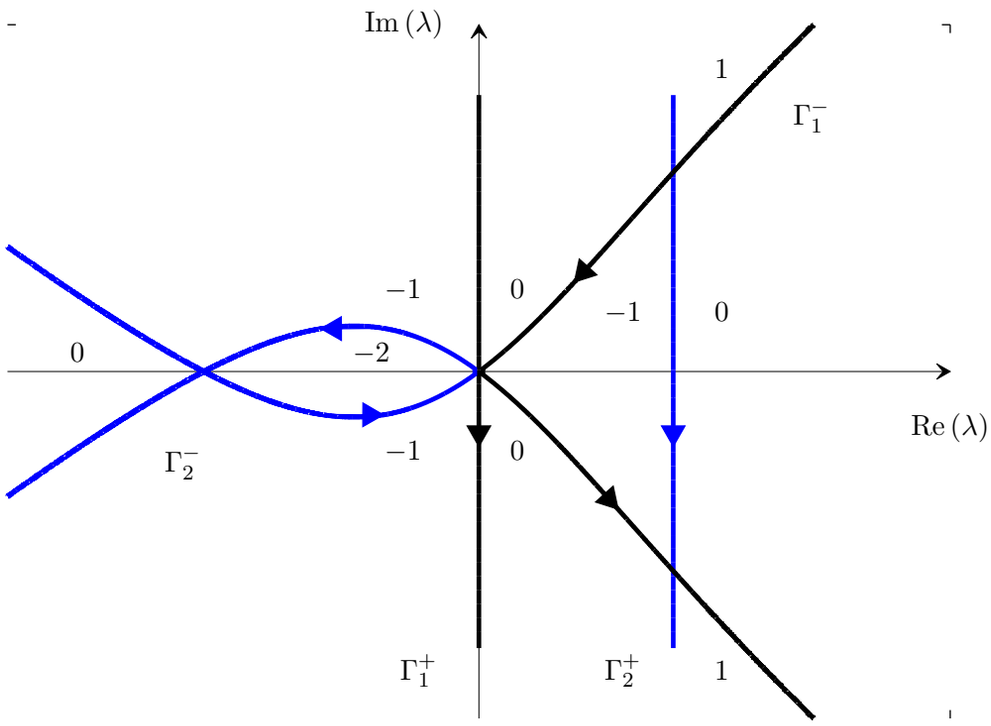

Figure 8.2: Operator spectrum for the linearized modulation equations at the isothermal traveling wave front. Curves in the complex plane are the Fredholm borders $\Gamma^{\pm}_{1,2}$ with their orientation given by the solid arrows. Fredholm indeces assigned to the regions which are enclosed by the Fredholm borders. Complex λ belongs to the spectrum if the Fredholm index is not zero.

The purely imaginary eigenvalues $\nu = i\mu$ with $\mu \in \mathbb{R}$ parametrize curves in the complex plane

$$\begin{aligned}
&\Gamma_1^+ : \mu \mapsto i\mu(\hat{\omega}'(k_z^+) - C_z),\\
&\Gamma_2^+ : \mu \mapsto i\mu(\hat{\omega}'(k_z^+) - C_z) - \eta_\rho \hat{\omega}'(k_z^+),\\
&\Gamma_1^- : \mu \mapsto -i\mu C_z + \sqrt{a_- N(i\eta_\rho \mu + \mu^2)},\\
&\Gamma_2^- : \mu \mapsto -i\mu C_z - \sqrt{a_- N(i\eta_\rho \mu + \mu^2)}.
\end{aligned} \tag{8.55}$$

These curves are called the Fredholm borders. They are plotted in the complex plane in Figure 8.2 for the same $O(1)$-parameters that we used to compute the traveling wave front for Figure 5.4. The union of the Fredholm borders gives us precisely the spectrum of the asymptotic operator $\mathcal{L}_Y^\infty$. If we consider $\mathcal{L}_Y$ as a well-behaved

perturbation of $\mathcal{L}_Y^\infty$, we can deduce the spectrum of the original operator $\mathcal{L}_Y$ because perturbations do not change the Fredholm properties. It is shown in Kapitula and Promislow (2013, Remark 3.1.15.) that the Fredholm index $\mathrm{ind}(\mathcal{L}_Y - \lambda\,\mathrm{id})$ changes by 1 if one moves in the complex plane crossing a Fredholm border. Precisely, the Fredholm index

(i) increases by 1 when crossing Γ^+ from right to left with regard to its orientation,

(ii) decreases by 1 when crossing Γ^- from right to left with regard to its orientation.

The orientation of a curve is given by the derivative with respect to its parametrization. For our Fredholm borders, the orientations are depicted by arrows on the curves in Figure 8.2. In terms of definition (8.51) we could compute the complete essential spectrum of $\mathcal{L}_Y$ if we only had one Fredholm index in some region being enclosed by the Fredholm borders. It is usually assumed that points with $\mathrm{Re}(\lambda) \gg 1$ must not be in the spectrum. If not, the wave is prone to high-frequency instabilities (Kapitula and Promislow 2013, p 52). So, we assume the Fredholm index to the right of Γ_2^+ shall be zero. The complete spectrum is now depicted in Figure 8.2 by the resulting Fredholm indeces. Due to (8.51) some λ belongs to the spectrum of $\mathcal{L}_Y$ if its Fredholm index is not 0.

Now, as we know the spectrum of the operator, we can analyze it with respect to instability which means to check for positve, real valued λ in the spectrum. We can already see in Figure 8.2 for this particular choice of parameters that the spectrum reaches far into the right half of the complex plane. And indeed we find from (8.55) that Γ_2^+ always has positive real part $-\eta_\rho \omega'(k_z^+)$ because $\eta_\rho < 0$ as the background density decreases always with height and $\omega'(k_z^+) > 0$ which is a prerequisite of the traveling wave front. Also, Γ_1^- is always encountered on the positive real side for any set of reasonable parameters which we can proof if we consider the square root in its definition (8.55). By the principal square root for complex numbers

$$\sqrt{z} = \sqrt{\frac{|z| + \mathrm{Re}(z)}{2}} \pm i\sqrt{\frac{|z| - \mathrm{Re}(z)}{2}}, \tag{8.56}$$

we find that $\mathrm{Re}\left(\sqrt{i\eta_\rho \mu + \mu^2}\right) \geq 0$ for all $\mu \in \mathbb{R}$.

We can therefore deduce that the traveling wave front is spectrally unstable against the modulation equations for every set of parameters defining the wave and the background. It also implies linear instability.

Let us give some final remarks on this section: An open question is, what would happen if we also allow the modulation equations to account for viscous damping. First of all, it is not obvious whether we would obtain frontal solutions again and second, if so, whether they can be stabilized by damping which is especially efficient in removing high-frequency instabilities. Experimental observations of atmospheric gravity waves show that they can propagate deep into the higher mesosphere where indeed viscosity plays a major role in the dynamics (Fritts et al. 2015). Taking this point of view, the choice to fix a first Fredholm index, by

assuming that $\mathrm{Re}(\lambda) \gg 1$ cannot belong to the spectrum, was somehow arbitrary. One could also argue the other way around. Since in the viscous limit one can expect high-frequency instabilities to get filtered out, one could equally assume that low-frequency instabilities shall not belong to the spectrum. However, the choice may alter the appearance of the spectrum but it cannot change the overall result that the waves are always unstable. This result, that it was feasible by spectral stability theory to show instability analytically, is remarkable. But as the modulation equations solve the scaled Euler equations asymptotically it remains fuzzy, how the physical manifestation of this instability looks like. Therefore, we will follow another approach in the next section where we will directly linearize the scaled Euler equations.

8.2 Stability of the scaled Euler equations

In the previous section we tested the isothermal traveling wave front with regard to stability against the modulation equations. This was convenient because the traveling wave front is an exact solution to them. When we linearized the modulation equations at the traveling wave, we obtained an eigenvalue problem for a linear differential operator depending only on the vertical translational coordinate. The spectrum of the operator told us when, i.e. for which initial, boundary, and background conditions, the wave becomes unstable. It is always unstable.

In this section we want to test the stability of not only a particular traveling wave solution but traveling waves in general against the governing equations which are the scaled Euler equations. As the traveling waves solve them asymptotically, we cannot expect to straightforwardly get an eigenvalue problem whose spectrum is the answer to stability. Since the scaled Euler equations pose a multiple scale problem, we would rather expect that after linearization, we still face multiple scales that need further assumptions on the nature of the perturbation to design an asymptotic solution.

Our approach how to investigate the stability of the traveling wave solutions against the scaled Euler equations is mainly inspired by the work of Lombard and Riley (1996). They examined the stability of gravity waves within the framework of Boussinesq theory. Their ansatz was based on studies of Mied (1976), Drazin (1977), and Klostermeyer (1991) who used the fact that finite amplitude plane waves solve the uniform, nonlinear Boussinesq equations exactly.

To simplify the system, Lombard and Riley (1996) introduced an orthogonal coordinate transformation composed of translation in combination with rotation in a fashion that the new coordinates follow the wave. The plane wave now solves the transformed Boussinesq equations, such that it is stationary in the translational, rotated frame of reference. It is furthermore periodic with respect to the phase following coordinate, whereas it is homogenous in the coordinate orthogonal to that.

After linearizing the transformed equations at the plane wave and inducing a normal mode ansatz for the perturbation, they obtained an ODE system in the phase

following coordinate. The coefficients of the ODE depended on two parameters, namely one temporal and one spatial eigenvalue, and in addition to that, the coefficients were periodic functions in the phase following coordinate.

This very fact enabled the authors to apply Floquet theory. The Floquet theorem states that ODEs of the aforementioned type have solutions that are of a specific form: the product of a periodic function having the same periodicity as the coefficients multiplied by a not necessarily periodic function (Floquet multiplier) possessing a certain parameter (Floquet exponent) that must be determined. A sound overview about Floquet theory and its application for stability problems is given by Kapitula and Promislow (2013). A first application of Floquet theory with regard to the stability of internal gravity waves was conducted by Mied (1976).

The periodic function part of the solution was expanded in a Fourier series which converted the ODE to an infinite algebraic problem whose solvability determines the three unknown parameters, that are the temporal, spatial eigenvalues and the Floquet exponent, respectively. The authors continued with a numerical parameter study to compute the temporal eigenvalue with highest positive real part by solving an optimization problem providing the fastest growing modes of an instability.

We also discovered a coordinate transformation (Chapter 7) which we used to justify the weak asymptotic ansatz. This translational, orthogonal, curvilinear transformation shall be used in the following sections to construct a simplified system in the same fashion as described above. After transforming the scaled Euler equations in Section 8.2.1, we will linearize them in Section 8.2.2 at the traveling wave solutions which will, as expected, result in a multiple scale problem. It is approximated asymptotically by a WKB approach in Section 8.2.3 that allows us subsequently to apply Floquet theory in Section 8.2.4. We will arrive at a system that can only be solved numerically, but similarities with studies about the stability of the Boussinesq model allows to apply known results in Section 8.2.5.

8.2.1 The scaled Euler equations with translational, curvilinear, orthogonal coordinates

In Chapter 7 we introduced a translational, curvilinear, orthogonal coordinate transformation that we derived from the horizontally traveling wave solutions (C1). But we also noted that it is equally applicable for the isothermal traveling waves (C2). In both cases, we found plane waves as particular solutions. A remarkable fact is that for those plane waves the curvilinear transformation becomes a rather simple rotation. This equivalence motivates us to explore the same path as Lombard and Riley (1996) who used a rotational, translational transformation but with our more general translational, curvilinear transformation.

Let us transform the scaled Euler equations into the coordinate system F of (7.1). For this purpose we need some more ingredients that we collect in the following. By the aid of the Lamé coefficients from (7.10), we can transform the slow nabla

operator, so

$$\nabla_\varepsilon = \frac{1}{\|\mathbf{h}_\Phi\|}\mathbf{e}_\Phi\partial_\Phi + \frac{1}{\|\mathbf{h}_\Psi\|}\mathbf{e}_\Psi\partial_\Psi = k\mathbf{e}_\Phi\partial_\Phi + \frac{K_x}{k_z}k\mathbf{e}_\Psi\partial_\Psi \tag{8.57}$$

according to Lebedev et al. (2010). The covariant vertical unit vector can be expressed in terms of the contravariant unit vectors like

$$\mathbf{e}_z = \frac{k_z}{k}\mathbf{e}_\Phi - \frac{K_x}{k}\mathbf{e}_\Psi. \tag{8.58}$$

Let us also introduce some fast independent variables that vary on the same scale as the original x, z-coordinates,

$$\varphi = \frac{\Phi}{\varepsilon} \quad \text{and} \quad \psi = \frac{\Psi}{\varepsilon}. \tag{8.59}$$

So, the original nabla operator therefore becomes

$$\nabla = k\mathbf{e}_\Phi\partial_\varphi + \frac{K_x}{k_z}k\mathbf{e}_\Psi\partial_\psi. \tag{8.60}$$

Providing the scaled Euler equations (2.15) in vector form, i.e.

$$\begin{aligned} D_t\mathbf{v} + \nabla P - NB\mathbf{e}_z &= \varepsilon N^2 P\mathbf{e}_z - \varepsilon NB\nabla P + \text{h. o. t.} \\ D_t B + N\mathbf{v}\cdot\mathbf{e}_z &= -\varepsilon(N^2+\eta_N)\mathbf{v}\cdot\mathbf{e}_z \\ \nabla\cdot\mathbf{v} &= -\varepsilon(N^2+\eta_\rho)\mathbf{v}\cdot\mathbf{e}_z + \text{h. o. t.} \end{aligned} \tag{8.61}$$

with

$$D_t = \partial_t + \mathbf{v}\cdot\nabla \tag{8.62}$$

we can now transform the vectors and differential operators using (7.11), (8.58), (8.59), and (8.60). The scaled Euler equations in the translational, curvilinear coordinates read

$$\begin{aligned} D_t\underline{u} + \frac{K_x}{k_z}k\partial_\psi P + \frac{K_x}{k}NB &= -\varepsilon\left(NB\frac{K_x}{k_z}k\partial_\psi P + \frac{K_x}{k}N^2P\right) + \text{h. o. t.} \\ D_t\underline{w} + k\partial_\varphi P - \frac{k_z}{k}NB &= -\varepsilon\left(NBk\partial_\varphi P - \frac{k_z}{k}N^2P\right) + \text{h. o. t.} \\ D_tB + N\left(\frac{k_z}{k}\underline{w} - \frac{K_x}{k}\underline{u}\right) &= -\varepsilon(N^2+\eta_N)B\left(\frac{k_z}{k}\underline{w} - \frac{K_x}{k}\underline{u}\right) \\ \frac{K_x}{k_z}k\partial_\psi\underline{u} + k\partial_\varphi\underline{w} &= -\varepsilon(N^2+\eta_\rho)\left(\frac{k_z}{k}\underline{w} - \frac{K_x}{k}\underline{u}\right) + \text{h. o. t.}. \end{aligned} \tag{8.63}$$

We abbreviate but do not ignore higher order terms with h. o. t.. They are not explicitly given here for the sake of readability as they do not occur in the later derivations. The material derivative transforms to

$$D_t = \partial_t + (\underline{u} - C_\Psi)\frac{K_x}{k_z}k\partial_\psi + (\underline{w} - C_\Phi)k\partial_\varphi \tag{8.64}$$

where

$$\begin{aligned} C_\Phi &= \mathbf{C}\cdot\mathbf{e}_\Phi = \frac{K_x}{k}C_x + \frac{k_z}{k}C_z \\ C_\Psi &= \mathbf{C}\cdot\mathbf{e}_\Psi = \frac{k_z}{k}C_x - \frac{K_x}{k}C_z, \end{aligned} \tag{8.65}$$

$$\begin{aligned} \underline{u} &= \mathbf{v}\cdot\mathbf{e}_\Psi \\ \underline{w} &= \mathbf{v}\cdot\mathbf{e}_\Phi \end{aligned} \tag{8.66}$$

are the relative velocity and the wind vector projected onto the contravariant unit vectors, respectively. Note that all the background coefficients in (8.63) not only depend on one, i.e. Z, but both the slow space variables Φ and Ψ, now.

8.2.2 Linearization of the scaled Euler equations in curvilinear translational coordinates

In order to compute the evolution of an infinitesimal perturbation, we linearize the scaled Euler equations in curved coordinates (8.63) at the traveling wave that we denote by U. The infinitesimal perturbation of U shall be $\widetilde{U}$. The resulting system can be written in terms of a linear differential operator $\mathcal{S}$ as

$$\mathcal{S}\widetilde{U} = 0. \tag{8.67}$$

The operator in matrix form is given by

$$\mathcal{S} = \begin{pmatrix} D_t + \frac{K_x k}{k_z}\partial_\psi \underline{u} & k\partial_\varphi \underline{u} & \frac{K_x}{k}N & \frac{K_x k}{k_z}\partial_\psi \\ \frac{K_x k}{k_z}\partial_\psi \underline{w} & D_t + k\partial_\varphi \underline{w} & -\frac{k_z}{k}N & k\partial_\varphi \\ \frac{K_x k}{k_z}\partial_\psi B - \frac{K_x}{k}N & k\partial_\varphi B + \frac{k_z}{k}N & D_t & 0 \\ \frac{K_x k}{k_z}\partial_\psi & k\partial_\varphi & 0 & 0 \end{pmatrix} + \text{h. o. t.}. \tag{8.68}$$

We did not give h.o.t. terms here explicitly for the sake of brevity, although they are taken into account completely but turn out to be irrelevant in later calculations.

If we find a solution $\widetilde{U}$ to (8.67), the complex conjugate $\widetilde{U}^*$ must solve it as well. Because the linear combination of the linearly independent solutions must be real valued to match physical initial conditions.

In the curvilinear translational coordinate system both the C1 and C2 traveling wave solutions can be written to leading order as

$$U(\Psi, \Phi, e^{i\varphi}; \varepsilon) = \hat{U}_{0,0}(\Psi, \Phi) + \left(\hat{U}_{0,1}(\Psi, \Phi)e^{i\varphi} + \text{c. c.}\right) + O(\varepsilon). \tag{8.69}$$

As the traveling wave depends on Ψ and Φ as well as φ, the linear operator of equation (8.67)

$$\mathcal{S} = \mathcal{S}(\Phi, \Psi, e^{i\varphi}; \partial_\varphi, \partial_\psi, \partial_t; \varepsilon) \tag{8.70}$$

defines a multiple scale problem. It exhibits slow variations in the coordinates Ψ and Φ, but a rapid oscillation in φ. So, if the amplitude and the background vary on

an order unity range spanned by Φ, the traveling wave envelope incorporates $O(1/\varepsilon)$ wave periods on that range. However, we obtained a significant simplification of the problem due to the transformation as there is no dependency on Ψ in the phase anymore. Since the traveling wave solutions are plane waves in the curvilinear coordinates, so that the phase is linear, only the background and the envelope of the wave vary slowly in the direction orthogonal to the phase.

8.2.3 WKB theory for linearized system

In order to construct an asymptotic solution to (8.67), we follow Miles (1961) who studied the stability of sheared flows. The flow, that was investigated in this paper, was statically stable, but a vertically sheared horizontal wind induced dynamical instabilities. The shear was heterogeneous, so that it was given by some function of the vertical coordinate. The arising instabilities though were of the same kind as the Kelvin-Helmholtz instabilities that were investigated by Goldstein (1931), who examined a two layered shear flow (piecewise homogeneous), where the instability appeared as a "cat eye" along the interface of the horizontal wind discontinuity. Both studies had a typical vertical scale defining the shear layer thickness. The evolution of a perturbation was obtained by a normal-mode ansatz which assumes a spatially bounded, horizontally oscillating field. It was found that highest exponential growth rates occurred when the horizontal wavelength of the perturbation was of the same order of magnitude as the shear layer thickness. These flows hardly capture the dynamics of our traveling wave solutions as the shear induced by the traveling wave solutions is not vertical but tilted.

However, we can translate these considerations to our gravity waves in order to fix the scales since in the limit of pure horizontal waves, we should obtain similar results. We can therefore identify the shear layer to be the wavelength of our traveling wave solution which is also assumed to be statically stable. In terms of wave numbers, we therefore assume that the wave number of the normal mode of the perturbation α, i.e. the wave number in Ψ-direction, is of the same order as the wave number of the traveling wave solution k, so

$$\frac{\alpha}{k} = O(1) \quad \text{as } \varepsilon \to 0. \tag{8.71}$$

This ansatz now allows for a WKB approach for the perturbation

$$\widetilde{U}(\varphi, \psi, t; \varepsilon) = \widetilde{U}(\varphi, \Psi; \varepsilon) e^{i\Theta(\Psi)\varepsilon^{-1} + \sigma t} \tag{8.72}$$

where the horizontal wave number of the perturbation becomes a slowly varying function

$$d_\Psi \Theta(\Psi) = \alpha(\Psi). \tag{8.73}$$

So, we replace the normal mode by a WKB phase which depends on the slow coordinate but induces fast variations due to ε^{-1}. Therefore, we allow the perturbation

to oscillate in Ψ-direction on the same scale as the traveling wave. As the phase is a function it still accounts for the slow modulation of the traveling wave. The dependence on φ is not further specified, yet. Since we linearized at a stationary solution, the coefficients in the linear operator do not depend on time and hence the linear system must have solutions of the form $e^{\sigma t}$. Note that σ is not an eigenvalue at least not for the operator $\mathcal{S}$. Because in the leading order of $\mathcal{S}$ there appears no time-derivative for the kinetic pressure of the perturbation $\widetilde{P}$.

In general, the parameter σ is a complex number that we may write as

$$\sigma = \sigma_R + i\sigma_I \quad \text{and} \quad \sigma_R, \sigma_I \in \mathbb{R}. \tag{8.74}$$

Solutions with $\sigma_R > 0$ correspond to unstable modes as they grow exponentially in time. Our objective is to find largest σ_R that solves (8.67).

The coefficients in the WKB ansatz (8.72) have a usual formal series expansion, so

$$\widetilde{U} = \widetilde{U}_0 + \varepsilon \widetilde{U}_1 + O(\varepsilon^2). \tag{8.75}$$

Due to our transformation, the phase of the traveling wave solution depends only on φ. So, $\varepsilon = 0$ has become an ordinary point and we can hence expand all coefficients in $\mathcal{S}$ depending on $\Phi = \varepsilon\varphi$ in a Taylor series at $\varepsilon = 0$ with φ, Ψ fixed

$$\begin{aligned}
\eta_f(\varphi, \Psi) &= \eta_f(0, \Psi) + O(\varepsilon) \\
U(\varphi, \Psi) &= \hat{U}_{0,0}(0, \Psi) + \big(\hat{U}_{0,1}(0, \Psi) e^{i\varphi} + \text{c. c.}\big) + O(\varepsilon) \\
\partial_\varphi U(\varphi, \Psi) &= i\hat{U}_{0,1}(0, \Psi) e^{i\varphi} + \text{c. c.} + O(\varepsilon) \\
\partial_\psi U(\varphi, \Psi) &= O(\varepsilon)
\end{aligned} \tag{8.76}$$

where $\Phi = 0$ is some reference point.

Let us now compute the transformed leading order velocity field (8.66) of the traveling wave in terms of the modulation variables using the Taylor series expansions (8.76), the polarization relation (3.27), and (3.28):

$$\underline{u} = \frac{k_z}{k} \hat{u}_{0,0} - \big(iAe^{i\varphi} + \text{c. c.}\big) + O(\varepsilon), \tag{8.77}$$

$$\underline{w} = \frac{K_x}{k} \hat{u}_{0,0} + O(\varepsilon). \tag{8.78}$$

Since $\underline{u}$ is the wind speed in Ψ-direction and $\underline{w}$ in Φ-direction, i.e. parallel to the phase velocity, we clearly see the character of the traveling wave solution: it is a shear wave. The wave induces a shear parallel to its phase velocity.

If we insert the WKB ansatz (8.72) into (8.67), then we obtain correct to $O(\varepsilon)$ as $\varepsilon \to 0$ with φ, Ψ fixed an equation for $\widetilde{U}_0$ of the form

$$\mathcal{B}\widetilde{U}_0 + \mathcal{C}\partial_\varphi \widetilde{U}_0 = 0 \tag{8.79}$$

with the matrix

$$\mathcal{B} = \begin{pmatrix} \hat{\sigma} & kAe^{i\varphi} + \text{c. c.} & \frac{K_x N}{k} & i\frac{K_x k}{k_z}\alpha \\ 0 & \hat{\sigma} & -\frac{Nk_z}{k} & 0 \\ -\frac{K_x N}{k} & \left(ikAe^{i\varphi} + \text{c. c.}\right) + \frac{Nk_z}{k} & \hat{\sigma} & 0 \\ i\frac{K_x k}{k_z}\alpha & 0 & 0 & 0 \end{pmatrix} \tag{8.80}$$

where

$$\hat{\sigma} = \sigma + i\left(\frac{k_z}{k}\hat{u}_{0,0} - \left(iAe^{i\varphi} + \text{c. c.}\right) - C_\Psi\right)\frac{K_x k}{k_z}\alpha, \tag{8.81}$$

and a matrix

$$\mathcal{C} = \begin{pmatrix} K_x\hat{u}_{0,0} - kC_\Psi & 0 & 0 & 0 \\ 0 & K_x\hat{u}_{0,0} - kC_\Psi & 0 & k \\ 0 & 0 & K_x\hat{u}_{0,0} - kC_\Psi & 0 \\ 0 & k & 0 & 0 \end{pmatrix}. \tag{8.82}$$

This system is very similar to the results of Lombard and Riley (1996) who performed the same steps but for the Boussinesq dynamics. As our coordinate transformations differ so do the coefficients that depend on the wave numbers, but in general we obtain the same terms to leading order. However, there are some major differences: we obtain additional terms including the mean flow. The mean flow was not considered in Lombard and Riley (1996) as it does not contribute to the exact plane wave solution of the nonlinear Boussinesq equations. Also, we acount for a slowly varying background in contrast to the uniform atmosphere as all background and traveling wave variables depend on the slowly varying coordinate Ψ. In this sense we add generalization to the established theory.

8.2.4 Floquet theory

The equation (8.79) can be identified as an ODE in φ if we keep Ψ constant. Since no further Ψ-derivatives appeared to leading order, setting it constant is justified, so that the solution for our perturbation has no modulation in Ψ-direction, it is a periodic wave. Let us rewrite the ODE as

$$\mathcal{A}(\varphi)\widetilde{U}_0(\varphi) = \partial_\varphi \widetilde{U}_0(\varphi) \tag{8.83}$$

with the coefficient matrix

$$\mathcal{A} = -\mathcal{C}^{-1}\mathcal{B}. \tag{8.84}$$

Since φ-dependencies only occur in the form of $e^{i\varphi}$, we deduce that the coefficient matrix is periodic, so that

$$\mathcal{A}(\varphi) = \mathcal{A}(\varphi + 2\pi) \tag{8.85}$$

with a period of 2π. Therefore, (8.83) is in the canonical form of a Floquet system. When we use the dispersion relation (5.12)

$$\mathbf{k} \cdot \mathbf{C} = \hat{\omega} + K_x \hat{u}_{0,0}, \tag{8.86}$$

we can simplify the diagonal entries of $\mathcal{C}$ and terms in $\hat{\sigma}$, respectively, by

$$\begin{aligned} K_x \hat{u}_{0,0} - k C_\Psi &= -\hat{\omega} \text{ and} \\ \frac{K_x k}{k_z} \left(\frac{k_z}{k} \hat{u}_{0,0} - C_\Psi \right) &= -\hat{\omega} + \frac{k^2}{k_z} C_z \end{aligned} \tag{8.87}$$

which removes the mean-flow wind from the equations. Hence, the inverse in (8.84) exists if

$$\det(\mathcal{C}) = -k^2 \hat{\omega}^2 \neq 0 \tag{8.88}$$

which is true as long as there is a traveling wave. We can now compute the coefficient matrix

$$\mathcal{A} = \begin{pmatrix} \frac{\hat{\sigma}}{\hat{\omega}} & \frac{k}{\hat{\omega}} A e^{i\varphi} + \text{c. c.} & \frac{N K_x}{k \hat{\omega}} & i \frac{k K_x}{k_z \hat{\omega}} \alpha \\ -i \frac{K_x}{k_z} \alpha & 0 & 0 & 0 \\ -\frac{N K_x}{k \hat{\omega}} & \frac{N k_z}{k \hat{\omega}} + \left(i \frac{k}{\hat{\omega}} A e^{i\varphi} + \text{c. c.} \right) & \frac{\hat{\sigma}}{\hat{\omega}} & 0 \\ -i \frac{K_x \hat{\omega}}{k k_z} \alpha & -\frac{\hat{\sigma}}{k} & \frac{N k_z}{k^2} & 0 \end{pmatrix}. \tag{8.89}$$

As mentioned above, we must check whether the complex conjugate of any solution also gives a solution in order to match physical, i.e. real valued, initial conditions. We therefore need to verify that

$$\mathcal{A}(-\sigma_I, -\alpha) \widetilde{U}_0^* = \partial_\varphi \widetilde{U}_0^* \tag{8.90}$$

holds assuming that $\widetilde{U}_0$ solves (8.83). It can be easily shown that

$$\mathcal{A}(-\sigma_I, -\alpha) = \mathcal{A}(\sigma, \alpha)^* \tag{8.91}$$

and hence by taking the complex conjugate of (8.90) the claim is always true.

We now proceed in finding a solution that gives us the nature of an instability. Floquet systems have a general solution of the form

$$\widetilde{U}_0(\varphi) = e^{\gamma \varphi} \widetilde{U}_{\text{per}}(\varphi) \tag{8.92}$$

where

$$\widetilde{U}_{\text{per}}(\varphi + 2\pi) = \widetilde{U}_{\text{per}}(\varphi) \tag{8.93}$$

is periodic with the same period as the coefficient matrix (Kapitula and Promislow 2013). The parameter γ is called the Floquet exponent. Note that in general γ is a complex valued number. It is the eigenvalue of the monodromy matrix which is

constructed via the fundamental matrix solution that we obtain writing all linearly independent solution vectors, of which there are four, into one matrix (Kapitula and Promislow 2013, p. 17). So, there exists as many γ's as there are linearly independent solutions. In general, it is neither possible to determine the fundamental matrix solution directly nor to compute the Floquet exponents. However, some information can be obtained when we apply Liouville's formula onto the fundamental matrix solution which links the Floquet exponents to the integral over the trace of the coefficient matrix:

$$\prod_j e^{2\pi\gamma_j} = \exp\left(\int_0^{2\pi} \mathrm{Tr}(\mathcal{A})\mathrm{d}\varphi\right). \tag{8.94}$$

We insert (8.89) and take the logarithm to get

$$2\pi \sum_j \gamma_j = \int_0^{2\pi} 2\frac{\hat{\sigma}}{\hat{\omega}}\mathrm{d}\varphi. \tag{8.95}$$

By plucking in (8.81) and computing the integral, we obtain

$$\sigma = \frac{1}{2}\hat{\omega}\sum_j \gamma_j + i\alpha\left(\hat{\omega} - \frac{k^2}{k_z}C_z\right). \tag{8.96}$$

If we decompose each Floquet exponent into its real and imaginary part,

$$\gamma = \nu + i\mu, \tag{8.97}$$

then it appears that

$$\sigma_I = \frac{1}{2}\hat{\omega}\sum_j \mu_j + \alpha\left(\hat{\omega} - \frac{k^2}{k_z}C_z\right), \tag{8.98}$$

$$\sigma_R = \frac{1}{2}\hat{\omega}\sum_j \nu_j. \tag{8.99}$$

Therefore, instabilities, i.e. positive σ_R, coexist with some real valued γ. If there is an unstable solution, then at least one of the Floquet exponents must posses a real part. This result in turn implies that solutions exist that grow exponentially in space which means they are not spatially bounded.

In our search for a particular, unstable solution, we restrict ourselves only to spatially bounded solutions, because otherwise one can probably not define an energy for the initial condition of the perturbation. As the energy must somehow be defined as a spatial integration, its convergence cannot be guaranteed. This rather vague, physically motivated argument has a rigorous counterpart in spectral stability theory (Sandstede 2002). But as we did not receive an eigenvalue problem for σ here, so that the σ's are not given by the spectrum of the linear operator, the prerequisites for the corresponding theorems are not fulfilled. The restriction of spatial boundedness also implies that α shall be purely real valued.

Let us discuss the role of the Floquet exponent more in detail. If we assume that a particular solution is spatially bounded, then it must be of the form $\gamma = i\mu$. In case $\mu = 0$ the solution will be 2π-periodic according to (8.92). The perturbation would therefore have the same periodicity as the traveling wave and can be called in resonance. The same holds for $\mu = 1, 2, \ldots$. Actually, one even finds that if any $\mu \in \mathbb{R}$ has a solution to the Floquet system, then $\mu + 1$ generates the exact same solution. The Floquet exponents are hence non-unique. If on the other hand $\mu = 1/2$, then the perturbation exhibits double the periodicity of the traveling wave. For $\mu = 1/3$ it is thrice the periodicity and so on. In conclusion, every rational μ generates periodic solutions whereas irrational μ produce consequently non-periodic solutions.

It is usually only possible for very idealized systems to compute the Floquet exponents explicitly. Nevertheless, it is possible to deduce one particular Floquet exponent for our system. Since it stems from a nonlinear system, there must exist some nonlinear function f, such that

(i) the traveling wave U solves $\partial_\varphi U = f(U)$ and

(ii) its Jacobian at the traveling wave $\mathcal{J}_f(U) = \mathcal{A}$ is our coefficient matrix.

Thus, if one replaces U in (i) by $U + V$ and linearizes at the solution U, then one has the Floquet system

$$\partial_\varphi V = \mathcal{J}_f(U)V = \mathcal{A}V. \tag{8.100}$$

To deduce the one Floquet exponent, we compute the derivative of (i) and insert (ii), so that

$$\partial_{\varphi\varphi} U = \partial_\varphi f(U) = \mathcal{J}_f(U)\partial_\varphi U = \mathcal{A}\partial_\varphi U. \tag{8.101}$$

If we now let $\partial_\varphi U = V$, then

$$\partial_\varphi V = \mathcal{A}V, \tag{8.102}$$

reproduces the Floquet system. Since U has period 2π, so has V and the corresponding Floquet exponent is zero. So, there is a perturbation that resonates with the traveling wave, i.e. it has the same periodicity.

Another way to deduce the trivial Floquet exponent zero is presented in Drazin (1977) by the observation that all periodic components in the Floquet matrix $\mathcal{A}$ from (8.84) share the same coefficient A being the amplitude of the underlying traveling wave. In the absence of the traveling wave, i.e. when $A = 0$, the system reduces to the linearized Boussinesq equations for the perturbation possessing the plane wave solution. This plane wave must have period 2π. So, the perturbation with Floquet exponent zero is the one which also solves in the limit of a vanishing traveling wave.

We now continue to manipulate the Floquet system in order to find a solution. We can decompose $\mathcal{A}$, such that the ODE (8.83) becomes

$$\mathcal{A}_1 \widetilde{U}_0 e^{i\varphi} + \mathcal{A}_0 \widetilde{U}_0 + \mathcal{A}_{-1} \widetilde{U}_0 e^{-i\varphi} = \partial_\varphi \widetilde{U}_0 \tag{8.103}$$

where the partitioned matrices are now independent of φ, so

$$\mathcal{A}_1 = \begin{pmatrix} \frac{\hat{\sigma}_1}{\hat{\omega}} & \frac{k}{\hat{\omega}}A & 0 & 0 \\ 0 & 0 & 0 & 0 \\ 0 & i\frac{k}{\hat{\omega}}A & \frac{\hat{\sigma}_1}{\hat{\omega}} & 0 \\ 0 & -\frac{\hat{\sigma}_1}{k} & 0 & 0 \end{pmatrix} \tag{8.104}$$

with $\hat{\sigma}_1 = \frac{K_x k}{k_z} A\alpha$,

$$\mathcal{A}_0 = \begin{pmatrix} \frac{\hat{\sigma}_0}{\hat{\omega}} & 0 & \frac{NK_x}{k\hat{\omega}} & i\frac{kK_x}{k_z\hat{\omega}}\alpha \\ -i\frac{K_x}{k_z}\alpha & 0 & 0 & 0 \\ -\frac{NK_x}{k\hat{\omega}} & \frac{Nk_z}{k\hat{\omega}} & \frac{\hat{\sigma}_0}{\hat{\omega}} & 0 \\ -i\frac{K_x\hat{\omega}}{kk_z}\alpha & -\frac{\sigma_0}{k} & \frac{Nk_z}{k^2} & 0 \end{pmatrix} \tag{8.105}$$

with $\hat{\sigma}_0 = \sigma - i\left(\hat{\omega} - \frac{k^2}{k_z}C_z\right)\alpha$, and

$$\mathcal{A}_{-1} = \begin{pmatrix} \frac{\hat{\sigma}_{-1}}{\hat{\omega}} & \frac{k}{\hat{\omega}}A^* & 0 & 0 \\ 0 & 0 & 0 & 0 \\ 0 & -i\frac{k}{\hat{\omega}}A^* & \frac{\hat{\sigma}_{-1}}{\hat{\omega}} & 0 \\ 0 & -\frac{\hat{\sigma}_{-1}}{k} & 0 & 0 \end{pmatrix} \tag{8.106}$$

with $\hat{\sigma}_{-1} = -\frac{K_x k}{k_z} A^*\alpha$. Since we know that $\widetilde{U}_{\text{per}}$ is periodic in φ, we can expand it in a Fourier series like

$$\widetilde{U}_{\text{per}}(\varphi) = \sum_{m=-\infty}^{\infty} \widetilde{U}_m e^{im\varphi}. \tag{8.107}$$

If we pluck it into (8.103), we obtain

$$\sum_{m=-\infty}^{\infty} \left(\mathcal{A}_1 e^{i(\mu+m+1)\varphi} + \mathcal{A}_0 e^{i(\mu+m)\varphi} + \mathcal{A}_{-1} e^{i(\mu+m-1)\varphi} - i(\mu+m)e^{i(\mu+m)\varphi}\right)\widetilde{U}_m = 0. \tag{8.108}$$

By shifting indices and using the orthogonality of the Fourier modes, we get an recursive algebraic equation for the Fourier coefficients

$$\mathcal{A}_1\widetilde{U}_{m-1} + (\mathcal{A}_0 - i(\mu+m))\widetilde{U}_m + \mathcal{A}_{-1}\widetilde{U}_{m+1} = 0, \tag{8.109}$$

which can be written as a homogenous matrix equation

$$\begin{pmatrix} & \ddots & & & & & \\ 0 & \mathcal{A}_1 & \mathcal{A}_0 - i(\mu-1) & \mathcal{A}_{-1} & 0 & & \\ & 0 & \mathcal{A}_1 & \mathcal{A}_0 - i\mu & \mathcal{A}_{-1} & 0 & \\ & & 0 & \mathcal{A}_1 & \mathcal{A}_0 - i(\mu+1) & \mathcal{A}_{-1} & 0 \\ & & & & & \ddots & \end{pmatrix} \begin{pmatrix} \vdots \\ \widetilde{U}_{-1} \\ \widetilde{U}_0 \\ \widetilde{U}_1 \\ \vdots \end{pmatrix} = 0. \tag{8.110}$$

The system matrix can be identified as an infinite block tridiagonal matrix

$$\mathbf{T} = \text{blocktridiag}(\mathcal{A}_1, \mathcal{A}_0 - i(\mu + m), \mathcal{A}_{-1}) \tag{8.111}$$

where in particular $\mathbf{T} = \mathbf{T}(\sigma, \mu, \alpha)$. The system (8.110) has nontrivial solutions only if

$$\det(\mathbf{T}) = 0. \tag{8.112}$$

This determinant gives us the condition to find the instability growth rates. In order to compute an approximate solution, one has to truncate the Fourier series, such that the block matrix $\mathbf{T}$ becomes finite. The approximated determinant can then be computed numerically and we arrive at a parameter study.

This numerical study would be designed as follows. We would have to prescribe a particular background and a particular traveling wave solution. For example the analytic solutions we found for the C1-case (see Chapter 5): either the wave with non-uniform background but without shear or the one with shear but uniform background. All the $O(1)$-parameters that we presented in Sections 5.1.2 and 5.1.3 must be fixed.

At hand would now be an optimization problem where we would maximize the real part of σ by variation of the imaginary part of the Floquet parameter μ and the perturbation wave number in Ψ-direction α, such that the condition (8.112) is fulfilled. Such a parameter study would be rather cumbersome and it would only test stability of a very particular traveling wave propagating through a very particular background. One could certainly vary some wave properties, such as the wave number or amplitude and repeat the numerical calculations. For the rich classes of traveling waves, we have found in this work, it would still only be possible to investigate a small fraction numerically.

8.2.5 Comparison with stability results from Boussinesq theory

For the finite-amplitude plane wave in the uniformly stratified, inviscid Boussinesq environment, the Floquet system was numerically solved first by Mied (1976) and independently by Drazin (1977). Both authors found that gravity waves with even infinitesimal amplitude and arbitrary wave vector in a stably stratified atmosphere are prone to instabilities. These kind of instabilities with vanishing amplitude are called parametric. Drazin compared his result with the Kelvin-Helmholtz instabilities by computing the local Richardson number which measures the induced shear and found that for any Richardson number the waves are parametrically unstable.

Our linearized scaled Euler equations in combination with the WKB approximation for the perturbation, that replaced the common normal-mode approach, are to leading order in line with the uniformly stratified, inviscid Boussinesq model which were examined by the aforementioned authors. We already acknowledged that the systems differ by the slowly varying phase (normal mode) and amplitude of the perturbation due to the slow modulation of the underlying traveling wave and

the slowly varying background. Another discrepancy is given by the fact that our equations include a mean flow that was not present in the discussed papers. However, if we assume in our model uniform stratification allowing for a plane wave with no mean flow (cf. Sections 5.1.4 and 5.2.5), we get the exact same stability results as Achatz (2005), Drazin (1977), Klostermeyer (1991), Lombard and Riley (1996), and Mied (1976) who all studied the uniformly stratified, inviscid Boussinesq model.

But even in the most general case, that our model provides, the differences between our and the Boussinesq model can be resolved: the components of our coefficient matrix (8.89) depend on the slow coordinate Ψ, but as we solve the Floquet system, it can be kept constant. In this sense, the modulation of the perturbation is homogenous on lines with constant Ψ and its wave character is periodic in Ψ-direction with fixed wave number α. The mean flow was substituted in terms of the dispersion relation of the traveling wave (8.87). It then only appears in $\hat{\sigma}$ as a type of Doppler shift for the imaginary part σ_I of the temporal parameter. By the symmetry of the system, such a shift cannot change any stability results since (8.87) is always real valued.

Hence, we can safely transfer the results of Drazin (1977) and Mied (1976) and conclude that our traveling wave solutions are always, i.e. for every set of control parameters, unstable. So, for every background and for every traveling wave defined by its modulation properties there exists at least one perturbative, locally bounded, oscillating mode which grows exponentially in time, such that the underlying traveling wave becomes linearly unstable.

To put it in a nutshell: we linearized the most general scaled Euler equations at the traveling wave solutions which allow for finite slowly varying amplitude; nonlinear mean-flow interaction; arbitrarily strong non-uniform stratification; and nonlinear non-plane phase functions. A scaling assumption favorable for unstable shear flows enabled us to apply a WKB approach, that captures the slow modulation of background and traveling wave, replacing the common normal-mode ansatz. The arisen Floquet system was found to be equivalent to the results that one gets from finite-amplitude plane waves in a uniformly stratified Boussinesq model.

It is not quite a surprise, that the traveling wave solutions are inherently unstable with respect to the Euler dynamics. This result was already supported by the outcome from Section 8.1.2 where we found instability of the isothermal traveling wave front with regard to the modulation equations. This chapter has shown that it is also unstable against the scaled Euler equations.

We can expect, that the picture changes if we would also account for viscous effects. Viscosity effectively damps short wavelength perturbations, so that we can estimate that traveling waves would be stabilized by this mechanisms. The influence of viscosity on the gravity wave stability was discussed in Achatz (2005) in a Boussinesq framework. Recently, Fritts et al. (2015) investigated anelastic gravity waves numerically by large eddy simulations where the role of viscosity is also examined.

9 Conclusion and final remarks

This thesis had two main tasks: to find traveling wave solutions to the extended theory presented by Achatz et al. (2010) and to test these solutions with respect to stability.

We started our derivations from the dimensionless, fully compressible Euler equations. By assuming non-hydrostatic dynamics, a typical wavelength small in comparison with the temperature scale height, a pressure scale height of the same order, and large wave amplitudes, we reproduced the distinguished limit of Achatz et al. (2010). The scale separation parameter ε, which is the ratio of the typical wavelength and the temperature scale height, now became the only parameter appearing in the equations.

The scaled Euler equations were derived from a multiple scale ansatz that separated the wave from a hydrostatic background. We combined a spectral expansion approach with the WKB assumption of slow modulation of amplitude and phase. So, the frequency and wave numbers are defined locally as the temporal and spatial derivatives of the phase, respectively. Since the system is nonlinear and we allowed for wave-mean-flow interaction, even the leading order equations are contaminated by higher harmonics.

Instead of an averaging technique (e.g. Grimshaw 1974; Tabaei and Akylas 2007) that assumes *a priori* periodicity of the asymptotic solution with respect to the fast phase, we applied the more general approach presented in Danilov et al. (2003) of weak asymptotic solutions. A key ingredient for this method was to substitute the phase by a bijective, differentiable mapping.

Investigating the results of the asymptotic analysis leads to the modulation equations: equations of motion for the phase, wave action density, and the leading order mean-flow variables. These equations are in line with the findings of Achatz et al. (2010). But in addition to that we found an evolution equation for the argument of the complex valued amplitude and a constraint for the higher-order mean-flow horizontal wind which becomes necessary to close the equation system. Computing the energy budget revealed that these equations conserve the sum of wave and mean-flow energy.

We found two distinct classes of traveling wave solutions for the modulation equations: the horizontally traveling wave solution and the isothermal traveling wave solution. This finding is the first main result of this study.

For the horizontally traveling waves, we were able to construct two different analytic solutions. One with non-uniform stratification and a homogeneous mean flow and another one with uniform stratification but heterogeneous mean flow. The horizontally traveling wave solution with vanishing horizontal velocity of the

co-moving reference frame may be applied to model mountain lee waves for arbitrary stratification, background horizontal wind, and orography.

A prerequisite for the fulfillment of the non-acceleration theorem, that we stated, was that the solution is horizontally homogeneous. Even though, the horizontally traveling wave solutions are horizontally heterogeneous, they still satisfy the theorem, such that they can only accelerate the mean flow irreversibly in case they break. Nevertheless, due to their nonlinear interaction, they constantly lose energy to the mean flow as long as the mean-flow horizontal wind has a positive vertical shear and gains energy if it is negative.

With the additional assumption that the wave is horizontally periodic, we investigated the existence and the shape of the isothermal traveling wave solution. It resembles an upward propagating wave front. Quite surprisingly, the isothermal traveling wave front decelerates the mean flow in order to sustain its constant amplitude and in this process drains energy from the mean flow. It thereby violates the non-acceleration theorem as the wave is locally confined but alters the mean flow irreversibly. We also showed that backs, regardless if up- or downward propagating, cannot solve the modulation equations.

Both classes of traveling wave solutions are generally characterized by nonlinear phase functions. The plane wave, whose phase is linear, however turned out to be a solution for both classes.

The horizontally traveling waves with non-uniform stratification were validated numerically against the fully nonlinear Euler equations with the aid of the pincFloit model (Rieper, Achatz, et al. 2013). Exact solutions of the modulation equations fulfill the Euler dynamics asymptotically. The purpose of the numerical simulations was to clarify the consistency of the solutions, i.e. range of validity of the asymptotic approximation. The traveling wave solutions performed surprisingly well: they exceeded the analytically expected order of convergence of one, as the scale separation parameter tends to zero. The numerically computed order turned out to be around three. This result holds on a broad range of scale separation parameters which proves the consistency of the traveling wave solutions presented in this thesis.

A second numerical survey was performed with the purpose to apply the traveling wave solutions as a reference for a grid convergence study. We showed feasibility for a large range of resolutions and reproduced the convergence order which was also found by the designer of the model.

We continued with a comment on the existence of weak asymptotic solutions and gave the mapping for the aforementioned substitution explicitly in terms of a translational, curvilinear, orthogonal coordinate transformation.

Next, we investigated the stability of the traveling wave solutions which was the second main objective of this survey. As the traveling waves are exact solutions to the modulation equations, we linearized them in the translational coordinate system and analyzed the evolution of small perturbations. For this purpose we introduced the method of spectral stability for the much simpler plane waves of the Boussinesq model. We showed the condition for spectral instability which coincided with the modulational instability proposed by Grimshaw (1977). The method was then

applied to the isothermal traveling wave front. They were found to be spectrally unstable in all circumstances.

We proceeded to linearize the scaled Euler equations in the curvilinear translational coordinate system, that we found earlier, at the traveling wave solutions. The transformation gained a simplification since the traveling waves, which typically exhibit nonlinear phases, transform to plane waves. As they are asymptotic solutions, we needed an asymptotic method to solve for the evolution of the perturbation. After applying a scaling for shear-unstable waves we exploited a WKB approach which replaced the common normal-mode decomposition. The resulting system was treatable with Floquet theory and had the same structure as the one which was obtained by Mied (1976) for the Boussinesq equations. We were able to transfer their results and concluded that both traveling wave classes are unstable in all circumstances.

In the course of our analytical and numerical investigations we stumbled upon a few questions that are certainly worth further attention. They shall be presented here as an outlook: we found plane waves as solutions to both traveling wave classes. Although the structure is different from the traveling wave front, the modulation equations simplify in the same fashion. It is probably worthwhile to investigate these equations with respect to stability with the same spectral methods because in contrast to the front the plane wave exhibits an exponential amplitude-growth with height.

In order to derive the isothermal traveling wave fronts we assumed *a priori* that the mean flow is controlled completely by the wave, so we set a vertically varying offset to be constant. It turned out, however, that we could allow the offset to depend linearly on altitude, which would correspond to a constant shear rate of the mean flow, and still generate traveling wave solutions in the desired sense. This generalization complicates the situation but probably produces a broad variety of solutions like fronts, backs, and pulses.

We saw that the horizontally traveling waves resemble the structure of mountain lee waves. These waves are usually large-scale and hydrostatic but we assumed for the scaling small-scale, non-hydrostatic dynamics. Thus, it remains an open question, whether our theory is also a generalization for this situation.

We did not obtain analytic solutions for the traveling wave fronts, such that for an application they must be computed numerically by solving the according ODE. Despite this little complication, it would also be interesting to test them in the pincFloit environment. We found that the traveling waves are generally unstable. Though, the numerical simulations of the horizontally traveling waves performed much better than expected. This seemingly paradox situation may resolve by the numerical damping of the discretization. We saw in the stability analysis that small-scale perturbations produce the highest growth rates. By design pincFloit produces some small but physical damping, which effectively degrades the small-scale motions. So, probably we can expect that the traveling wave front stabilizes by the same effect in a numerical simulation.

Acknowledgments

My sincerest gratitude goes to my supervisor Rupert Klein who asked the toughest questions but fortunately gave me the mathematical tools and the physical intuition to tackle them. He taught me that patience and endurance are most often the key. I am thankful for the guidance, inspirations, and advices of Ulrich Achatz. Also I want to thank Erich Becker who supported me and drew my interest for atmospheric dynamics. I thank Gergely Bölöni. He introduced me to the magic of pincFloit. My thanks go to Phillip Berndt and Christopher Pütz who were and are great office mates and always had an open ear for whatever I came up with. Many thanks to the entire AG Klein for the warm and kind working atmosphere. I thank the MS-GWaves research group for inspiring meetings, workshops, and discussions. I wish to thank Peter Patzt for keeping the tension between pure and applied mathematics. Special thanks go to Lennart Schüler for friendship, coffee, and proofreading. I offer my regards to all of those who helped me in any respect during the completion of my thesis. A special thank to Ralph Jonzeck, my physics teacher in school. He got me enthusiastic about science. I want to thank my parents, Angela and Gerd. They always endorsed my curiosity. Finally, my deepest gratitude to my love, Christin. You were always there patiently supporting me. Without you this thesis would never have been possible. Thank you!

Nomenclature

$\mathcal{A}$	Wave action density
A	Complex wave amplitude
a	Specific wave action density
$\mathbf{C}$	Relative velocity vector of translational coordinate system
$\mathbf{c}_g$	Wave group velocity
c_p	Heat capacity at constant pressure
ε	Scale separation parameter (ratio of the typical wavelength and the potential temperature scale height)
η	Logarithmic background derivative
E	Energy density
Fr	Froude number
G	Wave action flux
g	Gravitational acceleration
H_θ	Potential temperature scale height
H_p	Pressure scale height
$\kappa = R/c_p$	Ideal gas exponent
$\mathbf{k}$	Wave number vector
Λ	Mean-flow horizontal wind vertical shear rate
Ma	Mach number
N	Local background Brunt-Väisälä frequency
$\hat{\omega}$	Intrinsic wave frequency
ω	Wave frequency
Φ	Phase function

π	Exner pressure
q	Wave-mean flow energy-exchange rate
$R \approx 287\ Jkg^{-1}K^{-1}$	Specific gas constant
θ	Potential temperature
$\mathbf{v}$	Two-dimensional velocity vector field

Bibliography

Achatz, U. (2005). "On the role of optimal perturbations in the instability of monochromatic gravity waves". In: *Phys. Fluids* 17.9, pp. 1–27.

Achatz, U. (2007). "Gravity-wave breaking: Linear and primary nonlinear dynamics". In: *Adv. Sp. Res.* 40, pp. 719–733.

Achatz, U., R. Klein, and F. Senf (2010). "Gravity waves, scale asymptotics and the pseudo-incompressible equations". In: *J. Fluid Mech.* 663, pp. 120–147.

Alexander, M. J. and T. J. Dunkerton (1999). "A spectral parameterization of mean-flow forcing due to breaking gravity waves". In: *J. Atmos. Sci.* 56.24, pp. 4167–4182.

Becker, E. (2012). "Dynamical control of the middle atmosphere". In: *Space Sci. Rev.* 168.1-4, pp. 283–314.

Bölöni, G., B. Ribstein, J. Muraschko, C. Sgoff, J. Wei, and U. Achatz (2016). "The interaction between atmospheric gravity waves and large-scale flows: an efficient description beyond the non-acceleration paradigm". In: *J. Atmos. Sci.* pages.

Bühler, O. (2009). *Waves and mean flow*. first Ed. New York: Cambridge University Press.

Chu, V. H. and C. C. Mei (1970). "On slowly-varying Stokes waves". In: *J. Fluid Mech.* 41, p. 873.

Danilov, V. G., G. A. Omelyanov, and V. M. Shelkovich (2003). "Weak asymptotics method and interaction of nonlinear waves". In: *Asymptot. methods wave quantum Probl.* Ed. by M. V. Karasev. 208th ed. Amer. Math. Soc., Providence, RI, pp. 33–163.

Dosser, H. V. and B. R. Sutherland (2011a). "Anelastic Internal Wave Packet Evolution and Stability". In: *J. Atmos. Sci.* 68, pp. 2844–2859.

Dosser, H. and B. R. Sutherland (2011b). "Weakly nonlinear non-Boussinesq internal gravity wavepackets". In: *Phys. D Nonlinear Phenom.* 240.3, pp. 346–356.

Drazin, P. G. (1977). "On the instability of an internal gravity wave". In: *Proc. R. Soc. Lond. A* 356.1686, pp. 411–432.

Durran, D. R. (1989). "Improving the anelastic approximation". In: *J. Atmos. Sci.* 46.11, pp. 1453–1461.

Fritts, D. C. (2003). "Gravity wave dynamics and effects in the middle atmosphere". In: *Rev. Geophys.* 41, pp. 1–64.

Fritts, D. C., B. Laughman, T. S. Lund, and J. B. Snively (2015). "Self-acceleration and instability of gravity wave packets: 1. Effects of temporal localization". In: *J. Geophys. Res. Atmos. Res.* 120, pp. 8783–8803.

Goldstein, S. (1931). "On the stability of superposed streams of fluids of different densities". In: *Proc. R. Soc. A Math. Phys. Eng. Sci.* 132.820, pp. 524–548.

Grimshaw, R. (1974). “Internal gravity waves in a slowly varying, dissipative medium”. In: *Geophys. Fluid Dyn.* 6, pp. 131–148.

– (1977). “The Modulation of an Internal Gravity-Wave Packet, and the Resonance with the Mean Motion”. In: *Stud. Appl. Math.* 56.3, pp. 241–266.

Haack, A., M. Gerding, and F.-J. Lübken (2014). “Characteristics of stratospheric turbulent layers measured by LITOS and their relation to the Richardson number”. In: *J. Geophys. Res. Atmos.* 119.18, pp. 10, 605–10, 618.

Kapitula, T. and K. Promislow (2013). *Spectral and Dynamical Stability of Nonlinear Waves*. Vol. 185. Applied Mathematical Sciences. New York, NY: Springer New York.

Kato, T. (1995). *Perturbation Theory for Linear Operators*. Vol. 132. 2. New York: Springer, pp. xxii+619.

Klein, R. (2010). “On the regime of validity of sound-proof model equations for atmospheric flow”. In: *ESMWF Work. non-hydrostatic Model.* November, pp. 8–10.

Klein, R., U. Achatz, D. Bresch, O. M. Knio, and P. K. Smolarkiewicz (2010). “Regime of validity of soundproof atmospheric flow models”. In: *J. Atmos. Sci.* 67.10, pp. 3226–3237.

Klostermeyer, J. (1991). “Two and three–dimensional parametric instabilities in finite amplitude internal gravity waves”. In: *Geophys. Astrophys. Fluid Dyn.* 61.April, pp. 1–25.

Lebedev, L. P., M. J. Cloud, and V. A. Eremeyev (2010). *Tensor Analysis with Applications in Mechanics*. first Ed. Singapore: World Scientific Publishing.

Lelong, M.-P. and T. J. Dunkerton (1998). “Inertia-Gravity Wave Breaking in Three Dimensions. Part I: Convectively Stable Waves”. In: *J. Atmos. Sci.* 55.1997, pp. 2473–2488.

Lipps, F. B. and R. S. Hemler (1982). “A scale analysis of deep moist convection and some related numerical calculations”. In: *J. Atmos. Sci.* 39, pp. 2192–2210.

Liu, W., F. P. Bretherton, Z. Liu, L. Smith, H. Lu, and C. J. Rutland (2010). “Breaking of progressive internal gravity waves: convective instability and shear instability”. In: *J. Phys. Oceanogr.* 40, pp. 2243–2263.

Lombard, P. N. and J. J. Riley (1996). “Instability and breakdown of internal gravity waves. I. Linear stability analysis”. In: *Phys. Fluids* 8.12, p. 3271.

McLandress, C. (1998). “On the importance of gravity waves in the middle atmosphere and their parameterization in general circulation models”. In: *J. Atmos. Solar-Terrestrial Phys.* 60.14, pp. 1357–1383.

Mied, R. P. (1976). “The occurrence of parametric instabilities in finite-amplitude internal gravity waves”. In: *J. Fluid Mech.* 78, pp. 763–784.

Miles, J. W. (1961). “On the stability of heterogeneous shear flows”. In: *J. Fluid Mech.* 10.4, pp. 496–508.

Miura, R. M. and M. D. Kruskal (1974). “Application of a Nonlinear WKB Method to the Korteweg-DeVries Equation”. In: *SIAM J. Appl. Math.* 26.2, pp. 376–395.

Muraschko, J., M. D. Fruman, U. Achatz, S. Hickel, and Y. Toledo (2015). “On the application of Wentzel-Kramer-Brillouin theory for the simulation of the

weakly nonlinear dynamics of gravity waves". In: *Q. J. R. Meteorol. Soc.* 141.688, pp. 676–697.

Muraschko, J., M. Fruman, U. Achatz, S. Hickel, and Y. Toledo (2013). "On the application of WKB theory for the simulation of multi-scale gravity wave interactions". In: *Q. J. R. Meteorol. Soc.* 14.D12, p. 24110.

Rieper, F., U. Achatz, and R. Klein (2013). "Range of validity of an extended WKB theory for atmospheric gravity waves: one-dimensional and two-dimensional case". In: *J. Fluid Mech.* 729, pp. 330–363.

Rieper, F., S. Hickel, and U. Achatz (2013). "A Conservative Integration of the Pseudo-Incompressible Equations with Implicit Turbulence Parameterization". In: *Mon. Weather Rev.* 141.3, pp. 861–886.

Sandstede, B. (2002). "Stability of travelling waves". In: *Handb. Dyn. Syst.* Ed. by B. Fiedler. Vol. 2. Gulf Professional Publishing, pp. 983–1055.

Schlutow, M., R. Klein, and U. Achatz (2017). "Finite-amplitude gravity waves in the atmosphere: traveling wave solutions". In: under review.

Sutherland, B. R. (2001). "Finite-amplitude internal wavepacket dispersion and breaking". In: *J. Fluid Mech.* 429, pp. 343–380.

– (2006). "Weakly nonlinear internal gravity wavepackets". In: *J. Fluid Mech.* 569, p. 249.

Tabaei, A. and T. R. Akylas (2007). "Resonant long-short wave interactions in an unbounded rotating stratified fluid". In: *Stud. Appl. Math.* 119.3, pp. 271–296.

Whitham, G. B. (1965). "A general approach to linear and non-linear dispersive waves using a Lagrangian". In: *J. Fluid Mech.* 22, p. 273.

– (1974). *Linear and Nonlinear Waves*. John Wiley & Sons, Inc., p. 654.

THIS PAGE IS INTENTIONALLY LEFT BLANK.

THIS PAGE IS INTENTIONALLY LEFT BLANK.